

Bates College

SCARAB

Honors Theses

Capstone Projects

5-2022

Road Salt Retention and Its Impacts on the Water Quality of the Impaired Hart Brook Watershed (Lewiston, Maine)

Chen Chen

Bates College, cchen@bates.edu

Follow this and additional works at: <https://scarab.bates.edu/honorstheses>

Recommended Citation

Chen, Chen, "Road Salt Retention and Its Impacts on the Water Quality of the Impaired Hart Brook Watershed (Lewiston, Maine)" (2022). *Honors Theses*. 393.

<https://scarab.bates.edu/honorstheses/393>

This Open Access is brought to you for free and open access by the Capstone Projects at SCARAB. It has been accepted for inclusion in Honors Theses by an authorized administrator of SCARAB. For more information, please contact batesscarab@bates.edu.

Road Salt Retention and Its Impacts on the Water Quality of the Impaired Hart Brook Watershed (Lewiston, Maine)

An Honor Thesis

Presented to

The Faculty of the Department of Earth and Climate Sciences

Bates College

In partial fulfillment of the requirements for the

Degree of Bachelor of Science

By

Chen Chen

Lewiston, Maine

March 30, 2022

Preface

就一身了一身者，方能以万物付万物。

还天下于天下者，方能出世间于世间。

– 洪应明，1560~1615，《菜根谭》

Only the one, who can appreciate the nature and understands its philosophy, can pursue the nature's scheme without disturbing its consistency;

Only the one, who can follow the nature's rhythm and obey the rules of the nature, can accomplish a harmonious and successful life.

- Hong Yingming, 1560~1615, Caigentan (translated by Yuming, Su)

Acknowledgements

I want to say thank you to all the faculties of the Earth and Climate Sciences Department: Beverly Johnson, Eshita Samajpati, Genevieve Robert, Michael J. Retelle, Philip Dostie, Raquel Portes, Rebecca Larkin Minor, and Shreya Arora. Thank you to the faculties of Lewiston Public Work and Watershed Working Group: Reggie Poussard and John D. Kuchinski. Additional thanks to Camille S. Parrish in the Department of Environmental Studies, Martin W. Montgomery in the Department of Mathematics, and Ryan Gordon at Maine Geological Survey.

I want to show my deepest gratitude to my advisor Beverly Johnson and Philip Dostie for their invaluable supports. I will never accomplish my thesis writing and in-field as well as lab works without their selfless help. Their expertise and passions within the field of water geochemistry inspired my spirits within these years.

Thanks to all Class of 2022 Earth and Climate Sciences majors for letting me know the department as where I belong. Thanks to all the mates I know in the school for challenging, inspiring, and supporting me throughout these four years.

Finally, I want to say thank you to my mom, Ling Xu, and dad, Yi Chen, for their endless supports, which have encouraged me to keep challenging and surpassing myself on the way pursuing sciences.

Table of Contents

Acknowledgements	ii
Table of Contents	iii
Table of Figures	vii
Table of Tables	viii
Abstract	ixx
1. Introduction	10
1.1 Overview	10
1.2 Road Salt Background	10
1.2.1 Road Salt Impact	10
1.2.2 Road Salt Tracer	11
1.2.3 Road Salt Retention	12
1.3 Groundwater, Surface Water, and Impervious Surface Cover (ISC)	13
1.4 Road Salt Transport Model	17
1.5 Hart Brook Background	20
1.5.1 Historical Data	20
1.5.2 Depletion of the Data	24
1.5.3 Bedrock and Surficial Geology of the Hart Brook	25
1.6 Purpose of the Study	28
2. Methods	29
2.1 Overview	29
2.2 Study Sites	29
2.3 Field Methods	32
2.4 Lab Methods	34
2.3.1 Titration for HCO_3^-	34
2.3.2 Titration for Cl^-	35
2.3.3 Sulfate (SO_4^{2-}) Concentration	36
2.3.4 Major Cations	36
2.3.5 Alternative Ion Chromatography Instrument (IC)	37
2.4 Data Analysis	37

2.4.1 Major Ion Examination	37
2.4.2 Logger Data Conversion	38
2.4.3 Baseflow and First Flush Analyses	38
2.5 Watershed Characterization	40
2.5.1 Volume of Annual Precipitation in the Watershed and Total Cl ⁻ Input	40
2.5.2 Annual Stream Cl ⁻ Flux	41
3. Results	42
3.1 Characterization of the Watershed	42
3.1.1 Infiltration Rate	42
3.1.2 Lane Lengths	45
3.2 Water Level, Precipitation, and Discharge	46
3.3 Specific Conductivity and Cl ⁻ Concentration	53
3.4 Seasonal Variation in Cl ⁻ Flux	60
3.4.1 Historical Discharge and Cl ⁻ Concentration and Extrapolation	60
3.4.2 Seasonal Variation in BC6	61
3.5 Major Ion Analysis	65
4. Discussion	72
4.1 Major Ion Concentrations and Seasonal Shift in Water Type	72
4.2 Spatial Variation	74
4.2.1 Clean Water in Goff Brook Area	74
4.2.2 Potential Source of Contamination in Industry Area	74
4.2.3 Downstream Site Conditions	76
4.3 Seasonal Variation	76
4.3.1 Connecting Discharge Measurements with Previous Records	76
4.3.2 Cl ⁻ Flux	77
4.4 Surficial Geology and Infiltration Rate Analysis	78
4.5 Rough Calculation of the Exported Cl ⁻	79
4.6 Precipitation Events Analysis	81
4.6.1 Storm Hydrograph	81
4.6.2 Baseflow Separation	83
4.6.3 First Flush Analysis	83
4.6.4 Chemical Responses	84

5. Conclusion and Recommendations	85
References	86
GIS Layers	90
Appendix 1: Field Work Schedule	91
Appendix 2: Hydrolab Data	93
Appendix 3: Major Ion Analysis Results	94
Appendix 4: Piper Diagram of Each Sample Set	96

Table of Figures

1. Introduction	10
1.1 (<i>Hart Brook Watershed Management Plan 2019</i>) SpC vs. Cl ⁻ concentration of Hart Brook	12
1.2 (a) (<i>Cunningham et al., 2009</i>) Cl ⁻ and NO ₃ -N concentration vs. %ISC in 5 sites of Hudson River	16
1.2 (b) (<i>Kaushal et al., 2005</i>) Cl ⁻ concentration vs. %ISC in the city of Baltimore	17
1.3 (<i>Shamseldin et al., 2011</i>) Classification of first flush curves	20
1.4 (<i>Hart Brook Watershed Management Plan 2019</i>) Ten sites being assigned for the watershed	22
1.5 (<i>Hart Brook Watershed Management Plan 2019</i>) HSG of the divided six subareas in the Hart Brook	23
1.6 (<i>Hart Brook Watershed Management Plan 2019</i>) 2016 DO concentration in the Hart Brook	24
1.7 (<i>Bedrock Geology Map of Maine</i>) Overview of the bedrock geology of the Hart Brook	26
1.8 (<i>Bedrock Geology Map of Maine</i>) Cross-section of the bedrock geology of the Hart Brook	26
1.9 (<i>Surficial Geology of the Lewiston Quadrangle</i>) Surficial geology of the Hart Brook	27
2. Methods	29
2.1 (<i>Hart Brook Watershed Management Plan 2019</i>) Locations of the study sites	30
2.2 (<i>USGS Water Science School, 2018</i>) Sketch of stream gaging methods	32
2.3 Deployed logger at BC6	33
3. Results	42
3.1 Surficial geology in the Hart Brook watershed from ArcGIS	43
3.2 Calculation of the average infiltration rate in the Hart Brook	44
3.3 Public roads in the Hart Brook watershed from ArcGIS	45
3.4 Water level of HB4 from 3/29/2021 to 6/28/2021	48
3.5 Water level of BC6 from 3/29/2021 to 6/28/2021	49
3.6 Precipitation in the Hart Brook from March to June	50
3.7 Water Level of BC6 from 9/2/2021 to 12/9/2021 from data logger (blue) and field measurements (orange)	51
3.8 Precipitation in the Hart Brook from September to early December	52
3.9 Rating curve for BC6	53
3.10 SpC data plotted on the water level graph of HB4 from 3/29/2021 to 6/28/2021	55
3.11 SpC data plotted on the water level graph of BC6 from 3/29/2021 to 6/28/2021	56
3.12 SpC data plotted on the water level graph of BC6 from 9/2/2021 to 12/9/2021	57
3.13 SpC readings of BC6 from 12/17/2021 to 2/17/2022	58
3.14 SpC (μS/cm) vs. Cl ⁻ concentration (mg/L)	59
3.15 Seasonal variation of SpC and Cl ⁻ concentration in BC6	62

3.16 Seasonal variation of discharge and Cl^- flux in BC6	63
3.17 Discharge through sites	65
3.18 Major anions in the watershed	65
3.19 Major cations in the watershed	67
3.20 Na^+ concentration vs. Cl^- concentration; red line represents the standard 1:1 ratio	70
3.21 Piper diagram of samples from 6/28/2021 to 12/9/2021	71
4. Discussion	72
4.1 (Hatari Lab) Interpretation of piper diagram with circles indicating the location of samples	73
4.2 Site condition of CCI	75
4.3 (Weatherspark.com) Historical precipitation in Lewiston in 2021	77
4.4 (Caswell, 1987) Groundwater water-level in Maine	78
4.5 Calculation of the stream flow contribution	80
4.6 (Weatherspark.com) Precipitation on 7/9/2021	83
4.7 SpC and water level in BC6 from 7/8/2021 to 7/12/2021	83
4.8 MFF of the storm event at BC6 between 7/8/2021 and 7/12/2021	84
4.9 Cl^- mass and discharge variations during storm at BC6 between 7/8/2021 and 7/12/2021	85
4.10 Molar ratio between Na^+ and Cl^- under storm and no-rain condition	85

Table of Tables

1. Introduction	10
1.1 (CCME; EPA; Kaushal et al., 2005) Summary of proposed Cl^- concentration guidelines in stream	11
1.2 (Arnold and Gibbons, 1996; Holland et al., 2004; Kim et al., 2016; Klein, 1979; Liu et al., 2013) General %ISC thresholds for water degradation	14
1.3 (Brabec et al., 2002) Summary of degradation measurements and their associated threshold findings	15
2. Methods	29
2.1 Longitude and latitude of the study sites	31
3. Results	42
3.1 Area and infiltration rate of each type of surficial geology	43
3.2 Raw data for the rating curve	53
3.3 Raw data for SpC ($\mu\text{S}/\text{cm}$) vs. Cl^- concentration (mg/L)	59
3.4 Calculation approaches of the monthly average of the discharge in BC6	60
3.5 Calculation approaches of the monthly average of the SpC in BC6	61
4. Discussion	72
4.1 (Hem, 1985) Concentration of ions in the watershed and the global average concentrations in river water	72
4.2 Road salt application amounts in the Hart Brook	80
4.3 Calculations of annual Cl^- exports	81

Abstract

The application of road salt (NaCl) as a deicing compound in the United States began in the 1930s, and the Hart Brook watershed, located in Lewiston, Maine, has experienced elevated specific conductivity (SpC) values presumably due to the road salt retention since the first measurement in 2011. While the year-long spatial and temporal changes of the road salt contamination in the Hart Brook remain unclear, the purpose of this study is to investigate the transport dynamics of road salt and its impacts on the water quality of this watershed in a period of a year, in the aim of improving the understanding and the regulations on the nonpointing sources of pollution in this area. From late March 2021 to mid-February 2022, water levels, SpC values, discharges, and major ions were analyzed from 7 sites on a biweekly/monthly basis. Consistent with former reports, Cl^- concentrations in the watershed present signals to surpass the chronically toxic level of 230 ppm suggested by EPA during summer and winter, reaching 435 ppm and 430 ppm due to drought conditions and road salt applications, respectively. As the application of road salt contributes to most of the Cl^- contamination in the watershed, increasing Cl^- flux during fall and the overall molar ratio of 0.9192 between Na^+ and Cl^- indicate the road salt residence in soils. Significant difference between the annual Cl^- input amounts from the government and the actual export amounts from the measurements may suggest the presence of unregulated private application of de-icing salt, salt retention from previous years, and extra sources of contamination outside the watershed. The transport dynamics of the road salt were analyzed through the characterization of the infiltration rate of the watershed and an observed first flush event during a storm in July. Further analyses on the watershed sub-surface, soil conditions, and % ISC owned by private companies or residences are necessary to further understand the road salt transport mechanisms within the Hart Brook.

1. Introduction

1.1 Overview

The application of road salt (NaCl) as a deicing compound in the United States has a long history since 1940, and the application amounts keep growing exponentially, reaching 15-32 million metric tons in recent years (Cary Institute of Ecosystem Studies). The rise of road salt loadings has resulted in the increasing Na^+ and Cl^- concentrations in the water bodies of the northern United States and affected or even impaired existing water systems (Kaushal et al., 2005; Kaushal et al., 2017; Zuidema et al., 2018). The Hart Brook watershed, located in Lewiston, Maine, the city with 68 inches of annual snowfall, is undoubtedly suffering in the contaminations of road salts that are applied 21 tons per road mile for maintenance (Hart Brook Watershed Management Plan 2019; Rubin et al., 2010). Mass balance studies indicate that road salt being applied in a particular year is unlikely to be exported from the watershed within the same year (Howard and Haynes, 1993; Kelly et al., 2008; Robinson and Hasenmueller, 2017); historical specific conductivity (SpC) readings in this local watershed also suggest that the salts may continuously enter the system throughout the year, keeping the water quality harmful for aquatic life. In this study, the water quality of the watershed will be continuously monitored through use of dataloggers and field samplings from the summer of 2021 to the spring of 2022. The results will be used to determine the annual flux of road salt through the watershed, identify seasonal changes in road salt contamination, and identify hot spots of road salt application. The results will be compared with datasets previously acquired by the City of Lewiston to assess the impact of recent efforts to curb the impact of road salt on the watershed. In addition, a storm event will be specifically focused on, to further understand the dynamics of road salt contamination under the relatively high percent impervious surface cover of the watershed. This chapter will briefly summarize the history of Hart Brook watershed, discuss existing literature related to the topic, and introduce the background information of this case study.

1.2 Road Salt Background

1.2.1. Road Salt Impacts

Road salt is halite, the mineral form of sodium chloride (NaCl) that is widely applied to de-ice via freezing point depression. The effects of its contamination appear in both environmental and public health.

Despite the presence of road salt will increase the salinity of water (Kaushal et al., 2018), the pH is unlikely to be changed with these salts alone as Cl^- is a weak conjugate base; nevertheless, high NaCl loads can result in accelerated deterioration of water-related infrastructures (Kaushal et al., 2017). Increasing Na^+ concentration in freshwater and soils is also likely to decrease soil aggregate ability and soil fertility through the leaching of Ca^{2+} and Mg^{2+} caused by cation exchange (Robinson and Hasenmueller, 2017).

Kaushal et al. (2005) state that the Cl^- concentration level above 1000 mg/L will lead to lethal as well as sublethal effects on aquatic plants and invertebrates. This proposed threshold is widely accepted. EPA has recommended the instantaneous level of 860 mg/L for Cl^- since 1988, the level that freshwater animals with acute sensitivity will likely be affected (one-hour average concentration does not exceed more than once every three years). The life-cycle and early life-stage tests being conducted by EPA with freshwater animals and plants also recommends a chronically toxic level of 230 mg/L (four-day average concentration does not exceed more than once every three years on average). Although physiological damage is rarely observed from fish under lower Cl^- concentration, smaller organisms being consumed by fish, may be sensitive to the same condition (Shambaugh and Vermont, 2008). Under heavy road salt application, the Canadian Council of Ministers of the Environment (CCME) have also provided their own guidelines for Cl^- concentration in surface freshwater (Table 1.1).

Cl^- conc. (mg/L) - Instantaneous	Cl^- conc. (mg/L) - Chronical	Source
860	230	EPA
1000		Kaushal et al., 2005
640	120	CCME

Table 1.1. summary of proposed Cl^- concentration guidelines in stream.

1.2.2. Road Salt Tracer

NaCl dissolves into Na^+ and Cl^- ions and increases the specific conductivity (SpC) of the water. There is a strong correlation between SpC and Cl^- concentrations such that the SpC value can be used as a proxy for Cl^- concentration in a waterbody. Both long-term logger monitoring and the measurements conducted in microcosms present similar linear regression models for plotting Cl^- concentration (mg/L) against SpC ($\mu\text{S}/\text{cm}$) with slopes ranging from 0.21 to 0.30 when Cl^- concentration is below 500 (Benbow and Merritt, 2004; Castellote et al., 2001; Peinado-Guevara et al., 2012; Perera et al., 2009; Zuidema et al., 2018). Notwithstanding, in the Hart Brook Watershed Management Plan 2019, the relationship between SpC and Cl^-

concentration is plotted in power fit instead of linear fit from the historical data of watershed (Figure 1.1). Regarding this relationship and the Cl^- concentration guideline from EPA, the MDEP uses SpC values of 1000 $\mu\text{S}/\text{cm}$ or higher to identify waters of chronic toxicity; the Hart Brook watershed appears to approach and exceed these levels frequently (Figure 1.1; Hart Brook Watershed Management Plan, 2019).

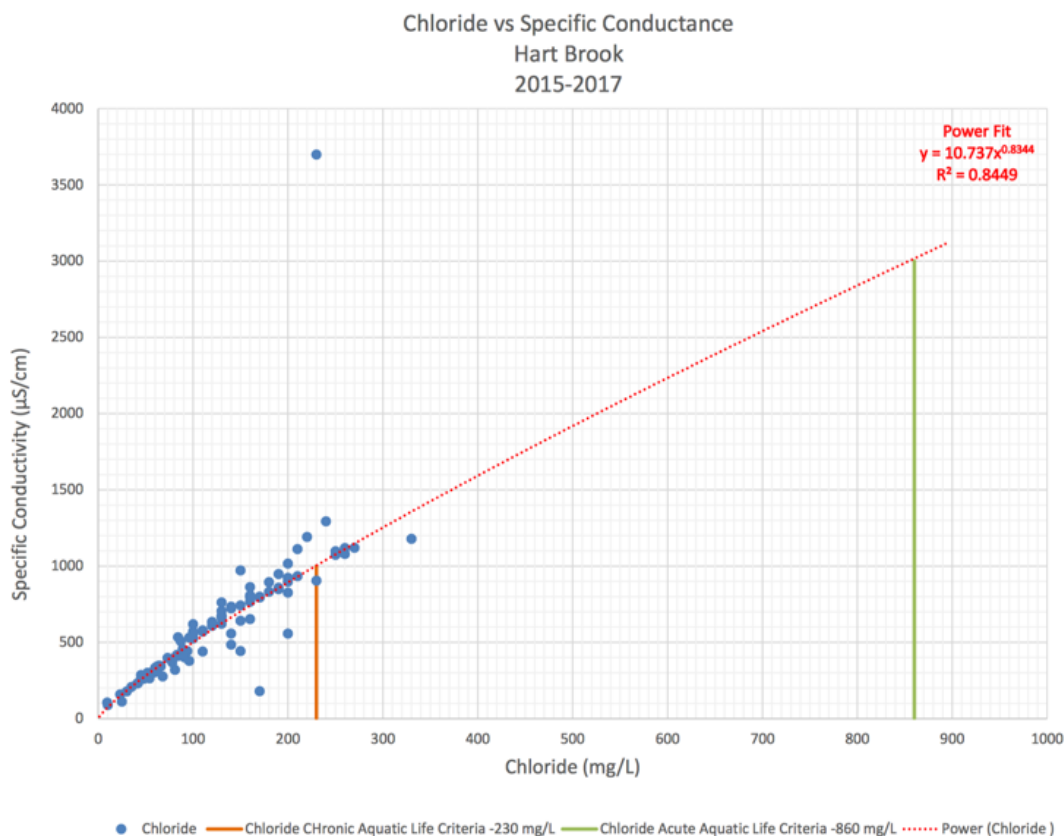


Figure 1.1. SpC vs. Cl^- concentration of Hart Brook (Hart Brook Watershed Management Plan 2019).

The strong correlation between SpC and Cl^- concentration thus enables the usage of datalogger/field sensors to monitor Cl^- concentration through the SpC readings. Cl^- concentration can be directly analyzed by titration, usually with Ag^+ substances, but are time consuming and expensive and are thus usually only performed to confirm the accuracy of the relationship between Cl^- and SpC (Robinson and Hasenmueller, 2017).

1.2.3. Road Salt Retention

Road salt is retained in soils. Na^+ is retained in soils through cation exchange; whereas Cl^- retention can be mostly attributed to the porewater retention, microbial uptake, and the formation of chlorinated organic compounds. Hence, the amounts of Cl^- may be observed continuously increasing during the time when road salt is not applied (Robinson et al., 2017; Snodgrass et al., 2017).

NaCl results in a 1:1 molar ratio of $\text{Na}^+:\text{Cl}^-$ upon dissolution. Assuming other sources of Cl^- , such as potassium chloride (KCl) and calcium chloride (CaCl_2) are negligible in the watershed, deviations from the expected 1:1 molar ratio between Na^+ and Cl^- provide useful information on tracking groundwater discharge into streams (Snodgrass et al., 2017). Retention rates of Na^+ and Cl^- are variable and depend on the watershed e.g., 66% and 62%, 30% and 20%, and 41% and 31% for Na^+ and Cl^- , respectively); however Na^+ tends to be retained more easily than Cl^- due to its higher affinity for negatively charged sites on soil surfaces than Cl^- (Robinson et al., 2017; Sun et al., 2012). Therefore, the regression line of $\text{Na}^+:\text{Cl}^-$ ratio of the stream water can serve as a signal of salt retention and an indicator for the degree of transport through either groundwater or surface runoff (Snodgrass et al., 2017). In general, the smaller the slope of the molar concentrations of Na^+ vs. Cl^- regression line, the greater the retention of Na^+ in the soil substrate and the greater degree the water is transported via the groundwater.

1.3 Groundwater, Surface Water, and Impervious Surface Cover (ISC)

Surface water is recharged by groundwater, surface water runoff, and direct precipitation. The process that the water naturally “seeps” through the soils to recharge the groundwater is known as infiltration and the process that the water drains into the surface water resources directly is called runoff. Streams receive Cl^- from both groundwater discharge as well as runoff from storm events and precipitation (Robinson and Hasenmueller, 2017).

When the surface water infiltrates through the soils with high Cl^- contents, the water grabs the retained Cl^- and joins the subsurface groundwater; the groundwater thus inputs Cl^- into the stream. Hence, the soil quality plays an essential role in the health of a water body.

At the same time, the Cl^- concentration in a stream is also highly related to the Impervious Surface Cover (ISC) level, because the annually applied road salts gradually turn into the loads of contaminations to the water sources through surface water runoff during melting and storming events (Cummington et al., 2009).

ISC refers to the land surface that does not allow water to infiltrate into the subsurface. A relatively higher density of these surfaces usually results from urbanization, when considerable amounts of landscapes are replaced by roads, parking lots, and buildings. Hence, urban areas tend to have larger ISC than suburban or rural areas. Under any circumstances, increasing ISC in the watershed area is linked to the deteriorating stream water quality as the contaminant accumulated on the impervious surface will be flush into streams through runoff (Liu et al., 2013; Kim et al., 2016). Two observable thresholds have been identified to present the relationship between ISC and water quality that: 1) water degradation occurs when the ISC exceeds 10% of local land cover and 2) over 30% ISC will lead to an unavoidable water degradation (Arnold and Gibbons, 1996). In fact, these thresholds being extrapolated through literature reviews are globally applicable. Kim et al.' (2016) study on Han River Basin, Korea, indicates the primary threshold of 10%, and Liu et al.'s study on the watersheds in Shenzhen, China, gives out the urban-watershed threshold of 36.9% for effective watershed management. Other studies on the same topic but different sites produce results in a similar range (Table 1.2).

%ISC - Start Degradation	%ISC - Unavoidable Degradation	Source
10	30	Arnold and Gibbons, 1996
10		Kim et al., 2016
	36.9	Liu et al., 2013
12	30	Klein, 1979
10-20	20-30	Holland et al., 2004

Table 1.2. general %ISC thresholds for water degradation.

Although these thresholds provide general quantitative references for ISC management, they are not universal regarding the types of impacts being introduced and distinctive characteristics of the topography, sewage, land-use type, etc. of a specific watershed, as summarized by Brabec et al. (2002) (Table 1.3).

	Impact Measurement	Percentage Impervious Threshold for Degradation	Study
Parameter type	Parameter		
Biotic	Benthic invertebrates	< 10 humans per hectare	Jones and Clark (1987)
		8	Horner et al. (1997)
		15	Klein (1979)
	Fish diversity	10 urbanized	Limberg and Schmidt (1990)
		12	Klein (1979)
		8	Miltner (1997)
		3.6	Booth and Jackson (1994)
		10	Wang et al. (forthcoming)
	IBI	8 urban land use	Yoder et al. (n.d.)
	Macroinvertebrate diversity	8 to 15	Shaver et al. (1994)
		8	Miltner (1997)
	Species diversity	10 to 15	Booth and Reinelt (1993)
Abiotic and biotic	IBI, habitat quality	10 to 20 urban land use	Wang et al. (1997)
	Mean event water-level fluctuation/ indicator species	10 TIA, 14 EIA	Taylor (1993)
	Variation of water depth and indicator species	15 to 21	Chin (1996)
Abiotic—physical	Temperature for cold-water biota	12	Galli (1990)
	Base flow	45	Klein (1979)
	Stream flow	> 21	Horner et al. (1997)
		Not defined	Krug and Goddard (1986)
	Peak flows	4.6	Booth and Jackson (1994)
	Channel enlargement and streambank erosion	Not given	Hammer (1972)
		34 urbanization	MacRae (1997)
		8 to 10	Booth and Reinelt (1993)
	Habitat assessment	30	May et al. (1997)
		10	Booth and Jackson (1994)
		4 to 9 impervious surface and 30 to 50 forest	Hicks and Larson (1997)
	Large woody debris	9	Horner et al. (1997)
	Sediment	20	Wydzga (1997)
		50	Horner et al. (1997)
		Not defined	Krug and Goddard (1986)
		43	Griffin et al. (1980)
		45	May et al. (1997)
Abiotic—chemical	Nutrients	42	Griffin et al. (1980)
	Phosphorous	45	May et al. (1997)
	Threshold of eutrophication based on TSS and TP	30	Todd et al. (1989)
	Chemical water quality	45	May et al. (1997)
	Oxygen	10	May et al. (1997)
		7.5 urbanized	Limburg and Schmidt (1990)
		43	Griffin (1980)
	Metals	50	Horner et al. (1997)
	Zinc	40	Horner et al. (1997)

NOTE: IBI = Index of Biotic Integrity; TIA = total impervious area; EIA = effective impervious area; TSS = total suspended solids; TP = total phosphorus.

Table 1.3. summary of degradation measures and their associated threshold findings (Brabec et al., 2002).

While Brabec et al. (2002) argued for “*defining accurate thresholds for a continuum of impervious surface impacts*”, investigations on the relationship between ISC and contaminants

concentrations were performed in Hudson River, NY, and Baltimore, MD (Cunningham et al. 2009; Kaushal et al., 2005). Cunningham et al. (2009) find that the impacts on the stream water quality are observed in low-density development area with the ISC level as low as 1% to 3% (Figure 1.2(a). Similarly, Kaushal et al., (2005) find road salt contamination in watersheds with less than 15% ISC (Figure 1.2 (b)). These indicate that there is essentially **no ISC threshold** for water quality and reiterates the need for individual investigation on different watersheds regarding their distinctive characteristics.

(a).

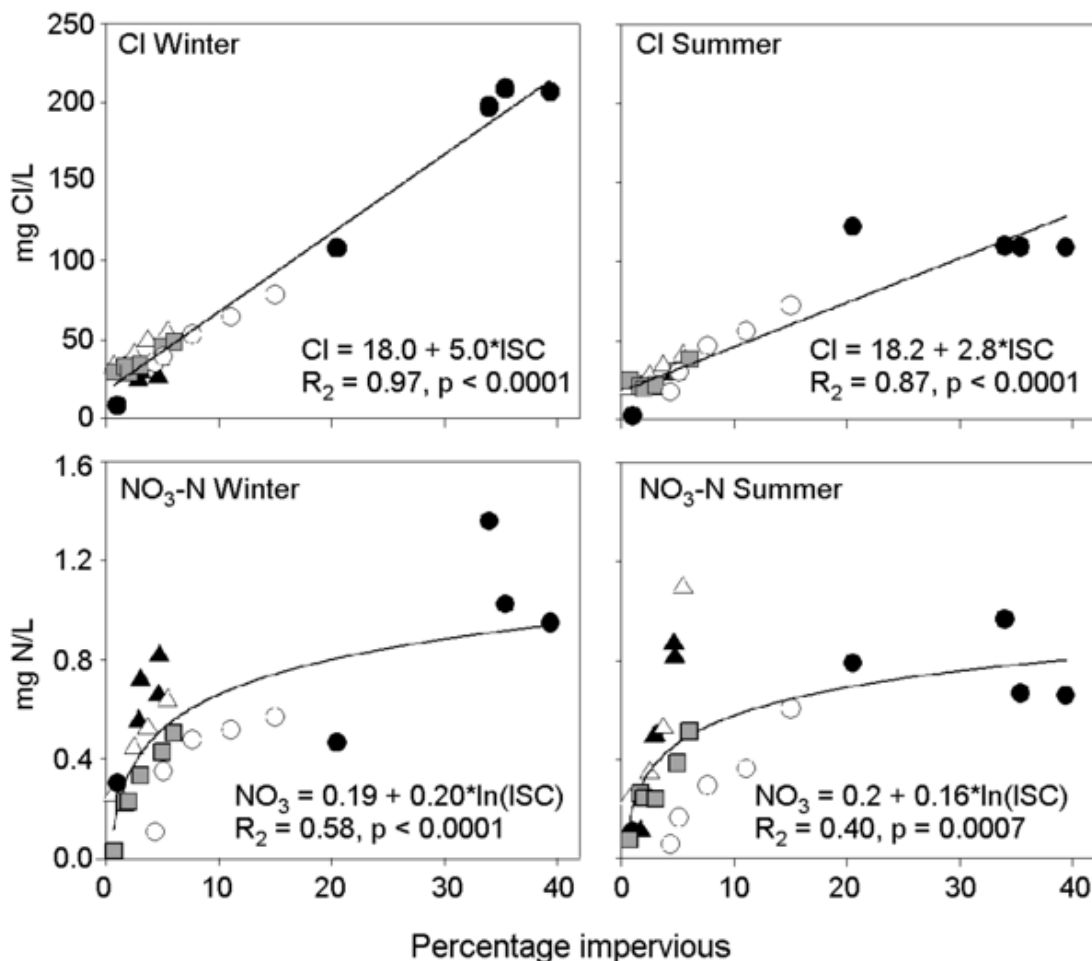


Figure 1.2. (a). Cl^- and $\text{NO}_3\text{-N}$ concentrations vs. %ISC in 5 sites of Hudson River (Cunningham et al. 2009)

(b).

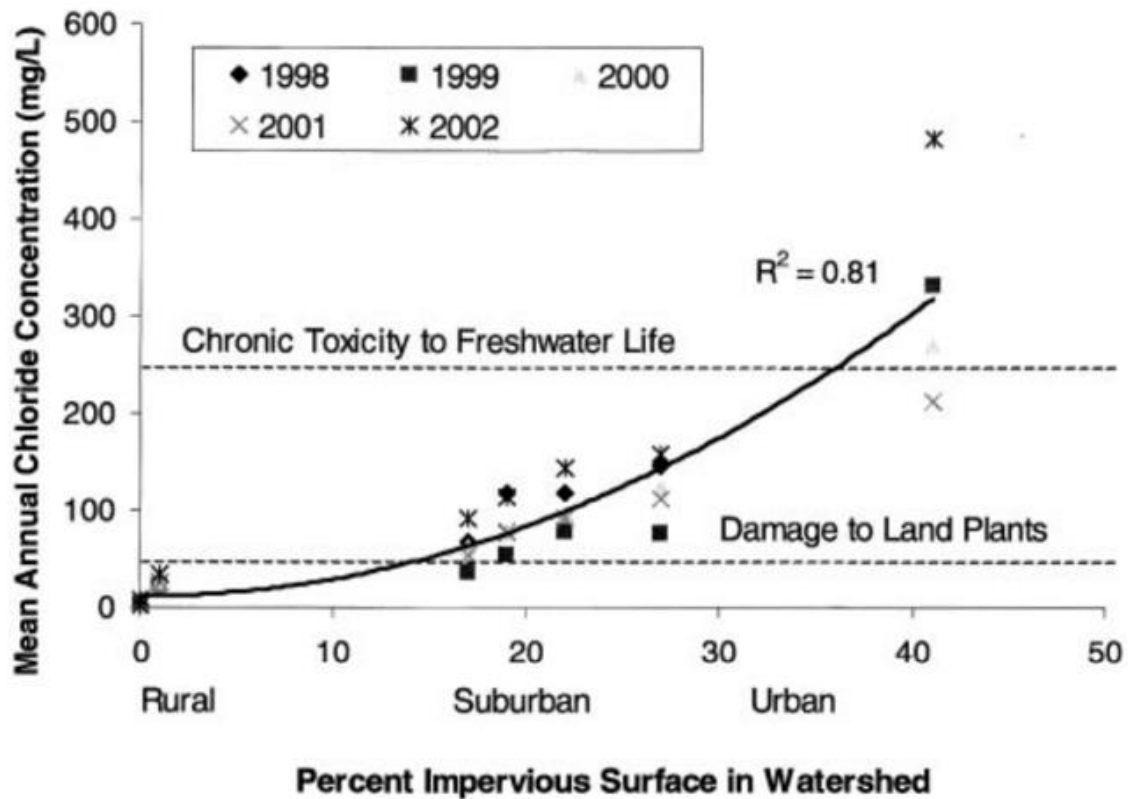


Figure 1.2. (b). Cl^- concentration vs. % ISC in the city of Baltimore (Kaushal et al., 2005)

1.4 Road Salt Transport Model

Road-salt contamination of surface water is a combination of both surface water runoff (immediate NaCl input) resulted from ISC and slower NaCl groundwater infiltration due to road salt retention (Godwin et al., 2003). Understanding the dynamics of its transport and its retention time in the watershed is essential in constructing effective management strategies (Gu et al., 2019; Robinson and Hasenmueller, 2017).

The modeling of Cl^- residence time is complicated due to the fact that it may not be fully flushed from a watershed from winter to winter and in between road salt application dates (Robinson and Hasenmueller, 2017). Arc/GIS techniques were used by Robinson and Hasenmueller (2017) to estimate the annually applied road salt amount in karst spring area, with calculated lane-length of roads in each recharge basin and application guidelines from local government and compared to measured values. Performing a two-year monitoring, they find the measured road salt export does exceed the estimated annual application amounts and thus suggest that the Cl^- residence time may be longer than one year in this setting. This implies that road salt is continuing to accumulate in the groundwater in this setting.

The key to analyzing the transport dynamics, as proposed by Robinson and Hasenmueller (2017), is to separate the baseflow and event flow of the stream, because both surface runoff and groundwater infiltration are highly related to floods. Baseflow (BF) is the groundwater contribution to the streamflow, or the “initial” and “older” water in the stream basin (discharging into the stream during the dry season), and the event flow (RO, standing for runoff) consists of the water added through direct precipitation and surface water runoff during storm, snow, and/or melt events.

Among numerical calibration models, one of the most applicable methods is known as SpC mass-balance method. This method assumes that the baseflow and event flow conductivity can be determined from the conductivity of the streamflow (Q_C) during extremely low-flow (dry) season and extremely high-flow (wet) season, respectively (Stewart et al., 2007). In other words, models with this method are based on the assumption that during extremely low-flow condition, the streamflow discharge (Q) is 100% consisted of BF, whereas it is 100% consisted of RO during extremely high-flow conditions/storm events. An alternative way is to assign the highest conductivity measurements during dry season as the conductivity of the baseflow (BF_C) and the lowest conductivity measurements during wet season as the conductivity of the event flow (RO_C) (Stewart et al., 2007; Robinson and Hasenmueller, 2017). That is because, theoretically, the streamflow would have its highest conductivity under the driest condition due to the lowest appearance of solvent, and vice versa. A more reliable identification of BF can be achieved by measuring precipitation samples and stream samples right before the rain event separately for every single storm event. The fraction of baseflow can thus be separated from the streamflow with the equation $BF = Q \frac{Q_C - \text{RO}_C}{\text{BF}_C - \text{RO}_C}$.

It is plausible to have the streamflow conductivity at the lowest flow representing the baseflow conductivity, because it is observable that little or no surface runoff is happening during driest season. Nevertheless, while Stewart et al., (2007) test the assumption of SpC mass-balance method, they find it is impossible to have no baseflow even at the most extreme high flows, which means the event flow conductivity will usually be selected higher than its actual value, and thus the baseflow contribution may be underestimated during short-term calibration.

The dynamics of Cl⁻ transport via event water can also be visualized via the monitoring of lag time and first flush events (Robinson and Hasenmueller, 2017). Lag time represents the delay in time between maximum rain fall and the peak discharge of a stream, and the first flush is known as the peak concentration of contaminants in storm water runoff occurring during the initial stage of a rainfall event (Stephenson et al., 2020; Su, 2007). As Su (2007) notes, first flush event usually contains a large percent of total pollution in a relatively small percentage of runoff volume, and thus is essential in storm water management.

The first flush event is characterized and quantified with mass first flush ratios (MFF) by Stenstrom and Kayhanian (2005) with the equation:

$$MFF_n \text{ (mass first flush ratio)} = \frac{\frac{\int_0^t M_{(t)} dt}{M}}{\frac{\int_0^t V_{(t)} dt}{V}}$$

$M_{(t)}$ and $V_{(t)}$ are the contaminant mass and the runoff volume as the function of time. M and V represent the normalized total mass of contaminant and total volume of runoff. Stenstrom and Kayhanian (2005) state that MFF is dimensionless, always starting at 0 and ending at 1, representing the start and the end of a storm. For each analysis, calculated MFF are plotted on the graph of %mass vs. %volume, together with a standardized MFF line of 1:1. The generated curve above the standardized line (namely, the curve with slope greater than 1) represents that the mass of contaminant is discharged at a faster rate initially and at low water volume, and thus indicates that first flush event exists. Below the 1:1 standardized line, the curve indicates the presence of pollutant delay, and thus the existence sub-catchment in the runoff area (Shamseldin et al., 2011) (Figure1.3).

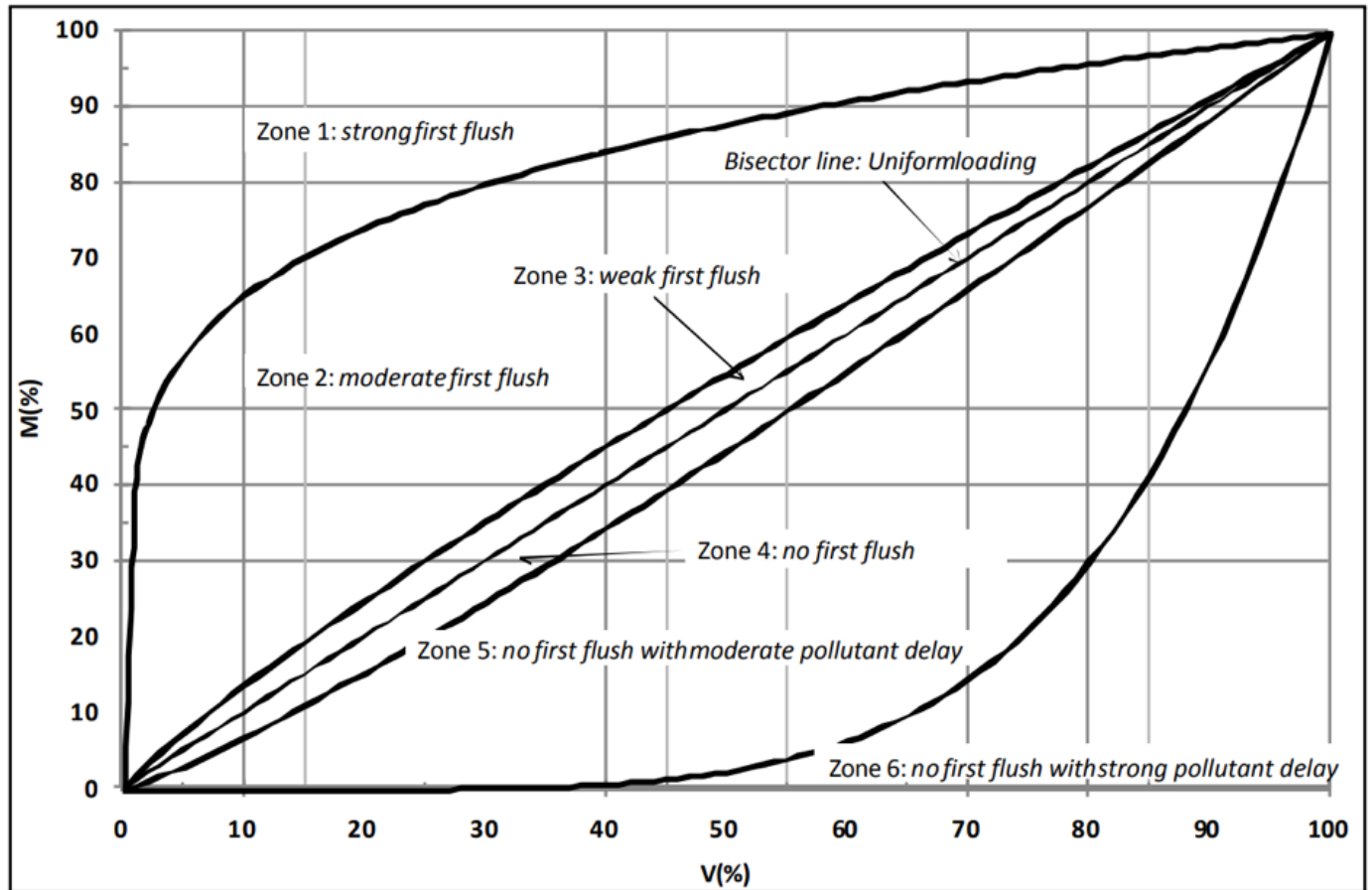


Figure 1.3. Classification of first flush curves (Shamseldin et al., 2011).

While zone 1, 2, 3 and zone 4, 5, 6 in Figure 1.3 describe the signals of the strengths of first flush event and pollutant delay event, respectively, in real cases, the first flush curve is not always maintaining its position above or below the standardized line. Among 62 first flush curves presented in Robinson and Hasenmueller (2017) study, significant amount of them appear to be above the standardized line at the beginning, but drop to be below the line as the %volume increases. This phenomenon is interpreted as the source depletion and contaminant dilution during flood response (Robinson and Hasenmueller, 2017; Shamseldin et al., 2011).

1.5 Hart Brook Background

1.5.1 Historical Data

The Hart Brook watershed is in the Lewiston, Maine. It is classified as Class B water by Maine Department of Environmental Protection (MDEP). According to Maine Revised Statutes (M.R.S.A. §465-B), Class B water must meet the water quality standards for DO (>85% of

saturation) and minimal E.coli (8 CFU per 100 mL in any 90-day interval or 54 CFU per 100mL in more than 10% of the samples in any 90-day interval) so that it is suitable for designated use of recreation and industrial processes and may not cause adverse impacts to estuarine and marine life. The watershed was found to be impaired due to the DO holding capacity of 75% saturation in 1998, 2003, and 2008 (TMDL summary, 2012).

Low DO is still a problem in certain areas of the watershed, particularly where the stream is channelized. The city of Lewiston currently has a grant to develop Best Management Practices (BMPs) to increase DO in the watershed. They are in the process of designing and building underground storage tanks and shading trees in Industrial Park to cool the water in key areas of the watershed so that it can hold more DO before releasing it back into the stream (Stormwater Management Plan, 2021; John D. Kuchinski).

Additional water quality impairments exist (conductivity/ Cl^- and unnaturally behaved stream channel) and are attributed to increasing ISC and non-pointing sources of pollution, such as urban stormwater runoff (Hart Brook Watershed Management Plan 2019). In 2007, a watershed management plan (WMP) divided the watershed into 6 subareas and aimed to address polluted salty stormwater via identification of sources of contamination, volunteer river monitoring program (VRMP), shade trees planting, roadway enhancements, and sanitary sewer assessments. (Woodard and Curran, 2007). Conductivity was included as a part of the water quality parameters in the monitoring starting from 2011 and was recorded since VRMP 2013 data report. Ten sites being assigned by the City of Lewiston and MDEP, which will be discussed in later section, were observed for almost a decade with the help of VRMP and CES Inc, and will be continuously monitored in next decade as stated by the Watershed Action Plan 2019 to 2029 (Figure 1.4).

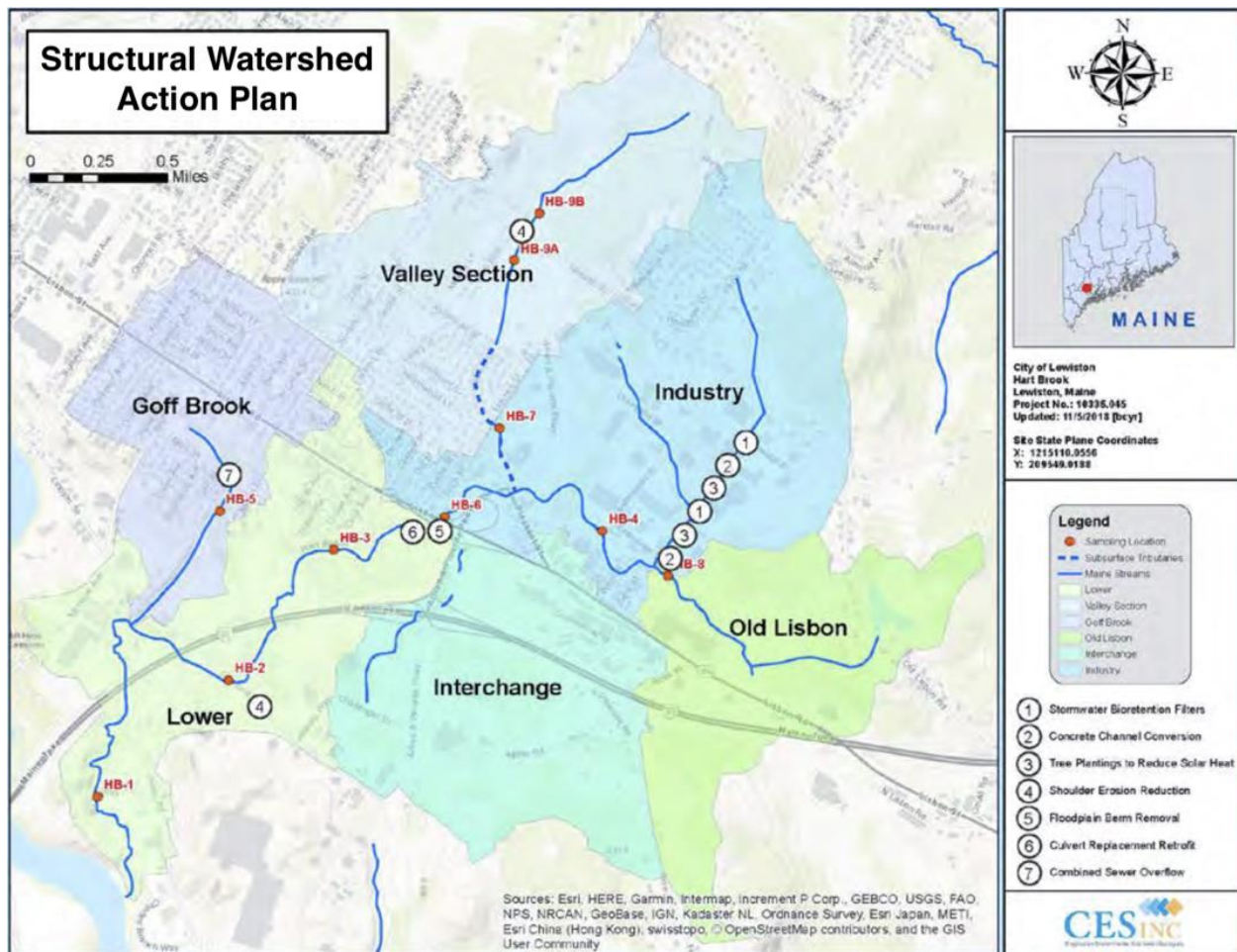


Figure 1.4. Ten sites being assigned for the watershed management plan (labeled 1-10) (Hart Brook Watershed Management Plan 2019).

Hart Brook watershed is about 2,100 acres, located entirely in the City of Lewiston, and flows into the Androscoggin River. The watershed contains 22% ISC and is divided into 6 subareas based on land use and land characteristics: Valley Section (396 acres), Industry (487 acres), Goff Brook (229 acres), Lower (376 acres), Interchange (342 acres), and Old Lisbon (279 acres) (Figure 1.4) (MDEP, 2007). There has been no significant change in land use from 2008 to 2018 (Slattery, 2018). Hydrologic Soil Groups (HSG) is the initial screening tool to identify the infiltration capacity and runoff potential of each sub-watershed, ranging from A, high infiltration rate and low runoff potential with >90% sand and <10% clay, to D, low infiltration rate and high runoff potential with <50% sand and >40% clay (Figure 1.5). No specific values are found for the city of Lewiston, but 50% of the precipitation is assumed to directly run off as the streamflow and 10-20% of precipitation is thought to infiltrate and recharge groundwaters in Maine

(Caswell, 1987).

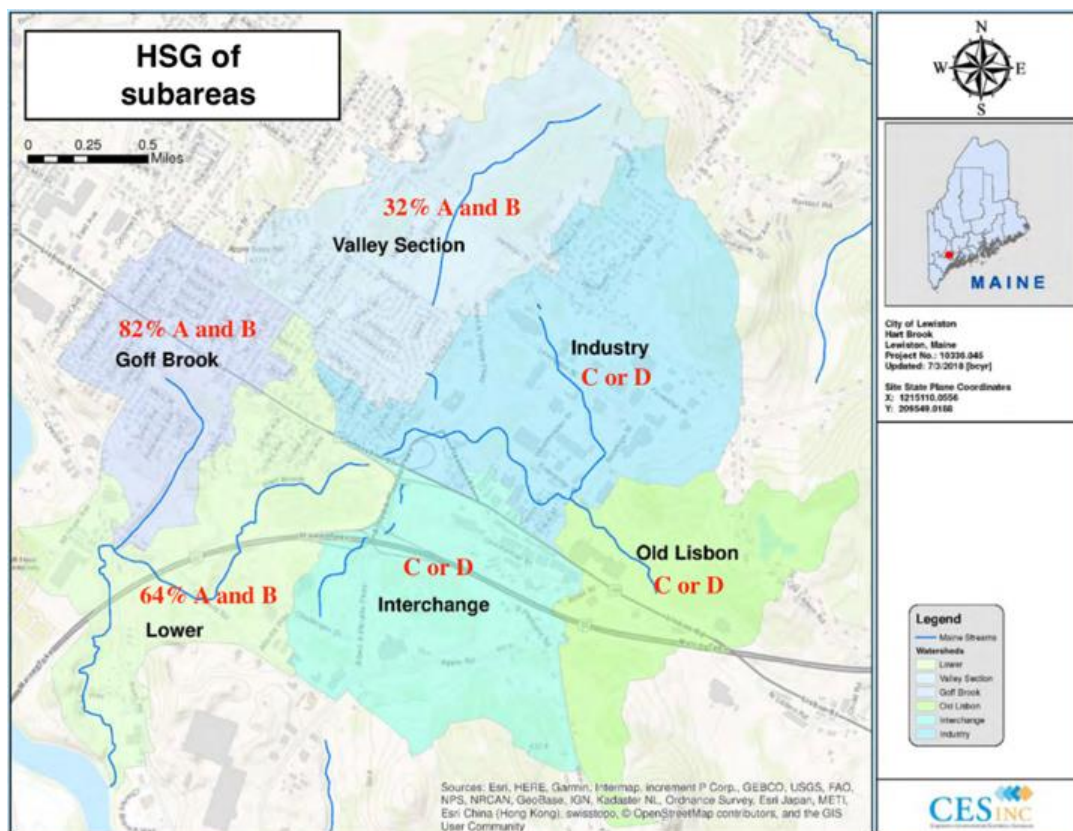


Figure 1.5. HSG of the divided six subareas in Hart Brook watershed (Hart Brook Watershed Management Plan 2019).

Ten sites are typically monitored in the Hart Brook, a stream with the main branch length of 3.8 miles. While the stream has only one entry into the Androscoggin River, two major stems converged before the entry; one of the stems derived in Goff Brook section, and the other stem derived in Industry section and Old Lisbon. Among the monitored ten sites, HB1 is located downstream of the confluence of the main stem of Hart Brook and Goff Brook. HB5 is located onstem of Goff Brook and is located in a residential area. HB8, 4, 6, 3, and 2 are located at the other main stem of the Hart Brook, and HB9 (AB) and HB7 are located at the joining tributary of this stem.

The water quality data exist at various points from 2011 till 2020; the complete dataset can be found in the Hart Brook Management Plan 2019 as well as Annual Hart Brook Monitoring Report 2020. In general, the SpC value and the Cl⁻ concentrations of these sites range from 36-

3699 $\mu\text{S}/\text{cm}$ and 9.5-330 mg/L , respectively (Hart Brook Watershed Management Plan 2019). Both values are positively correlated and appear to be the highest during summer and fall (June to October) for all of the sites. In addition, all of the sites, except for HB5 and HB7, usually have their SpC or Cl^- concentration surpassed the chronic criteria of 1000 $\mu\text{S}/\text{cm}$ or 230 mg/L at least once in a year; even these two cleanest sites have the average SpC values far exceeding that being monitored from lower Androscoggin river ($\sim 30 \mu\text{S}/\text{cm}$).

No annual trend is observed for DO concentrations on any sites, but the concentration tend to decrease as the temperature drops (from summer to fall), and it is not rare for DO saturation in this watershed to be less than 75% standard during the hottest and driest months in areas of the watershed that are channelized (Figure 1.6).

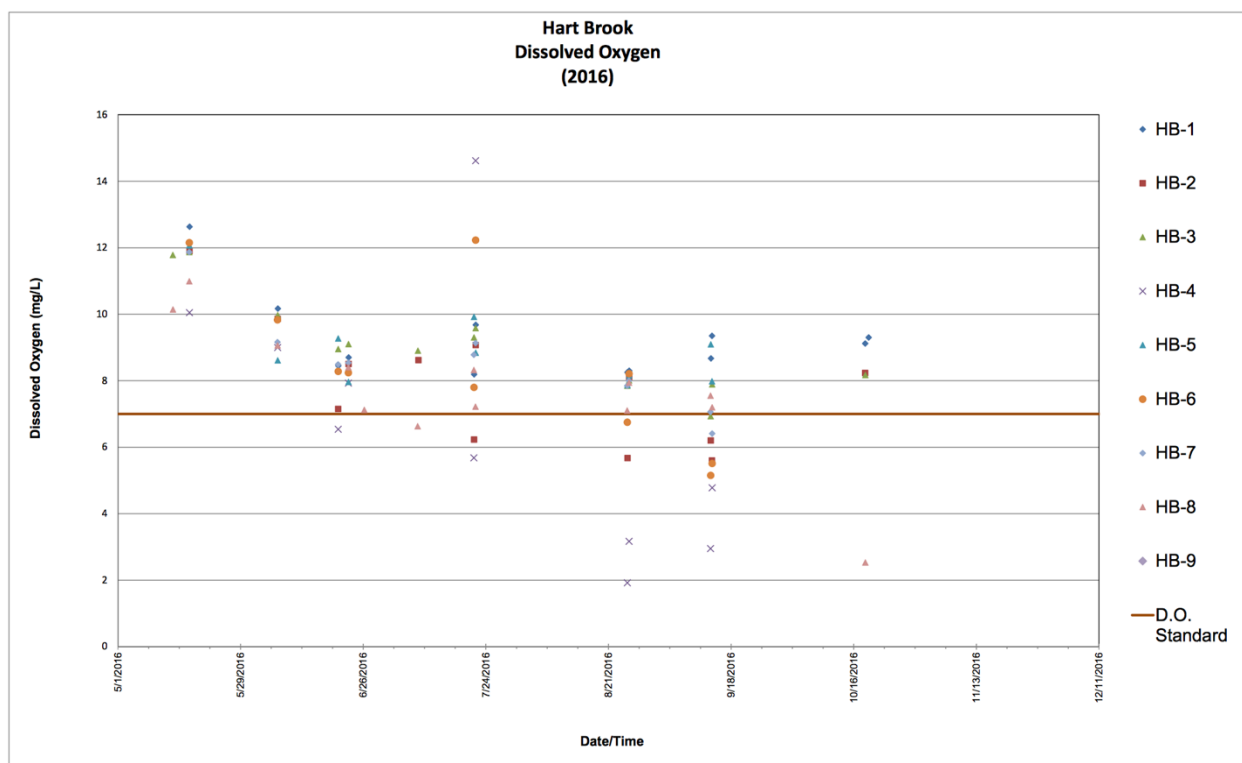


Figure 1.6. 2016 DO concentration in the Hart Brook (Hart Brook Watershed Management Plan 2019).

1.5.2 Depletion of the Data

It should be noted that, throughout the historical data of the Hart Brook watershed, great scarcity appears in the water quality data during winter and early spring (December – March), so that no strong evidence exists to correlate the road salt application with the increasing Cl^- in this

watershed.

Moreover, in the year of 2017, increasing SpC was observed from summer to fall, which seems conflicted with the fact that the discharge increases from summer to fall while no more Cl^- is manually input into the stream; however, no specific investigations were performed on the SpC and Cl^- concentration in this watershed.

1.5.3 Bedrock and Surficial Geology of the Hart Brook

Lewiston, as well as Hart Brook, is located on Paleozoic metamorphic and igneous bedrock (Figure 1.7), including the Patch Mountain Formation (Patch Mountain Limestone Member; shown in green, Sspm), and the Sangerville Formation (shown in yellow, SS), formed during early Silurian. The rocks are a mix of impure marbles, calc-silicate rocks, and pelitic schists, rich in potassium, magnesium, iron, and aluminum. These cations can easily bind with Cl^- and CO_3^{2-} . Similarly, the underlying Waterville Formation (shown in lighter yellow, Sw) and Vassalboro Formation (shown in light brown, SOv), formed during Silurian and Silurian-Ordovician, are biotite-sillimanite-muscovite-garnet schist and quartz-plagioclase-biotite and calc-silicate granofels, respectively. Granite (blue) appears in the watershed as well.

The abundant base cations (Na^+ , K^+ , Ca^{2+} , and Mg^{2+}) in the bedrock, hence, make the introducing of SO_4^{2-} and HCO_3^- to the stream through the chemical-weathering processes possible (Wilson and Grosell, 2003). However, silicate rocks weather very slowly and it is unlikely that the chemical weathering of these bedrocks will serve as the major contributor of ions in the watershed. This is evident by the low anion concentrations in the Androscoggin River, which drains similar rock types and should provide baseline concentrations of these contaminants.

The surficial geology of the watershed is mostly the deglacial marine silt and clay of the Presumpscot Formation, and marine nearshore deposits, glaciomarine ice-contact delta deposits, and minor esker deposits as well as Holocene stream alluvium are composed of sands, silts, and gravels (Figure 1.9; Lewiston Quadrangle, Maine).

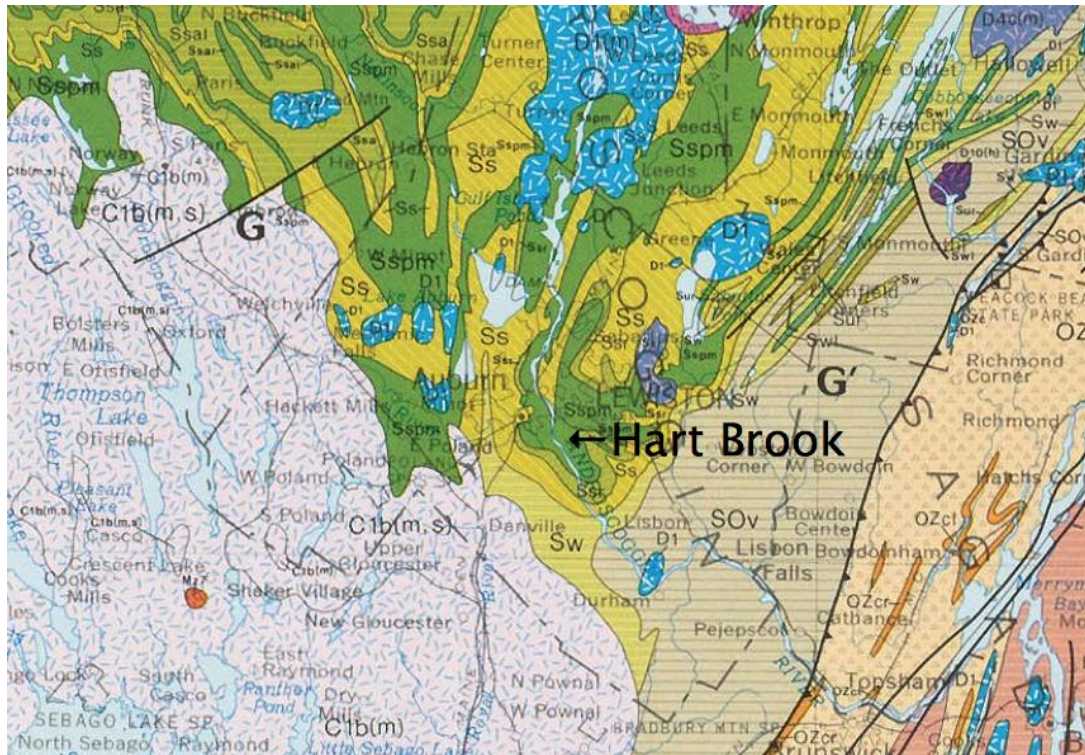


Figure 1.7. Overview of the bedrock geology of the Hart Brook (Bedrock Geology Map of Maine).

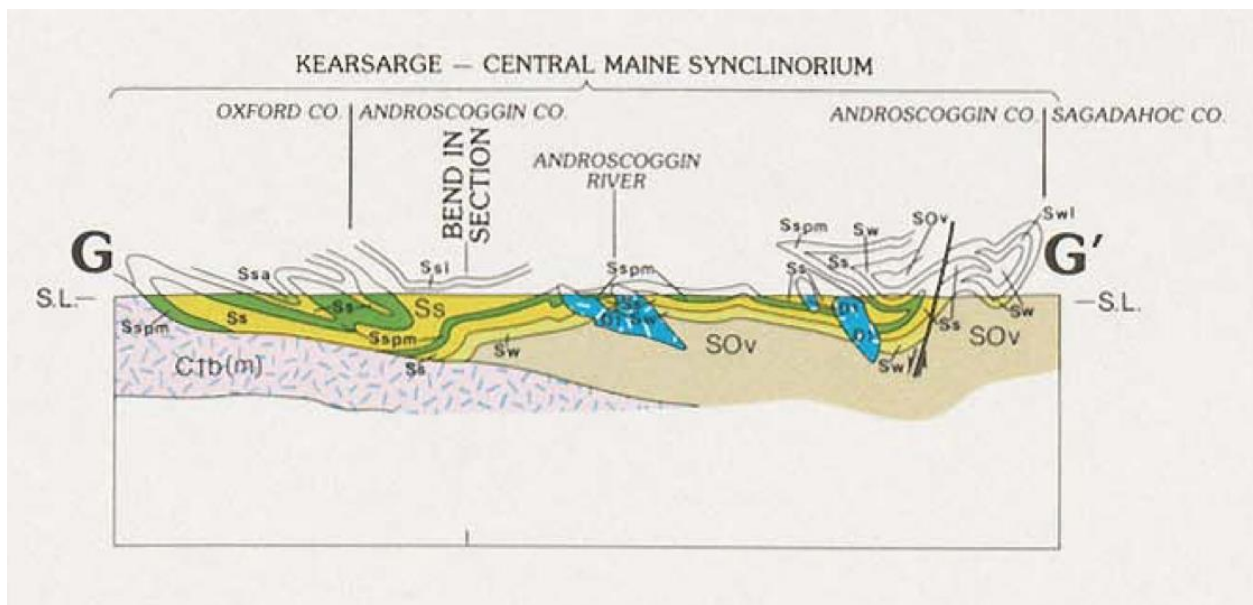


Figure 1.8. Cross-section of the bedrock geology of the Hart Brook (Bedrock Geology Map of Maine).

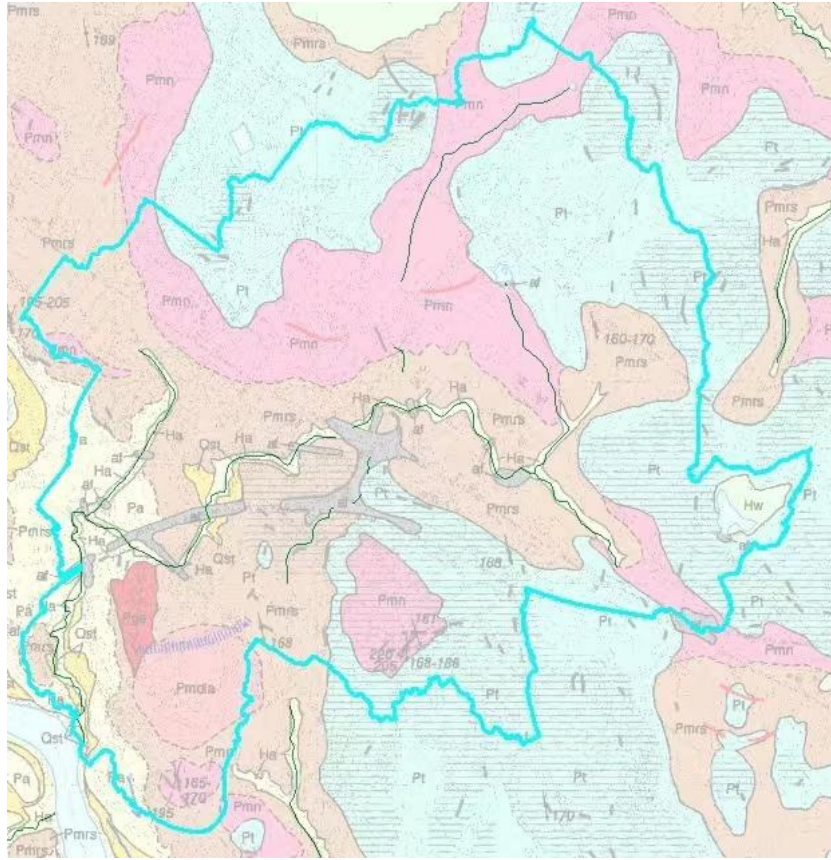


Figure 1.9. Surficial geology of Hart Brook (Surficial Geology of the Lewiston Quadrangle, Maine).

1.6 Purpose of the Study

Road salt is a relatively recent environmental concern in water management. In the Hart Brook, although the monitoring processes has been conducted for a decade, little is known about NaCl contamination in winter through spring. In addition, the road salt retention in the groundwater has not been specifically discussed, despite both annual report and revised management plan mention that the road salt may be entering the Hart Brook during the summer months from groundwater discharge. Although both topics have been studied in respect to other streams, it is important to focus on the case study of Hart Brook regarding to its own land use and land characteristics. Therefore, this study aims to 1) complete a full year monitoring on the water quality parameters, especially on SpC value and Cl^- concentration, of Hart Brook, in order to analyze the seasonal trend of road salt in the watershed and 2) calculate the annual road salt export from the watershed and identify the salt retention by comparing the measurements with theoretical input amounts, and 3) identify potential non-point sources of road salt pollution in the watershed. This study can be used to inform strategies for reducing road salt application in the water shed and for making improvements to storm water management in the Hart Brook Watershed.

2. Method

2.1 Overview

Water quality and stream discharge was monitored at various sites over the course of a year to better understand road salt contamination and transport in the Hart Brook watershed. SpC, DO, pH, temperature, and discharge of the sites were measured in a biweekly/monthly basis while water samples were simultaneously collected and analyzed for the major ion concentrations (Na^+ , K^+ , Ca^{2+} , Mg^{2+} , Cl^- , HCO_3^- , SO_4^{2-}). Datasondes (logger/sensor) were deployed in the downstream area of the watershed to measure SpC and water depth every 15 minutes. A relationship between SpC and Cl^- concentration and a Rating Curve addressing the relationship between the discharge and water level were established to convert the logger recordings into Cl^- concentration and discharge. Additionally, ArcGIS was used to determine the infiltration rate of the watershed based on the surface geology, and to estimate the amount of road salt being applied in the watershed through the calculation of lane lengths. The total flux Cl^- through the watershed, which is also considered as the annual exported amounts, was calculated from the field measurements and was compared to the estimated theoretical road salt input, in an attempt to better understand retention times of Cl^- in the groundwater.

This chapter will start with the introductions of the in-field techniques and the criteria to examine the stream flow properties and collect water samples, followed by the illustration of lab work and the elaborations of the constructions of the rating curve and the mathematical model of SpC vs. Cl^- concentration. At last, the chapter will explain the methods to identify road salt retentions and analyze watershed properties including infiltration rate and lane lengths.

2.2 Study sites

Six sites were studied within the HB watershed; 3 from the sub-watershed labeled Industry (CC1, CC2, HB4), 1 from the Goff Brook (HB 5), and 2 from Lower watershed (HB3 and BC 6) (Figure 2.1; Table 2.1). The Androscoggin was sampled just upstream of the Hart Brook outlet for baseline ion concentrations resulting from chemical weathering in the region. The longitude and latitudes of the sites can be found in Table 2.1.

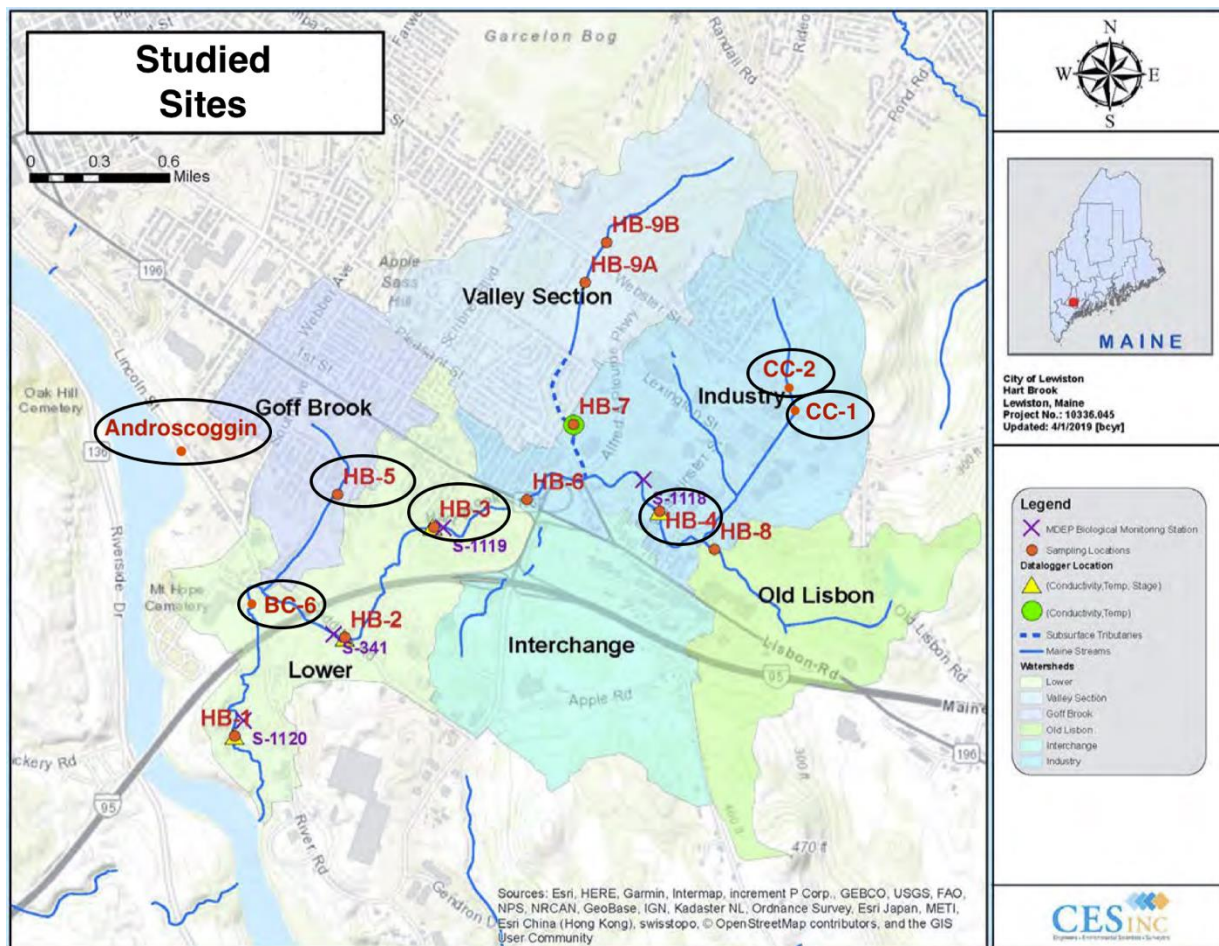


Figure 2.1. Locations of the study sites.

Sites	Longitude	Latitude
CC2	-70.167256	44.080624
CC1	-70.167544	44.078945
HB4	-70.17535134	44.07539636
HB3	-70.18875848	44.0746385
BC6	-70.2008036	44.07077299
HB5	-70.19558044	44.07603512
Androscoggin	-70.204610	44.077725

Table 2.1. Longitude and latitude of the sites.

HB4 is in Industry area, locating at the downstream of a compacted industrial zone, and it is one of the most contaminated sites with respect to SpC (238-1200 $\mu\text{S}/\text{cm}$; Hart Brook Watershed Management Plan 2019) and Cl^- concentrations. A logger was deployed in the site from 3/29/2021 to 6/28/2021. In order to better understand the source of contamination in this area, two new sampling sites were established upstream of HB4 (CC2 and CC1). CC1 was found within the industrial zone, and CC2 was found at the upstream of the industrial zone. Notably, a draining pipe was observed along the channel in CC1, and the water was sampled after the confluence. HB3 was locating at the downstream site of HB4, with the historical records of SpC reaching as high as 1233 $\mu\text{S}/\text{cm}$, thus was continue analyzed to identify the potential impacts of the contaminations in HB4.

HB5, in the Goff Brook area, is usually the cleanest site in this watershed, with the SpC recordings 191-830 $\mu\text{S}/\text{cm}$, and was monitored as it represents the water quality in a residential area.

In addition, BC6, as the confluence of the major stems before the entrance of the Androscoggin River, was especially focused on to represent the general water quality of the watershed. Dataloggers monitoring SpC and water depth were deployed over the following dates (3/29/2021-6/28/2021; 7/8/2021-7/12/2021; 9/2/2021-12/9/2021; 12/17/2021-2/17/2022).

2.3 Field Methods

Field work schedule can be found in Appendix 1.

A multimeter Hydrolab instrument was used for in situ measurements of temperature, pH, SpC, and DO. The pH, SpC, and DO sensors were calibrated before use with 4.0 and 7.0 pH solutions, 1.413 mS/cm solution, and instantaneous atmospheric pressure, respectively.

The estimation of stream discharge was conducted with USGS Stream gaging method (Figure 2.2). In short, the stream channel of each site was divided into rectangular subsections (shown in dash lines; usually 0.3 to 1.5 m in this study, shown as b_1, b_2, \dots, b_n in the sketch). The height (d_1, d_2, \dots, d_n) of the water surface and the flow speed (v_1, v_2, \dots, v_n) were measured at the middle of each subsection with a measuring tape and a **flow meter**. In some cases, when the flow meter was unavailable or inapplicable due to the shallow water depth, the flow speed was measured by timing the speed of visible bubbles/sticks over a fixed distance.

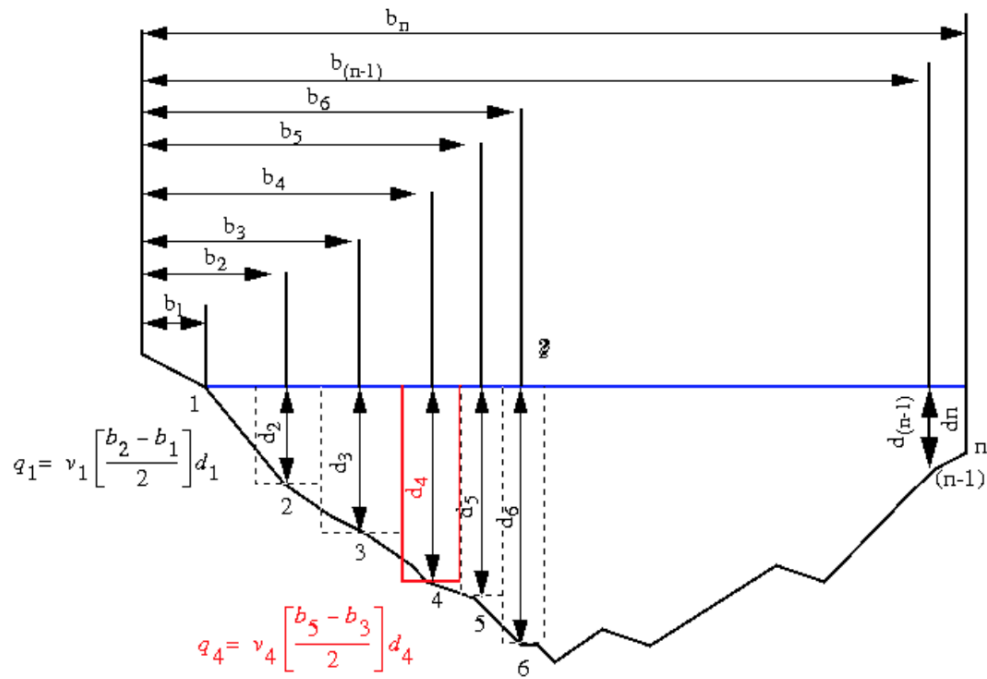


Figure 2.2. Sketch of stream gaging method (USGS Water Science School, 2018).

Regarding the bowl shape of the channel bed, this measurement was based on the assumption that the area being over-estimated at the two sides of the channel was equal to the area being under-estimated at the bottom of the channel. Summary calculation:

$$Discharge = v_1 \cdot d_1 \cdot \frac{(b_2 - b_1)}{2} + \sum_{i=2} v_i \cdot d_i \cdot \frac{(b_{i+1} - b_{i-1})}{2}$$

Water samples were collected in clean 1 L bottles that were rinsed three times with water upstream of each site, and were stored at 4 °C until analysis.

Loggers were deployed in HB4 and BC6. In order to eliminate the external effects in BC6, a semi-wrapped cylinder protector was designed according to *Applied Hydrogeology* (Fetter, 2018), in order to stabilize the logger and prevent it from being buried by fast moving sediments during storm events and to facilitate the measurements of actual water depth (Figure 2.3). Barro-loggers were deployed instantaneously near a window of the lab room (25 °C) to record atmosphere pressure in the areas.



Figure 2.3. Deployed logger at BC6.

2.4 Lab Methods

2.4.1 Titration for HCO_3^-

Water samples were titrated within 48 hours of collection using 0.1M hydrochloric acid (HCl) as the titrant and 0.5% methyl orange as the color indicator. The titrant was diluted from the stock solution of 12.1 M HCl with the equation: $C_1V_1 = C_2V_2$. A 100mg/L HCO_3^- solution was generated from the appropriate mass of pre-dried sodium bicarbonate (NaHCO_3), which was titrated and used as a secondary standard for determining the precise concentration of the titrant before titrating unknown samples.

Volumetric pipettes were used to transfer 50mL of standard solution and 50 mL of each *filtered* water sample to 150mL erlenmeyer flasks. Each sample was analyzed in triplicate and HCO_3^- concentrations were determined using the following equation:

The actual concentration of the titrant was calculated with the equation:

$$C_{(\text{HCl titrant})} = \frac{V_{\text{standard solution}} \cdot C_{(\text{standard solution})}}{M_{(\text{HCO}_3^- \text{ secondary std})} \cdot V_{\text{HCl titrated}}}$$

The concentration of the HCO_3^- in the sample water was then calculated with the equation:

$$C_{(\text{HCO}_3^-)} = \frac{V_{\text{HCl titrated}} \cdot C_{(\text{HCl titrant})} \cdot M_{(\text{HCO}_3^- \text{ secondary std})}}{V_{\text{sample}}}$$

Sample Calculation:

HCO_3^- has the molar mass of 61.0168 g/mol. For HCO_3^- titration of 08/18/2021 samples, the average titrating volume of HCl to the standard NaHCO_3 solution was 7.33mL. Therefore:

$$C_{(\text{titrant})} = \frac{50\text{mL} \times 100\text{mg/L}}{61.0168\text{g/mol} \times 7.33\text{mL}} = \frac{50\text{mL} \times \frac{1\text{L}}{1000\text{mL}} \times 100\text{mg/L} \times \frac{1\text{g}}{1000\text{mg}}}{61.0168\text{g/mol} \times 7.33\text{mL} \times \frac{1\text{L}}{1000\text{mL}}}$$
$$\approx 0.011\text{mol/L}$$

The average titrating volume of HCl to the sample collected from HB4 was 14.70mL, hence:

$$C_{(\text{HCO}_3^-)} = \frac{14.70\text{mL} \times \frac{1\text{L}}{1000\text{mL}} \times 0.011\text{mol/L} \times 61.0168\text{g/mol} \times \frac{1000\text{mg}}{1\text{g}}}{50\text{mL} \times \frac{1\text{L}}{1000\text{mL}}}$$
$$\approx 197.33\text{mg/L}$$

2.4.2 Titration for Cl^-

Samples were analyzed for Cl^- using the Mohr titration. In this titration, 30 mM silver nitrate ($AgNO_3$) solution was used as titrant, and 0.25M potassium chromate (K_2CrO_4) was used as the color indicator. A 100mg/L NaCl solution was used as a secondary standard to determine the precise concentration of the titrant. A volumetric pipet was used to transfer 100mL of each *filtered* sample water was transferred to 250mL erlenmeyer and samples were run in triplicate. Cl^- concentrations were determined using the overall equation below:

The actual concentration of the titrant was calculated with the equation:

$$C_{(AgNO_3 \text{ titrant})} = \frac{V_{\text{standard solution}} \cdot C_{(\text{standard solution})}}{M_{(Cl^- \text{ secondary std})} \cdot V_{AgNO_3 \text{ titrated}}}$$

The concentration of the HCO_3^- in the sample water was then calculated with the equation:

$$C_{(Cl^-)} = \frac{V_{AgNO_3 \text{ titrated}} \cdot C_{(AgNO_3 \text{ titrant})} \cdot M_{(Cl^- \text{ secondary std})}}{V_{\text{sample}}}$$

Sample Calculation:

Cl^- has the molar mass of 35.45 g/mol. For Cl^- titration of 8/18/2021 samples, the average titrating volume of $AgNO_3$ to the standard NaCl solution was 9.9mL. Therefore:

$$C_{(\text{titrant})} = \frac{100\text{mL} \times 100\text{mg/L}}{35.45\text{g/mol} \times 9.90\text{mL}} = \frac{100\text{mL} \times \frac{1\text{L}}{1000\text{mL}} \times 100\text{mg/L} \times \frac{1\text{g}}{1000\text{mg}}}{35.45\text{g/mol} \times 9.90\text{mL} \times \frac{1\text{L}}{1000\text{mL}}}$$

$$\approx 28.49\text{mmol/L}$$

The average titrating volume of $AgNO_3$ to the sample collected from HB4 was 22.77mL, hence:

$$C_{(Cl^-)} = \frac{22.77\text{mL} \times \frac{1\text{L}}{1000\text{mL}} \times 0.028\text{mol/L} \times 35.45\text{g/mol} \times \frac{1000\text{mg}}{1\text{g}}}{100\text{mL} \times \frac{1\text{L}}{1000\text{mL}}} \approx 225.98\text{mg/L}$$

2.4.3 Sulfate (SO_4^{2-}) Concentration

The SO_4^{2-} contents in the sample water was examined with DR-2000 direct-reading spectrophotometer from *HACH* company. 50mg/L SO_4^{2-} solution made from sodium sulfate (Na_2SO_4) was applied as the standard solution to ensure the operation of the spectrophotometer. During the process, 25mL standard solution and *non-filtered* water samples were transferred to 25mL sample cells in a set of three, and they were separately measured at 450nm wavelength after the addition of one package of SulfaVer 4 Sulfate Reagent Powder Pillow.

The spectrophotometer determines the concentration of target contaminants via the absorbance and transmittance. For this measurement, specifically, barium sulfate (BaSO_4) in the packets dissolves and barium chloride (BaCl_2) forms as a white precipitate. Light transmission through the sample decreases as BaCl_2 content increases. The spectrometer thus extrapolates the concentration of SO_4^{2-} through the level of cloudiness.

2.4.4 Major Cations

Concentrations of major cations, including Na^+ , potassium(K^+), calcium (Ca^{2+}), magnesium (Mg^{2+}) were measured with Inductively Coupled Plasma Optical Emission Spectrometer (ICP-OES). Other cations, including lead ion (Pb^{2+}), iron ion ($\text{Fe}^{2+/3+}$), and arsenic ion (As^{3+}), were also measured but not presented in this thesis.

Special multi-element standard solution with 2% nitric acid (HNO_3) was diluted from the stock of 70%, and was further diluted to 0.01ppm, 0.1ppm, 1ppm, 10ppm, and 100ppm for the calibration curve, which relates concentration to detector response. A new calibration curve was generated for each ICP run. For calibration curve with the R^2 value lower than 0.99990, standards solutions were remade and/or reran. ~10mL *filtered* water samples were transferred to 10mL disposable sample cells and acidified with one drop of concentrated HNO_3 , and analyzed on the ICP. The results with the most significant wavelengths were selected. The significance of measurements was determined via the existence of well-integrated peaks with minimal interference from other peaks. For this machine, readings for Na5895, K7664, Ca4226, Mg2795, Pb2203, Fe2599, and As1890 were recorded. The numbers following the element symbols refers to the wavelengths analyzed (in angstrom, 10^{-10} m). For Na, for example, the wavelength being measured was 589.5 nm.

Units of ppm were converted into mmol/L and milliequivalent per liter (meq/L) by multiplying the concentration in mmol/L with the number of charges present for each specific ion. The unit of meq/L describes the amounts of substances that will react with a certain number of hydrogen ions; therefore, the conversion was performed for later major ion examination. Summary conversion calculation:

$$C_{meqv/L} = \frac{C_{ppm}}{M_{ion}} \times |\delta^{+/-}|$$

2.4.5 Alternative Ion Chromatography Instrument (IC)

In order to eliminate the lab time with a large number of samples, SO_4^{2-} and Cl^- concentrations within the samples being collected after 10/08/2021 were determined via IC. Standard solutions for these two contaminants were prepared for calibration curve prior to the measurements. The concentration range of the standards were referred to the previous titrated data of the sites. For SO_4^{2-} , 6 standard solutions with the concentration of 0.1ppm, 1ppm, 5ppm, 10ppm, 25ppm, and 50ppm were made; similarly, 6 standard solutions with the concentration of 10ppm, 50ppm, 100ppm, 150ppm, 200ppm, and 250ppm were made for Cl^- measurements.

2.5 Data Analysis

2.5.1 Major ion examination

Given the concentrations of major ions in the water samples, analysis was performed on these concentrations to examine the relative abundancy of each ion/contaminant, in the aim of identifying the water type.

In order to check the validity and the quality of the lab measurements, sums of the concentrations (in meqv/L) of major cations and anions were calculated separately and were calculated for charge-balance error (CBE) with the equation: $\frac{\sum C_{(cations)} - \sum C_{(anions)}}{\sum C_{(cations)} + \sum C_{(anions)}}$ (Fetter, 2018). The value of CBE could be both positive and negative, depending on the relative abundancy of cations and anions. Usually, an acceptable water analysis was indicated by the CBE with the absolute value below 5%.

Further, the percentage of each ion in each sample water was calculated with the equation: $\frac{C_{(ion)}}{\sum C_{(cations/anions)}}$, and the percentages were then applied in piper plot plotting with GW-Chart program provided by USGS, in order to visualize the variations in each water quality parameter in each site (USGS, 2020).

Additionally, Na^+ concentration was plotted against Cl^- concentration in the unit of mmol/L to reflect the road salt residence in soils during transport (Snodgrass et al., 2017).

2.5.2 Logger data conversion

SpC and water depth in the site was recorded in a 15-minute interval by the deployed logger.

Corresponding water level and SpC measurements from the deployed sensors were found respectively for each biweekly field measurement of discharge and Cl^- concentration with the recorded sampling time. A rating curve was generated by plotting the discharge data against the collected water level.

A curve relating Cl^- concentration to SpC was created from the water samples collected. Best-fit lines were plotted for both graphs by comparing the R^2 value between exponential fit and linear fit, and the equations of the lines were applied to convert the water level and SpC recordings to discharge and Cl^- concentrations, respectively.

After the conversion of all recorded values, monthly averages of Cl^- concentration and discharge were determined, and monthly average Cl^- flux with the unit of milligram per second (mg/s) was calculated by multiplying the solved discharge (m^3/s) with the Cl^- concentration (mg/L).

2.5.3 Baseflow and First Flush Analyses

First flush analysis was performed during the storm from 7/8/2021 to 7/12/2021 at BC6 to visualize the chemical (Cl^-) and flooding responses. Baseflow separation was conducted to enable the analysis.

Conductivity mass-balanced approach (CMB) was decided to be the most applicable *base flow separation* method for this study. Regarding to the equation proposed by Stewart et al. (2007), the highest SpC recording during the period of the lowest recorded water level from the deployed logger was assigned as the BF_C , and the lowest SpC recording during the storm event with the highest recorded water level was assigned as the RO_C .

In order to adapt the recordings in every 15 minutes into the analysis, the “continuous” integral function proposed by Stenstrom and Kayhanian (2005) was changed to summation function, so that the generated plot was, instead of a line, a line formed with separate dots.

With the equation generated by the rating curve, the water level reading in every 15 minutes was converted into discharge (Q). The RO volume (m^3/s) was calculated by $Q \cdot (1 - \frac{Q_C - \text{RO}_C}{\text{BF}_C - \text{RO}_C})$

for every 15 minutes, and it was multiplied with the time (900s/15mins) to represent the RO volume of **1 step**, so that $V = \sum_{i=0}^i RO_i$, where $i = 1step$.

Logic flow:

$$\begin{aligned}
 & \text{Logger} \rightarrow \text{water depth } (d_1) \\
 & d_1 = 0.46 \cdot Q_1^{1.0716} \\
 & RO_1 = Q_1 \cdot \left(1 - \frac{Q_c - RO_c}{BF_c - RO_c} \right) \\
 & RO_{i=1} = RO_1 \cdot 900s \\
 & V = RO_{i=0} + RO_{i=1} + \dots
 \end{aligned}$$

The conductivity reading in every 15 minutes was converted to Cl^- concentration, and the Cl^- flux (mg/s) in RO was calculated by multiplying the Cl^- concentration with corresponding RO volume. The flux was then multiplied with the time (900s/15mins) to represent the mass of **1 step**, so that $M = \sum_{i=0}^i M_i$, where $i = 1step$.

In order to normalize the value from 0-100, the equation $\frac{100V_i}{V}$ and $\frac{100M_i}{M}$ was applied, respectively, and the calculated values were cumulatively formatted. $(\frac{100V_i'}{V} = \frac{100V_i}{V} + \frac{100V_{i-1}'}{V})$. Finally, the MFF line was graphed by plotting $\frac{100M_i'}{M}$ against $\frac{100V_i'}{V}$.

Precipitation data were acquired from the website of Weather Underground (<https://www.wunderground.com/history/daily/us/me/auburn/KLEW/date/2021-7-9>). The data were further used to interpret the peaks in the graphed water level records and to analysis of lag time and first flush dynamics in response to a rapid and intense rainfall (hereafter referred to as “flood response”, even though this was technically not a flood). The lag time was defined as the difference between the time of the peak precipitation and that of the peak discharge peak during the event.

2.6 Watershed Characterization

In the aim of identifying the Cl^- retention in the watershed, the theoretical annual Cl^- input and average Cl^- concentration of the Hart Brook stream were generated and compared with the

measured Cl^- export and annual monthly-average Cl^- concentration. The characterization of the watershed was conducted through infiltration rate characterization and lane lengths calculation with ArcMap 10.8.1.

2.6.1 Volume of Annual Precipitation in the Watershed and Total Cl^- Input

Theoretical concentrations of Cl^- in the watershed is estimated by dividing the total amount of road salt applied by the city of Lewiston by the total volume of water delivered to the watershed annually.

The total volume of water is estimated by multiplying the average annual precipitation amount (m) by the area of watershed (m^2) by the fraction of water that does not undergo evapotranspiration as follows:

$$V = \text{precipitation} * \text{watershed area} * (1 - \text{evapotranspiration rate}).$$

Two major assumptions were made during the calculation of the infiltration rate and the total delivered volume. First, the speed of infiltration was assumed to be equal to the speed of runoff, which is highly unlikely in most of the watershed. Second, the infiltration to the deeper bedrock was neglected.

The watershed area and the area of each surficial geology type within the watershed were calculated with MGS_Suficial_24K_Map_Data provided by Maine Geological Survey. The infiltration rate of each surficial geology type was obtained from the *Ground Water Handbook for the State of Maine* (Caswell, 1987). The overall infiltration rate for the entire watershed was calculated by summing up the weighted infiltration rate of each area.

The lane lengths of the city of Lewiston and the Hart Brook watershed were calculated using Maine DOT Public Road, and the annually applied amounts of road salt in Lewiston were acquired from the Department of Lewiston Public Works. The annual input of road salt in Hart Brook were thus calculated as:

$$\text{annual input} = \text{annually applied in Lewiston} \times \frac{\text{lane length}_{(HB)}}{\text{lane length}_{(Lewiston)}},$$

based on the assumption that the road salt is evenly applied in every public road. The theoretical annual average Cl^- concentration in this watershed was then acquired through dividing the Cl^- mass in the annually applied amounts of road salt by the theoretical total volume of water

delivered to the watershed every year.

2.6.2 Annual Stream Cl⁻ Flux

Measured monthly average Cl⁻ concentrations were multiplied by the average monthly discharge values and then added up for a year to determine the total annual Cl⁻ flux in the watershed.

3. Results

3.1 Characterization of the Watershed

3.1.1 Infiltration Rate

The surficial geology in this watershed was classified into 10 major types (Figure 3.1). According to Caswell, 1987, glacial sand and gravel in the state of Maine may yield as much as 50% recharge, Tills yields some water to the groundwater, and clays are poorly permeable. Therefore, dominant components of each surficial geology type are classified into “Sand, Gravel”, “Till”, “Clay-Silt”, and “Impervious surface” corresponding to the infiltration rates of 50%, 20%, 10%, and 0%, respectively (Table 3.1).

The GIS calculated the area of artificial fill of 218558 m², which is about 2.45% of the total watershed area. This calculated area may have only counted the major highways in the watershed, so that the value is significantly different from previous estimation of 22% (Slattery, 2018). In order to more accurately characterize the infiltration rate in the watershed without adding extra areas, the other impervious surface areas that should occupy 20% of the total watershed area is taken from the areas of the “marine nearshore deposits” and the “marine regressive sand deposits”, because the roads are mostly concentrated in the areas made by these two surficial geologies, according to the map of public road (Figure 3.2).

Afterall, the sand and gravel are calculated to occupy 23.1% of the total watershed; tills occupy 34.4%, and clay-silt sediments occupy 20.5%. By multiplying the infiltration rate of each sediment type with their occupied percentage, the total watershed infiltration rate is estimated to be 20.5% (Figure 3.2).

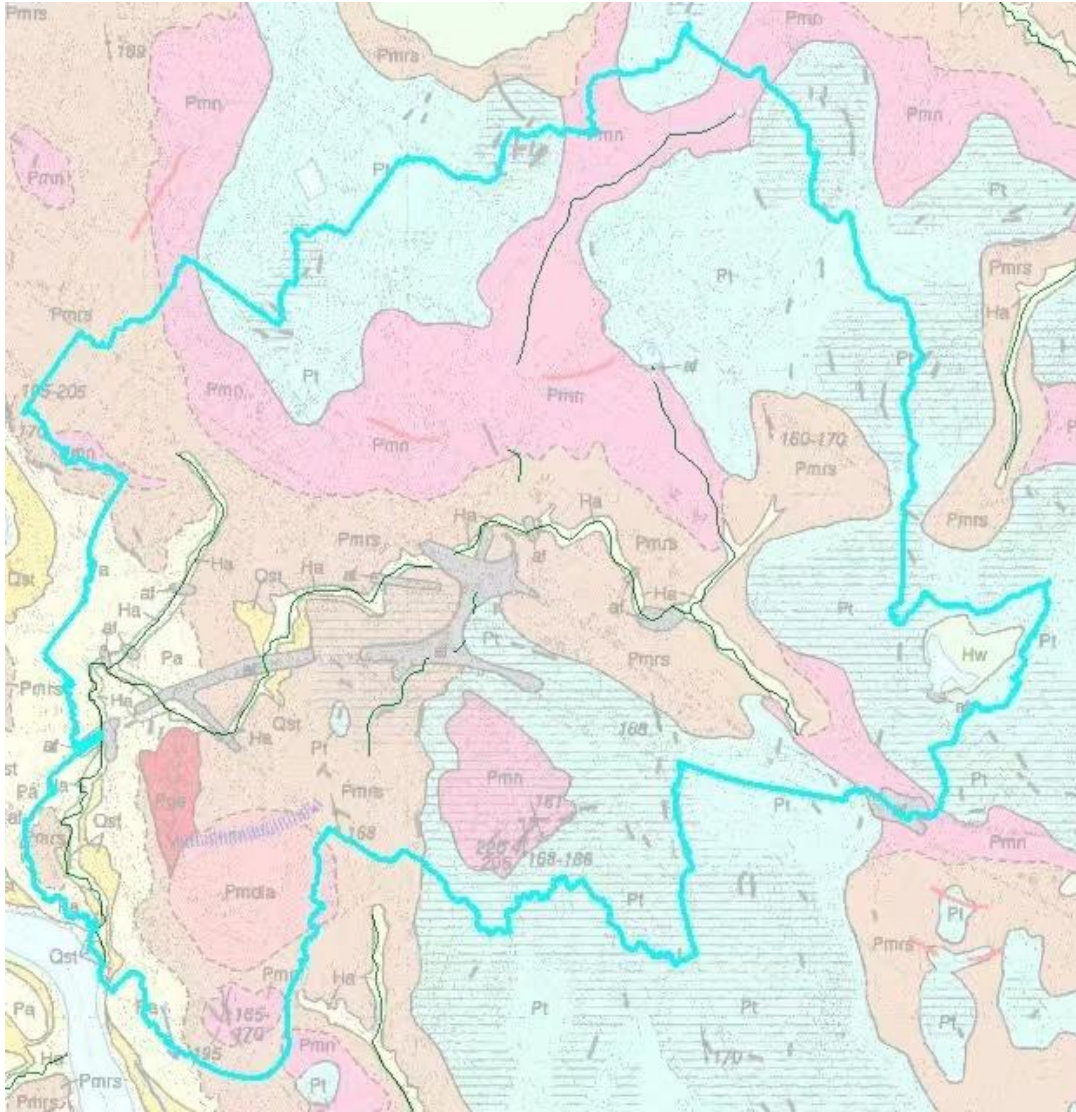


Figure 3.1. Surficial geology in the Hart Brook watershed from ArcGIS.

	Area (m ²)	% Area	Dominant Type	Infiltration rate
Stream Alluvium	252563	2.8	Sand, Gravel, Muck	50%
Braided Stream Alluvium	504286	5.7	Sand, Gravel, Muck	50%
Stream Terrace Deposits	86018	1.0	Sand, Gravel, Silt	50%
Armory Delta	269786	3.0	Sand	50%
Freshwater Wetland Deposit	56189	0.6	Sand, Muck, Peat	50%
Esker Deposits	79745	0.9	Sand, Gravel	50%
Marine Regressive Sand Deposits	2548846	28.6	Sand, Silt	50%

Till	3060529	34.4	Till	20%
Marine Nearshore Deposits	1827053	20.5	Clay-Silt	10%
Artificial Fill*	218558	2.5	Impervious Surface	0%
Total	8903573	100	N/A	20.5%*

Table 3.1. Area and infiltration rate of each type of surficial geology.

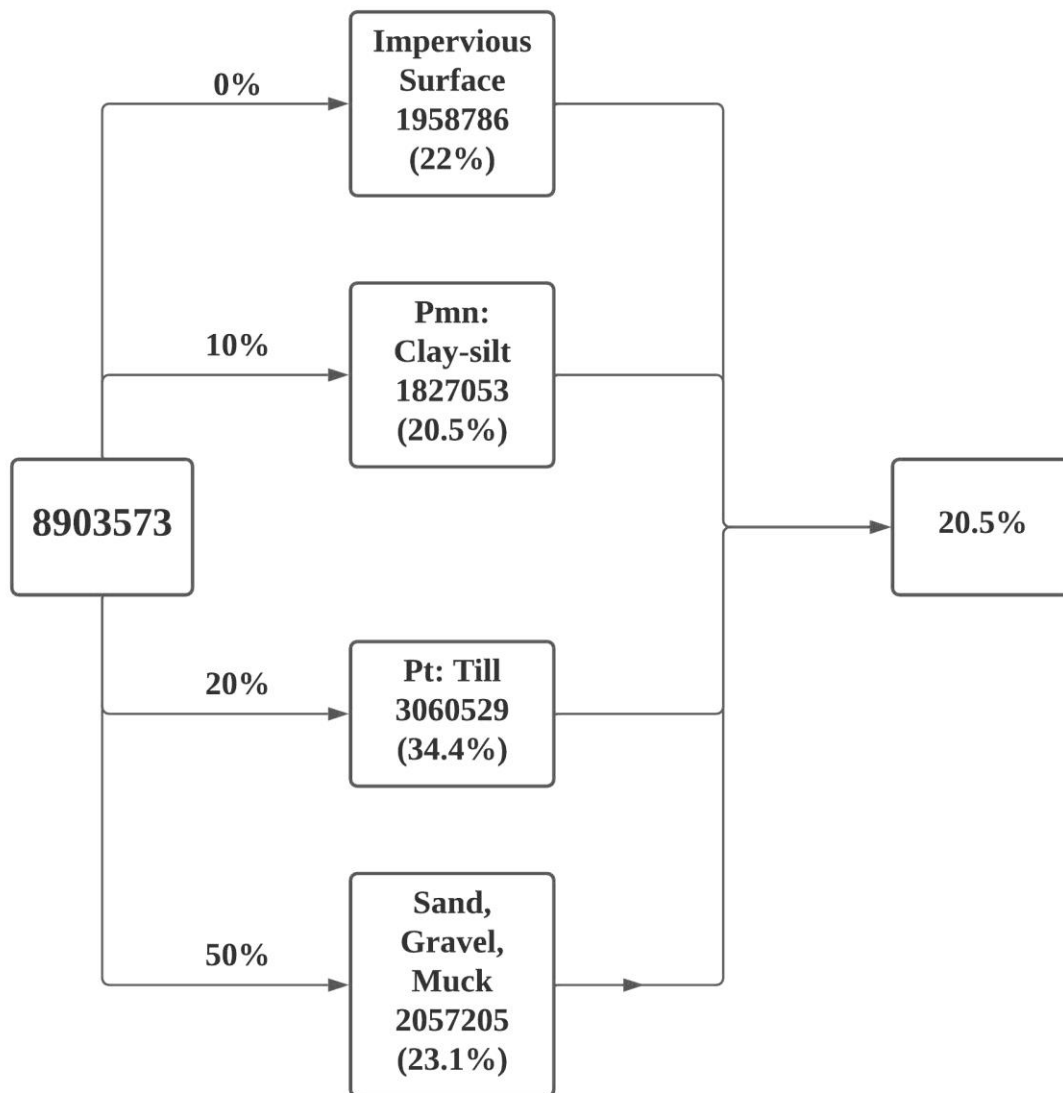


Figure 3.2. Calculation of the average infiltration rate in Hart Brook

3.1.2 lane lengths

The total lane lengths in the Hart Brook Watershed were characterized with GIS techniques (Figure 3.3). In this watershed, about 35.42 km public roads are available for road salts consumptions, which contribute 15.87% of the total lane lengths in the City of Lewiston that is about 359.66 km. The annual application amounts of road salt in Lewiston were about 4435 tons in 2020, according to Reggie Poussard, the operation manager from the Lewiston Public Work. Hence, the application amounts in the watershed were estimated to be about 704 tons through the ratio of 15.87%, which is equivalent to 19.84 tons per road mile.

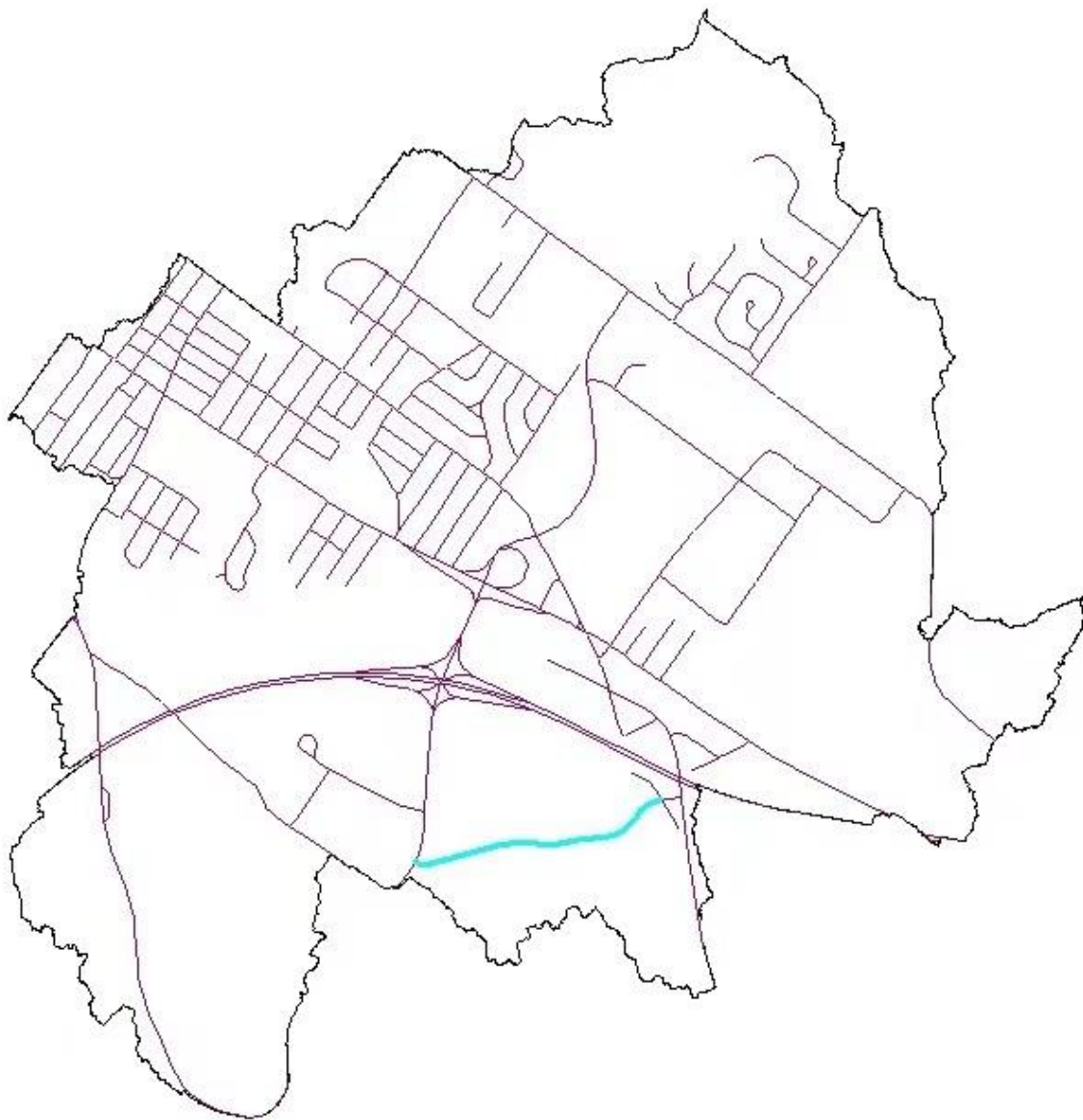


Figure 3.3. Public roads in the Hart Brook watershed from ArcGIS.

3.2 Water Level, Precipitation, and Discharge

In many cases, significant spikes in the water level data would correspond to large precipitation events (Figure 3.4-3.6 and Figure 3.7-3.8). However, occasionally the recorded precipitation events appear to occur one day after the measured increase in water level (Circled date in Figure 3.6 and 3.8). Since it is impossible to have water level increases prior to a precipitation event, and the logger's date was set correctly before use, this inconsistency may be due to the recording delay from the Weather Underground.

The data logger from HB4 shows a decreasing trend from spring (March) to summer (late June), in general. For a storm event, the site usually takes about 1-2 days to return to the normal water level (baseflow), which can be visualized from the peaks in Figure 3.4.

The logger deployed in BC6 during the first monitoring period started to give out invalid water depth data since 5/2 (Figure 3.6). This corresponds to a large precipitation event between 4/29 - 5/2. It is highly likely that the logger in BC6 was buried by the sediments after this large rain event. Despite that the apparent burying of the data sensor at BC 6, the valid data from 3/29 to 5/2 at the site still present a slightly decreasing trend in water depth from early spring (March) to early summer (June) (Figure 3.5).

The storm effects on the water level records may also appear in the second monitoring period from early September to late October (Figure 3.7 and 3.8). However, the rain events are relatively more frequent and the measured water level values do not stay the same as those being monitored from 4/30 to 6/28, the water level data for the entire second period is believed to be valid. The data show that the water level in BC6 does not have large variation in early fall, but it started to increase significantly since late fall (end of October). In addition to the water levels, in-field measurements of the discharge in the site in 9/14/2021, 10/8/2021, and 10/26/2021 are also plotted (Figure 3.7, orange diamonds). The discharge values, in fact, reveals the pattern that the discharge started to increase during the early fall period.

In addition to regular long-term monitoring processes, a storm event happened from 7/8/2021 to 7/12/2021 was monitored with the same processes, and the data will be shown in later sections.

The rating curve for BC6 is based on the discharge measurements and water level readings

from the data logger (Figure 3.9). The curve is an exponential-fit rating curve with the R^2 value of 0.9714. All water depths at BC6 were converted to discharge using the curve. (Table 3.2 and Figure 3.9).

HB4: Water Level from 3/29 to 6/28

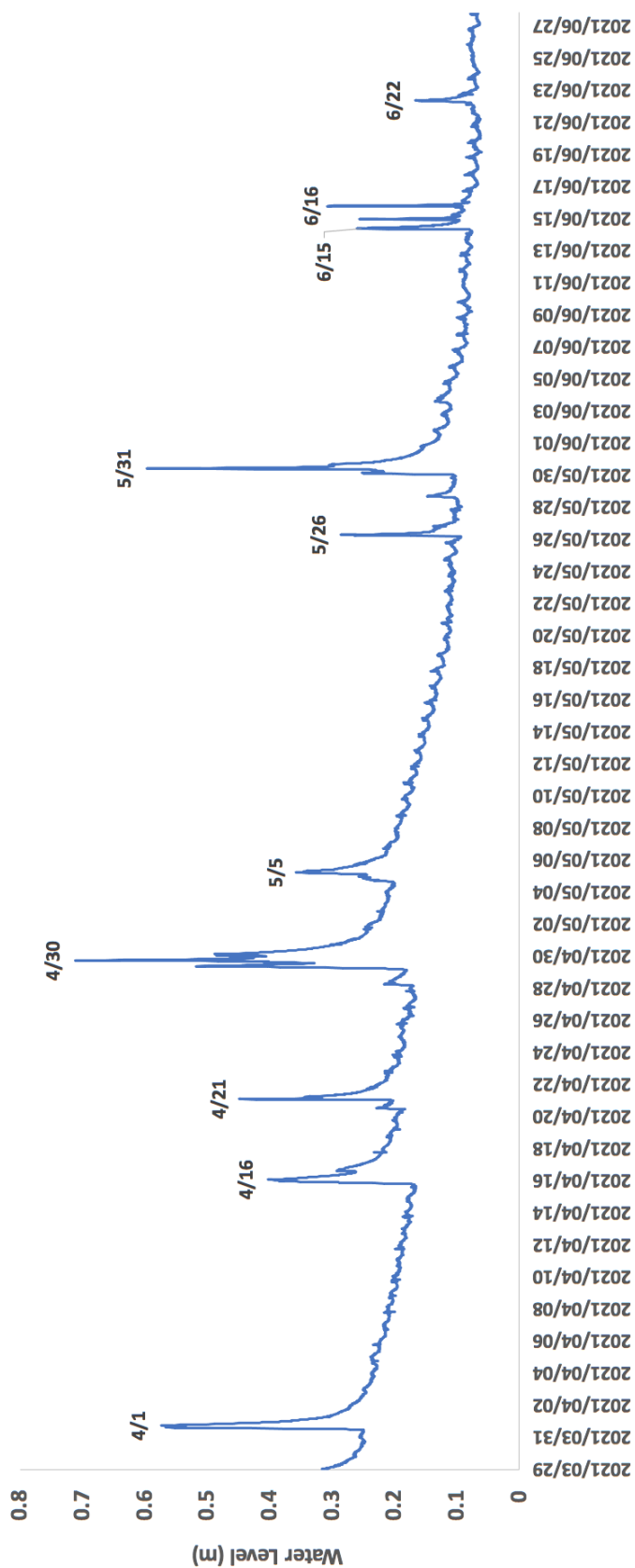


Figure 3.4. Water level of HB4 from 3/29/2021 to 6/28/2021.

BC6: Water Level from 3/29 to 6/28

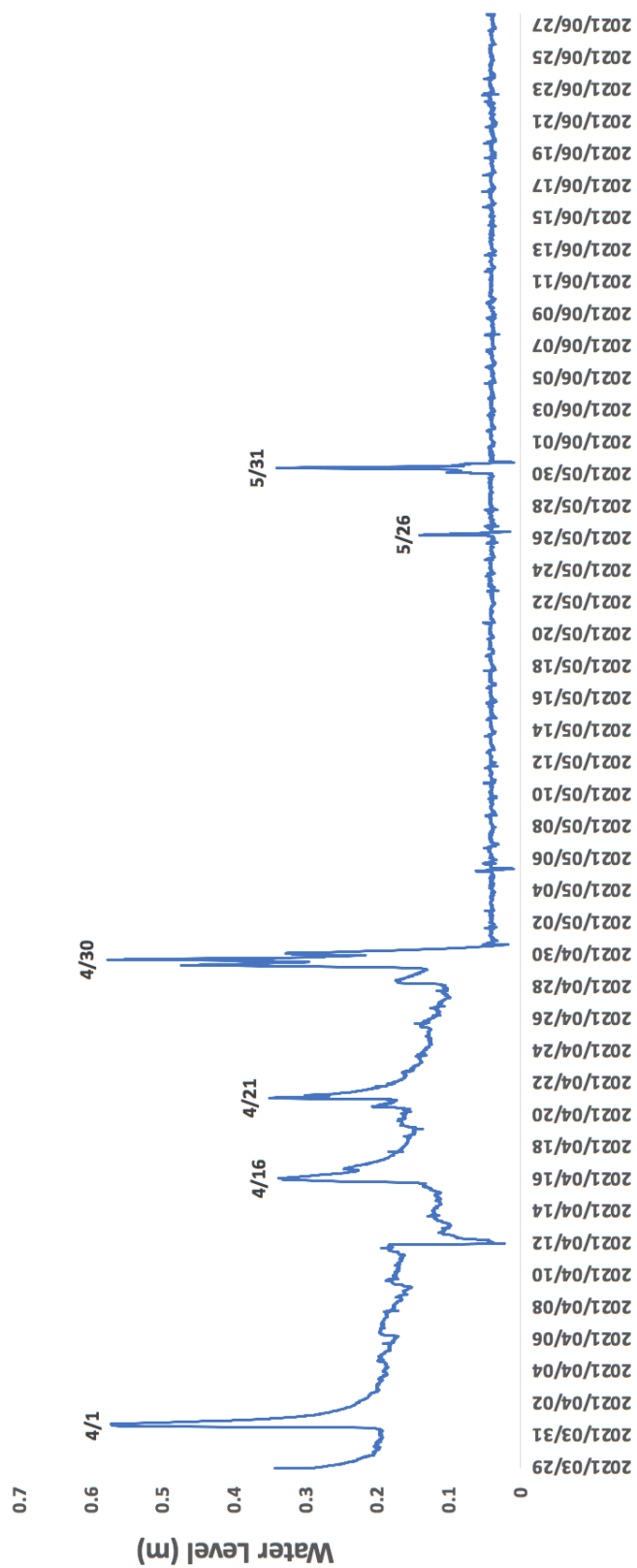


Figure 3.5. Water level of BC6 from 3/29/2021 to 6/28/2021

Lewiston Precipitation: March - June

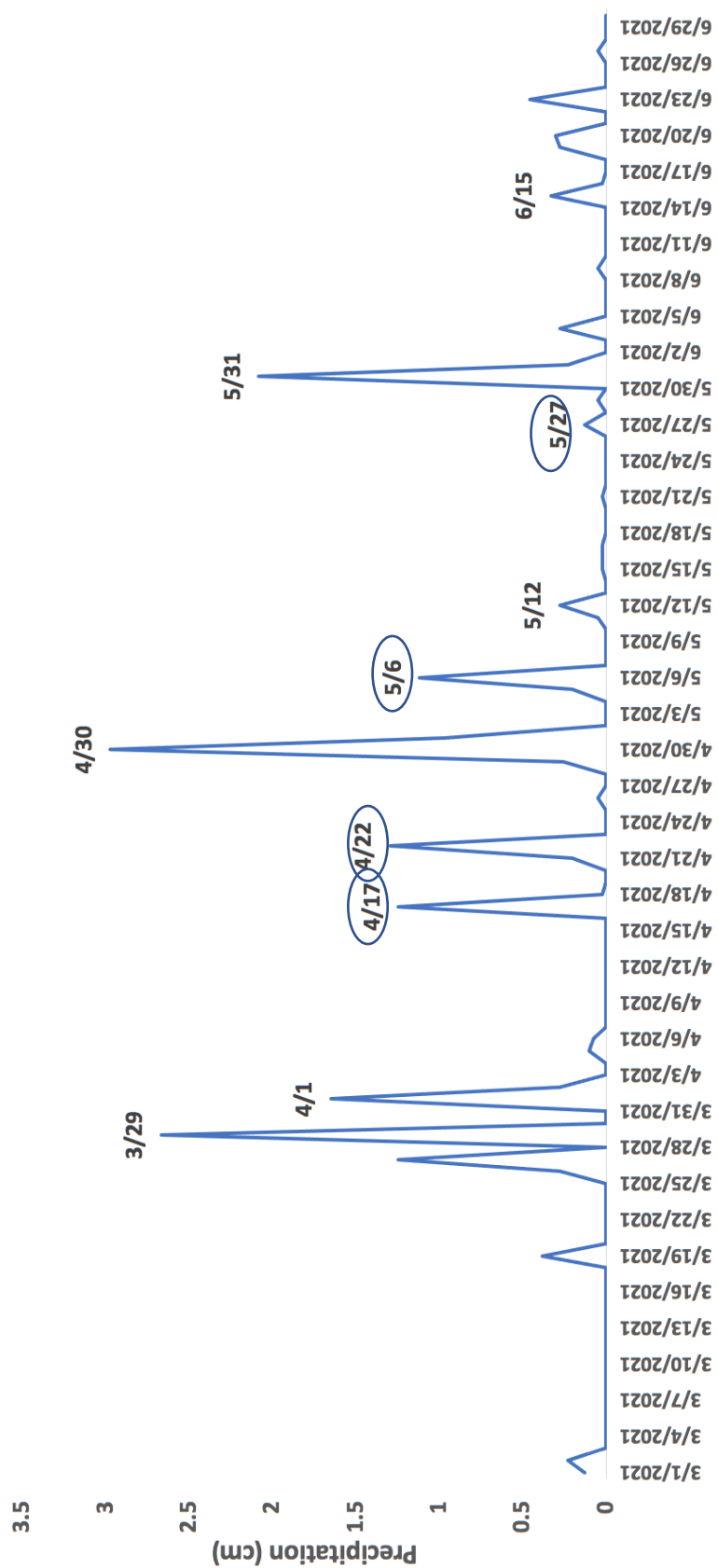


Figure 3.6. Precipitation in the Hart Brook from March to June.

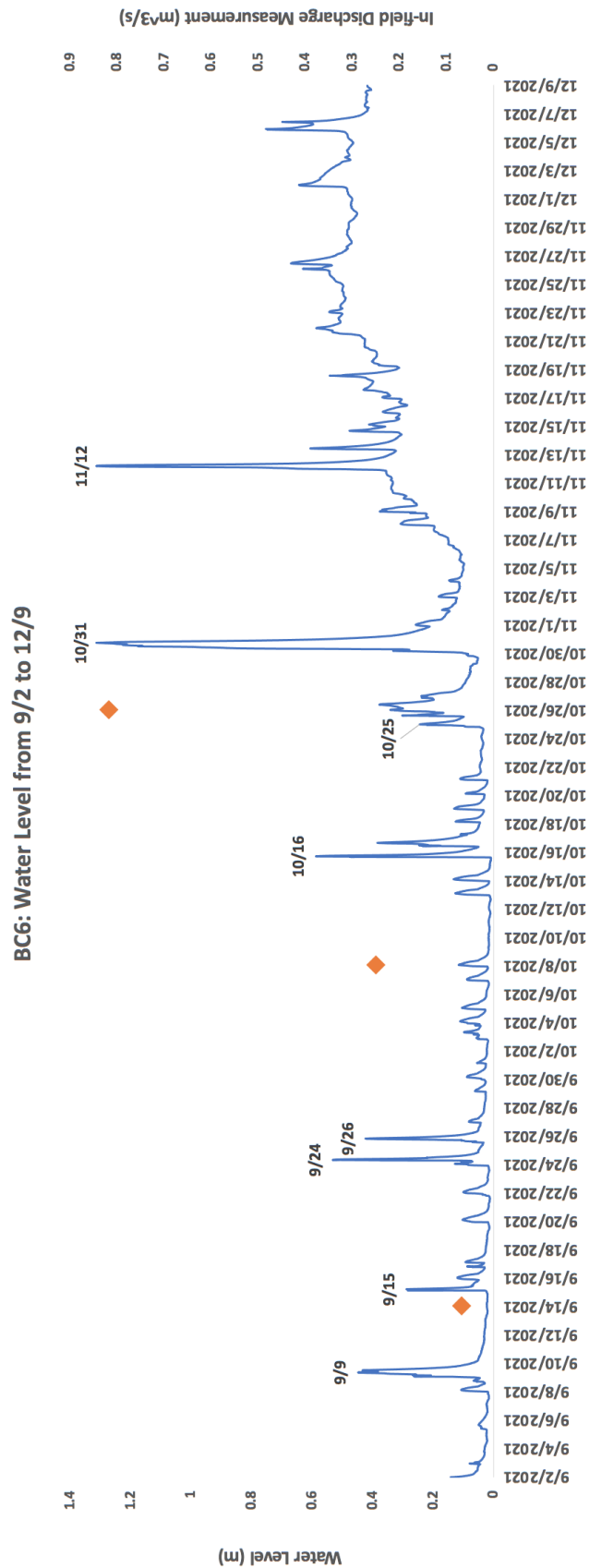


Figure 3.7. Water Level of BC6 from 9/2 to 12/9 from data logger (blue line) and from field measurements (orange diamonds).

Lewiston Precipitation: September - December

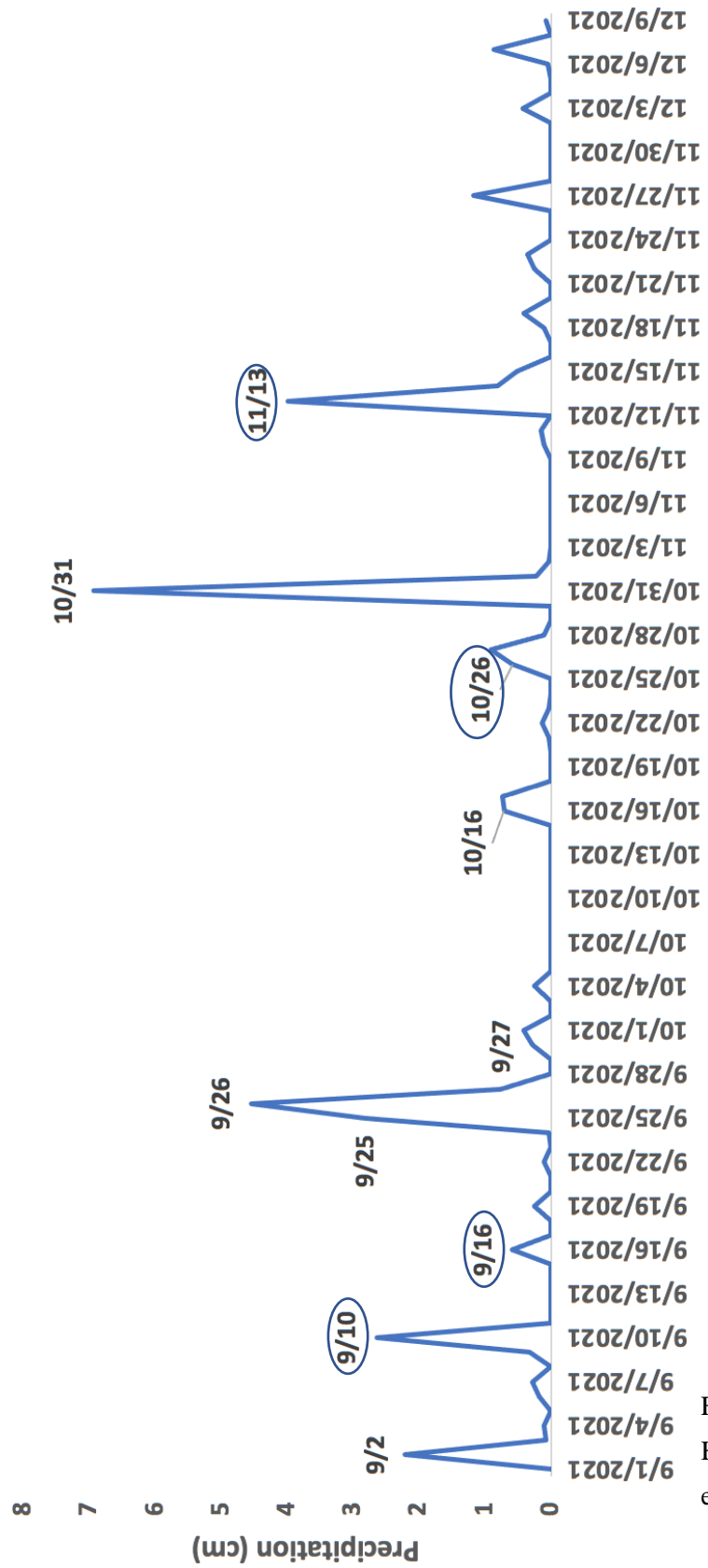


Figure 3.8. Precipitation in the Hart Brook from September to early December.

Date and Time	BC6 Water Level (m)	BC6 Discharge (m ³ /s)
7/8/2021 18:00:00	0.117	0.099
7/9/2021 11:45:00	0.167	0.465
7/10/2021 11:00:00	0.196	0.361
7/12/2021 10:15:00	0.064	0.149
9/14/2021 16:00:00	0.023	0.069
10/8/2021 16:15:00	0.116	0.251
10/26/2021 15:15:00	0.342	0.818

Table 3.2. Raw data for the rating curve.

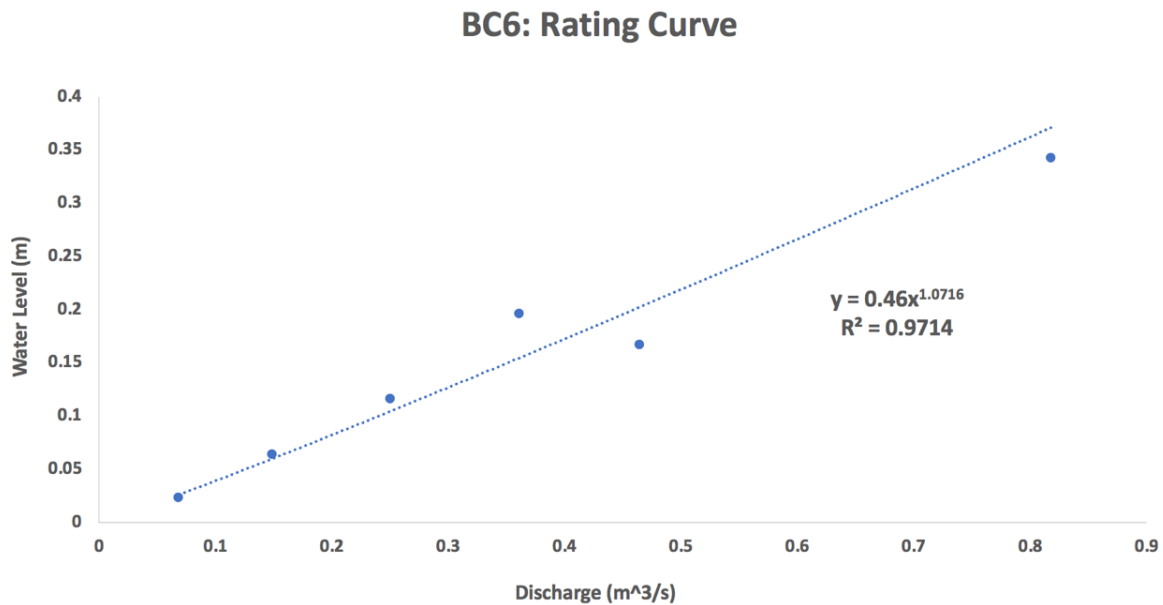


Figure 3.9. Rating curve for BC6.

3.3 SpC and Cl⁻ Concentration

The SpC readings from the loggers are plotted together with the water level data (Figure 3.10 for HB4, Figure 3.11 and Figure 3.12 for BC6). Additionally, a SpC logger was deployed to BC6 from 12/17/2021 to 2/17/2022 (Figure 3.13).

Similar to the water level sensor, the SpC sensors of the loggers deployed in BC6 were also affected by the moving sediments resulted from storm events, so that the readings from 5/2 to 6/28 (Figure 3.11) show identical patterns as the water level readings (Figure 3.6), and extremely

low values were recorded after every precipitation event from 9/2 to 10/16 (Figure 3.12).

However, by plotting out the SpC values together with the water level data, it was found that the SpC values change with the variations of the total discharge of the site.

From spring to midsummer, the SpC of the stream tend to inversely correlate with the water level; for the valid data in both graphs of HB4 (Figure 3.10) and BC6 (Figure 3.11) during this period, decrease in SpC is always observed in correspond to every precipitation event with significant increase in water levels. Moreover, as the water level in HB4 and BC6 present generally decreasing trend from spring to midsummer (Figure 3.4 and Figure 3.5), the SpC value within the sites show increasing pattern (Figure 3.10 and Figure 3.11).

Nevertheless, this relationship becomes more complex and tend to be reversed from early fall to early winter in BC6. Smaller precipitation events, such as that happened on 9/16 and 10/16, tend to increase the SpC readings in the stream (Figure 3.12). Notwithstanding, during larger precipitation events observed on 10/31 and 11/12 that have significantly increased the discharge in the site, the SpC readings show similar pattern with that during spring and summer (Figure 3.12).

By corresponding the measurements of Cl^- concentration from the grabbed samples with SpC readings from the in-field measurements with HydroLab, the relationship between Cl^- concentration and SpC is generated that: $\text{SpC}(\mu\text{S}/\text{cm}) = 9.6276 (\text{Cl}^-(\text{mg}/\text{L}))^{0.8463}$, and thus the logger readings on SpC can be converted into the monitoring of the Cl^- concentration in the site (Table 3.3 and Figure 3.14). According to this relationship, the chronically toxic level of Cl^- concentration of 230 mg/L can be converted into 960 $\mu\text{S}/\text{cm}$, and it was represented as the black dotted line in Figure 3.10-3.13.

HB4: SpC and Water Level from 3/29 to 6/28

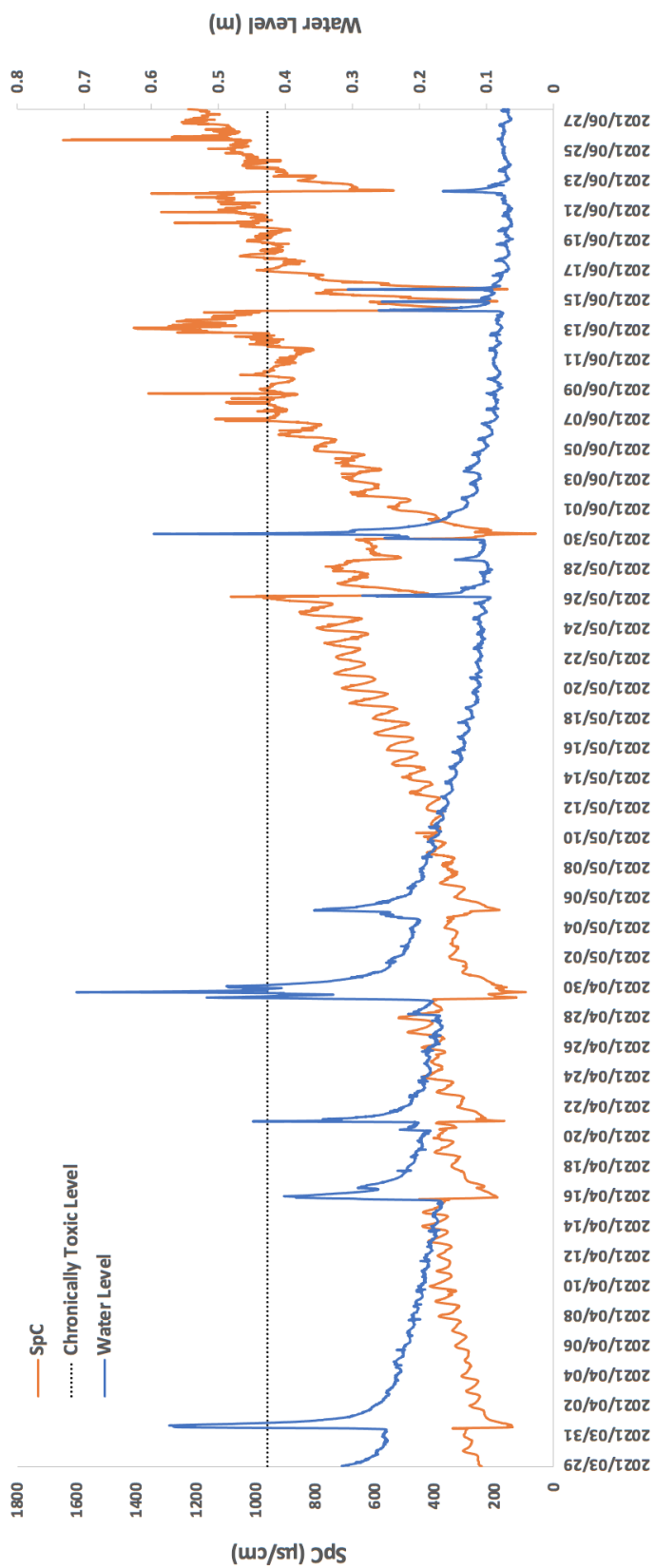


Figure 3.10. SpC data plotted on the water level graph of HB4 from 3/29/2021 to 6/28/2021.

BC6: SpC and Water Level from 3/29 to 6/28

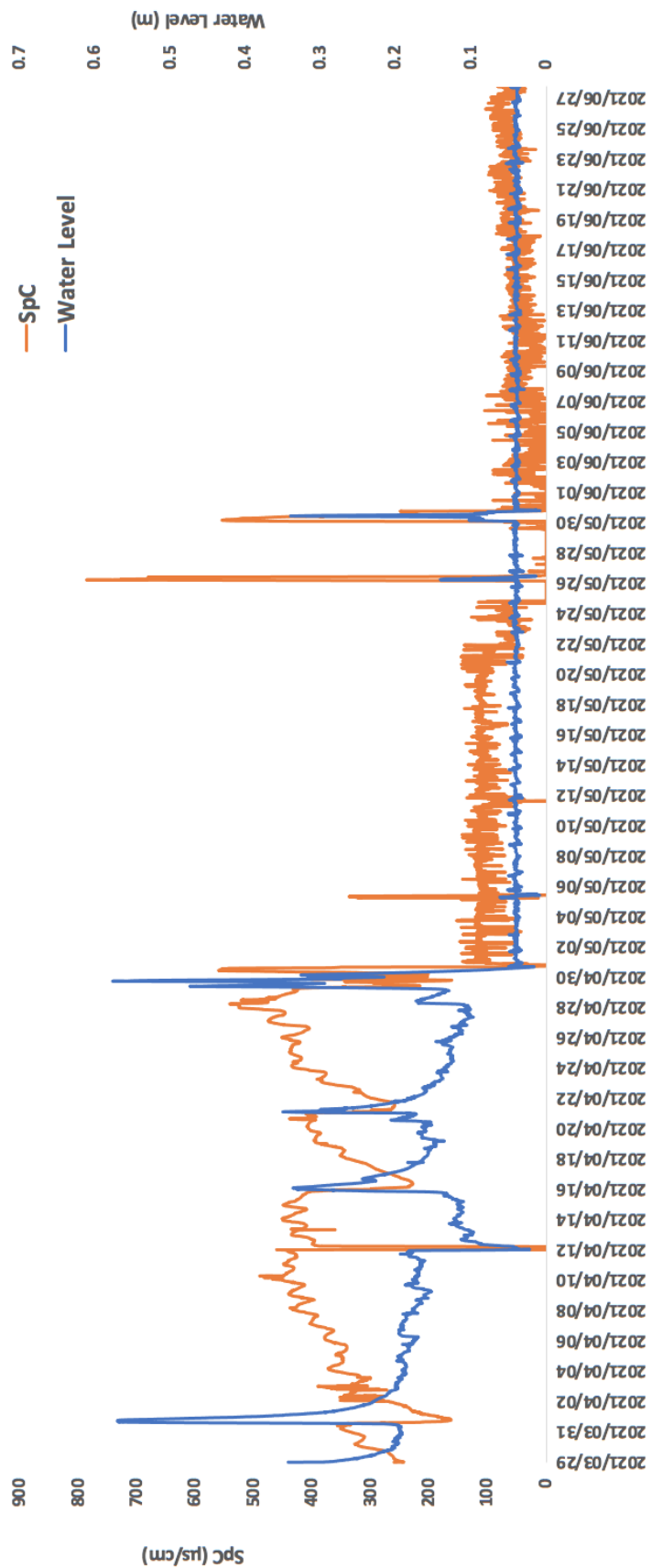


Figure 3.11. SpC data plotted on the water level graph of BC6 from 3/29/2021 to 6/28/2021.

BC6: SpC and Water Level from 9/2 to 12/9

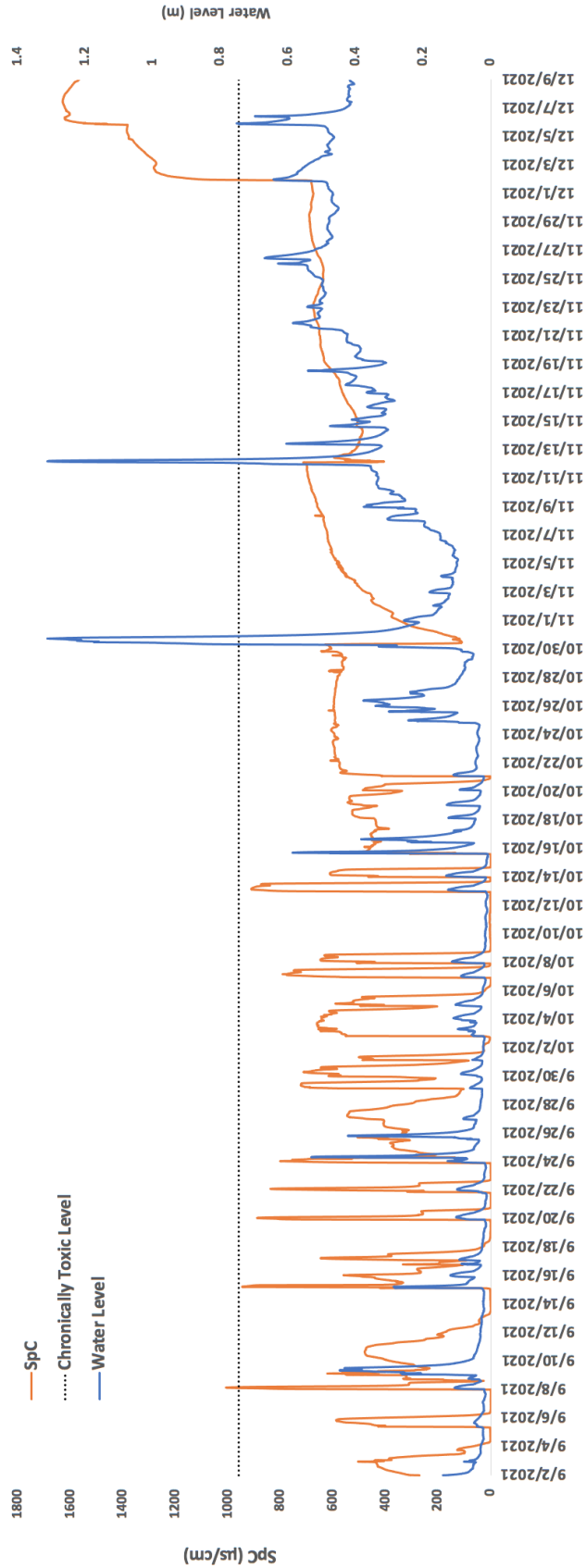


Figure 3.12. SpC data plotted on the water level graph of BC6 from 9/2/2021 to 12/9/2021.

BC6: SpC from 12/17 to 2/17

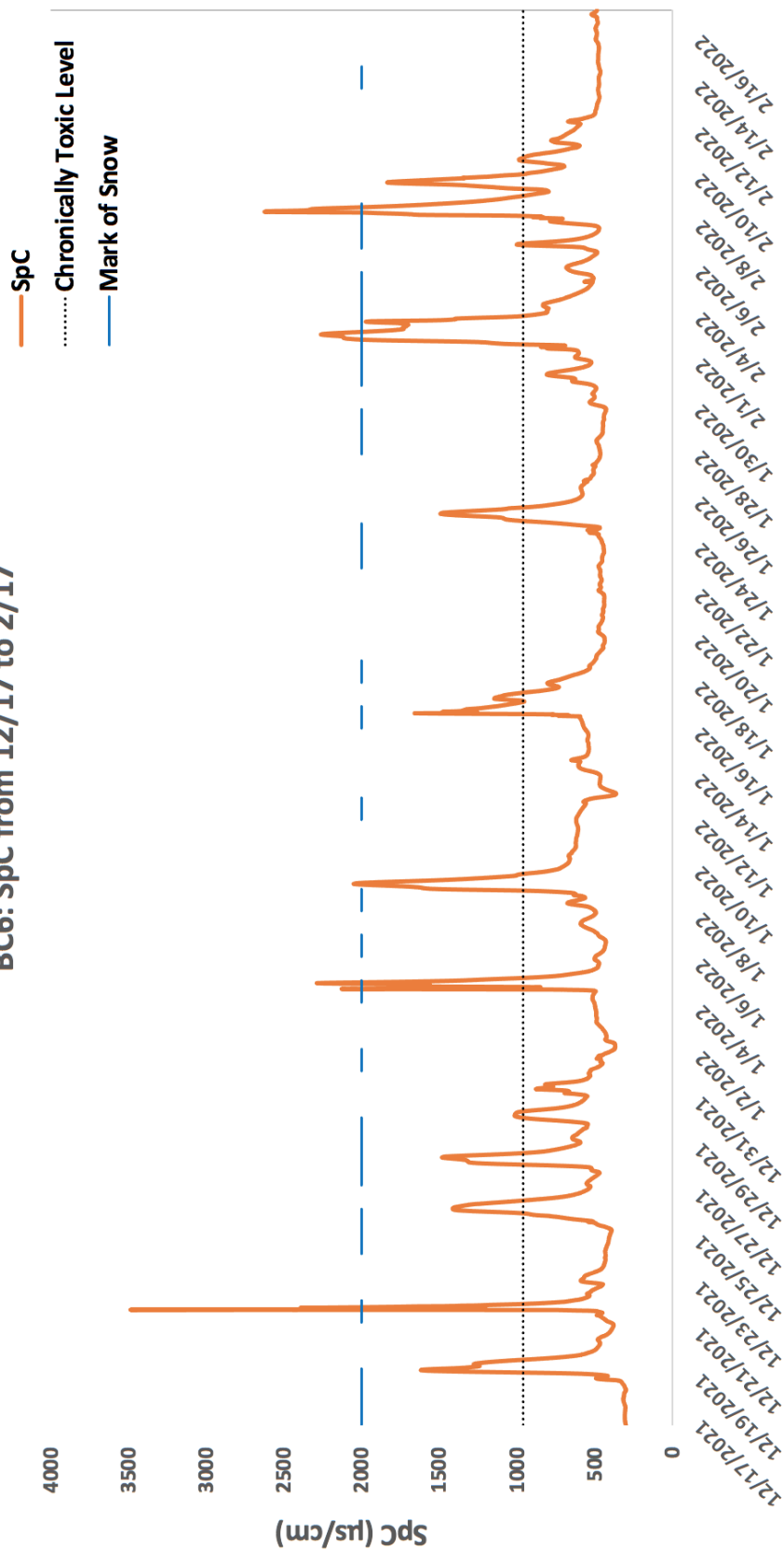


Figure 3.13. SpC readings of BC6 from 12/17/2021 to 2/17/2022, the blue dashes mark snow events.

Date & Site	Cl conc. (mg/L)	SpC (µs/cm)	Date & Site	Cl conc. (mg/L)	SpC (µs/cm)
6/28 HB4	289.06	1176	8/20 BC6	113.68	500
6/28 HB3	229.47	923	8/18 HB5	106.79	513
6/28 BC6	162.14	402	9/14 CC2	89.78	486
6/28 HB5	85.02	383	9/14 CC1	129.31	629
7/8 HB4	161.67	717	9/14 HB4	179.39	903
7/8 HB3	51.34	233	9/14 HB3	175.88	835
7/8 BC6	68.73	301	9/14 BC6	168.34	786
7/8 HB5	84.65	403	9/14 HB5	78.22	390
7/9 BC6	97.33	434	10/8 CC2	88.90	460
7/10 HB4	84.33	399	10/8 CC1	127.51	652
7/10 HB3	84.00	408	10/8 HB4	195.79	920
7/10 BC6	85.14	407	10/8 HB3	36.92	205
7/10 HB5	94.40	499	10/8 BC6	126.17	555
7/12 HB4	120.56	581	10/8 HB5	67.67	344
7/12 HB3	144.12	674	10/8 Andro	9.59	72
7/12 BC6	154.19	712	10/26 BC6	48.13	258
7/12 HB5	110.65	563	11/5 CC2	72.76	358
7/28 HB4	140.50	582	11/12 CC1	21.58	129
7/28 HB3	158.47	644	11/12 HB4	30.60	173
7/28 BC6	170.23	679	11/12 HB3	46.20	245
7/28 HB5	87.45	370	11/12 BC6	53.50	277
8/18 CC2	109.98	584	11/12 HB5-1	16.90	105
8/18 CC1	141.38	720	11/12 HB5-2	17.71	110
8/18 HB4	229.37	1041	12/9 BC6	249.18	1027
8/18 HB3	214.60	947			

Table 3.3. Raw data of SpC (µS/cm) vs. Cl⁻ concentration (mg/L)

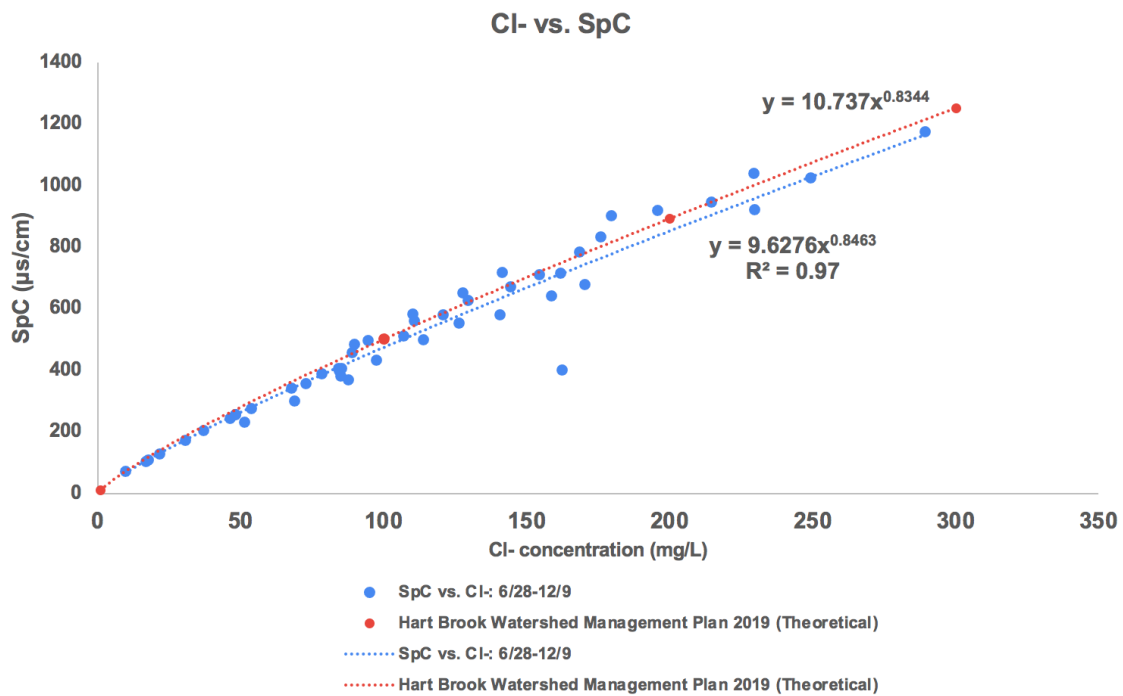


Figure 3.14. SpC (µS/cm) vs. Cl⁻ concentration (mg/L)

3.4 Seasonal Variations in Cl⁻ Flux

3.4.1. Historical Discharge and Cl⁻ concentration and Extrapolations

Since BC6 is located at the confluence of the streams in the watershed and is also where the streams start to discharge into the Androscoggin river, the site is considered to be representative for the water quality in the watershed, and thus is used to reveal the general seasonal variation trend of the entire watershed.

Both the monthly average of Cl⁻ concentration and discharge within the site was determined via direct measurement and extrapolation, depending on the months (Table 3.4 and Table 3.5). Loggers' direct measurements were the prioritized (refer as "measurements"). However, loggers may produce invalid and inaccurate data (ie. Figure 3.5, water level of BC6) or not be available (from 6/28 to 9/2); therefore, the monthly average values, under these circumstances, were extrapolated from biweekly/monthly sampling results, historical value, and other data analysis approaches (refer as "extrapolation").

The average discharge is calculated with the logger data for March, April, May, September, October, November, and December. During the time when the logger was not deployed, discharges were manually measured in field in June (6/28), July (7/28), and August (8/18). Nevertheless, the only measurement during August was immediately after a storm event; therefore, with the flood responses generated during storm analyses (discussed in later section), the monthly average discharge during August at BC6 was estimated by subtracting the flood effects from the in-field measurements.

During the time when the logger was not functioning and the in-field measurements were not applicable due to the 2-feet ice cover on the site of BC6 in January and February, the average discharge in these two months is estimated by the ratio of precipitation with that in December:

$$Q_{Jan.} = Q_{Dec.} \times \frac{Precipitation\ Depth_{Jan.}}{Precipitation\ Depth_{Dec.}}$$

Summarized data measurements and extrapolation approaches for the monthly average discharges were included in Table 3.4.

	Month Average Discharge Measurement	Discharge Extrapolation
Mar.-May	Average of data logger	Average of logger data
June - July.	Hydrolab	Hydrolab
August	Hydrolab	Hydrolab - Flood Response
Sept. - Dec.	Average of logger data	Average of logger data
Jan., Feb.	N/A	Estimated by the ratio of precipitation with that in December

Table 3.4. Calculation approaches of the monthly average of the discharge in BC6.

The average Cl^- concentration of the Androscoggin river is 9.6 mg/L (Table 3.3, highlighted in red), which corresponds to a calculated SpC of 65 $\mu\text{S}/\text{cm}$. This represents baseline levels of Cl^- in the region, so that all the SpC recordings at BC6 that are below this value are considered void.

The monthly average SpC values were calculated for March, April, and May, with the direct measurements from the deployed logger.

During June, July, and August, when the logger was not deployed, the monthly average SpC was determined through the in-field measurements. However, as only one data point was acquired from this approach for each of these three months, which may lead to large variations, these measurements were decided to be compared with the historical data. Although the water quality parameters at BC6 were not officially measured by the government, Hart Brook Watershed Management Plan 2019 provides data for HB1, which was located at the downstream of BC6 before the stream's entry to the Androscoggin River and should present similar water quality parameters as BC6 (Figure 2.1).

The SpC sensor being deployed from 12/17/2021 to 2/17/2022 was found 11.2% lower than the actual value, giving out 1255 $\mu\text{S}/\text{cm}$ for the standard of 1413 $\mu\text{S}/\text{cm}$. Therefore, the extrapolated monthly average SpC values for these months was 1.12 the actual measurements.

Summarized data measurements and extrapolation approaches for the monthly average SpC values were included in Table 3.5.

	SpC Measurement	SpC Extrapolation
Mar.-May	Average of logger data	Average of logger data
June - Aug.	Hydrolab	Historical data from HB1
Sept. - Dec.	Tossed SpC below 65 $\mu\text{S}/\text{cm}$	Tossed SpC below 65 $\mu\text{S}/\text{cm}$
Jan., Feb.	Average of logger data	Average of logger data times 1.12

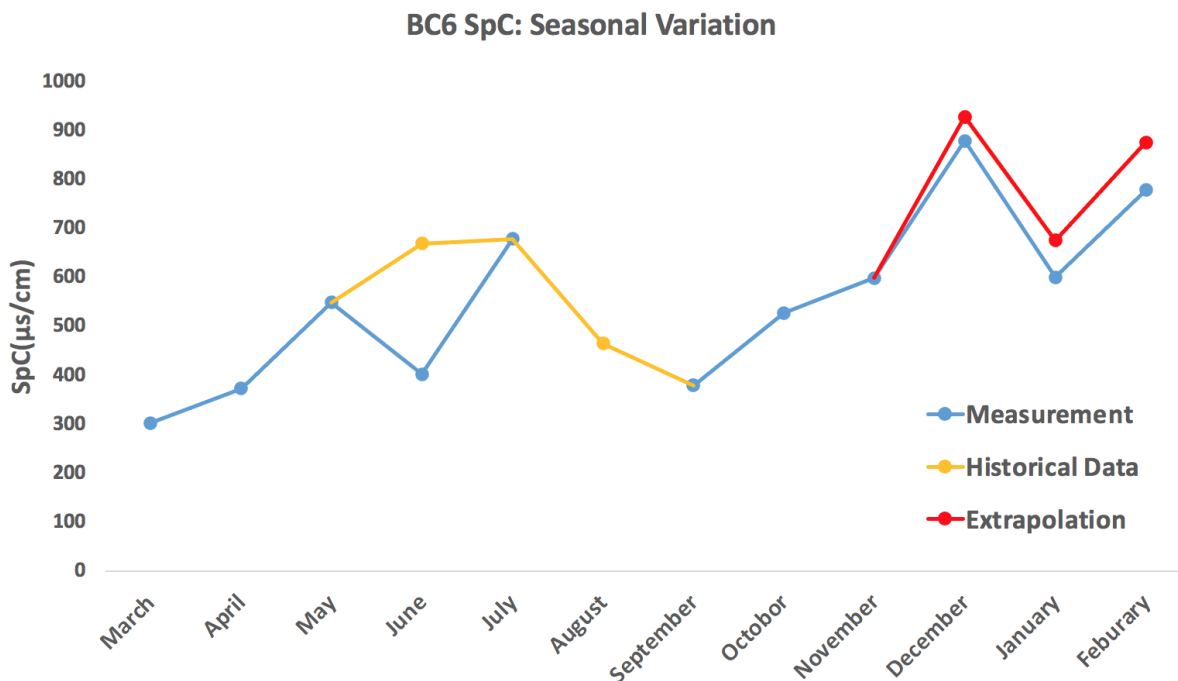
Table 3.5. Calculation approaches of the monthly average of the SpC in BC6.

3.4.2. Seasonal Variation in BC6

The measurements (blue), historical data (yellow), and extrapolations (red) of the average of the SpC values and discharges were plotted for BC6 (Figure 3.15 and Figure 3.16). The graphs were also converted into the Cl^- concentration and Cl^- flux. Both SpC and Cl^- concentration graphs revealed increases in ion concentration from March to June (spring to summer), likely due to a combination of factors, including continued mobilization of Cl^- in the watershed and/or the decreasing discharge within the period (Figure 3.16). Decrease in ion concentration from July to September (summer to fall) may correspond to the increase in discharge and perhaps export of much of the salt from previous year's application (Figure 3.16). Transiting from Fall to Winter

(Sept. to Dec.), both ion concentration and discharges within the site significantly increased, which may be resulted from the snow fall and the following application of road salt (Figure 3.15). Overall, two peaks in both SpC and Cl^- concentration were observed during mid-summer and winter, because of the drought (low-flow) condition and the application of road salt, respectively.

According to Figure 3.15 and 3.16, higher observed Cl^- concentration does not necessarily indicate higher Cl^- fluxes. In fact, the Cl^- flux in the stream is dependent on the discharge and the Cl^- concentration. For example, although a peak in Cl^- concentration was extrapolated for the summer, the flux was actually extremely low, because of the low-flow condition within this period; the only peak being observed in the Cl^- flux happened in winter period, which was consistent with the seasonal pattern of the discharge. Interestingly, although road salt was not applied, the calculated Cl^- amounts within the stream increase from summer to fall with the increasing discharge (Figure 3.16).



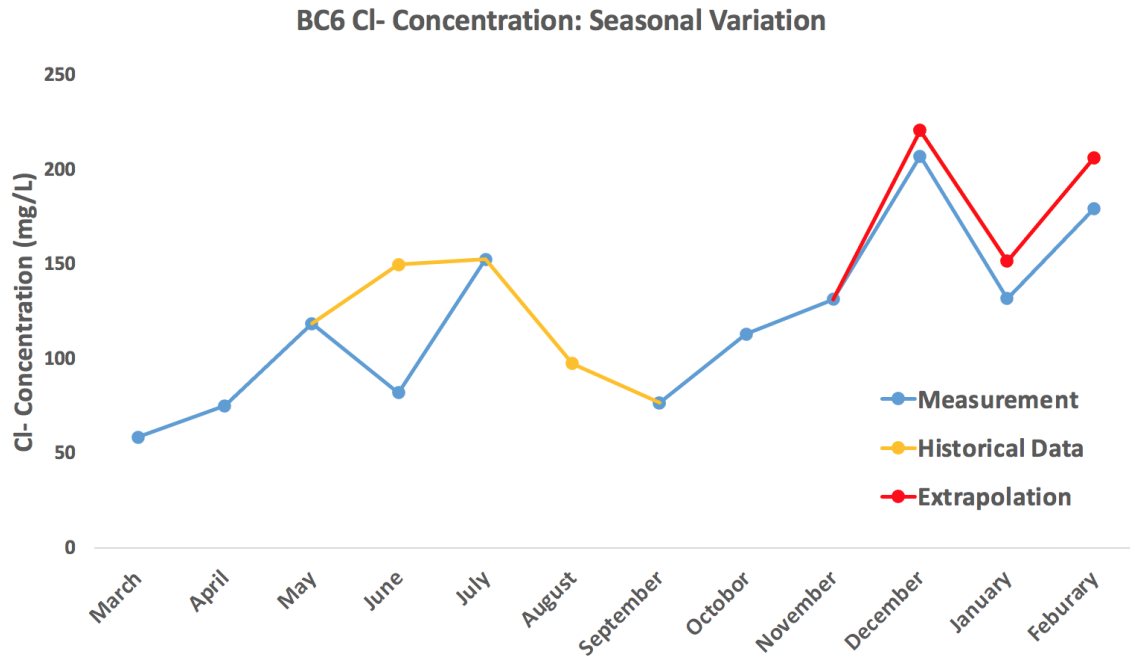
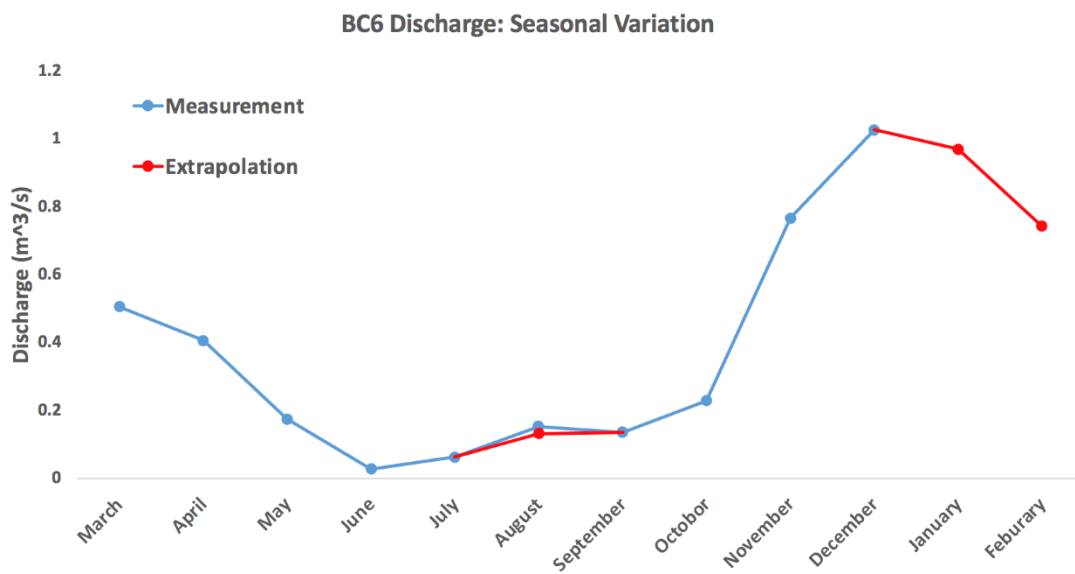


Figure 3.15. SpC and Cl⁻ concentration seasonal variation in BC6.



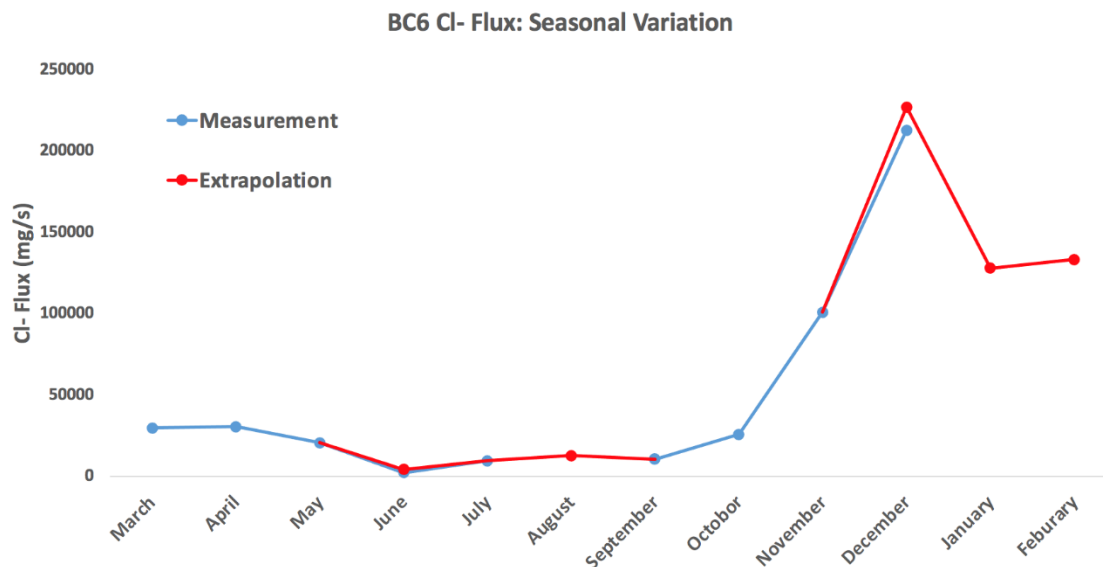


Figure 3.16. Discharge and Cl⁻ flux seasonal variation in BC6

3.5 Major Ion Analysis

In-field monitoring data (Hydrolab data) and the results of major ion analyses from the acquired samples from 6/28/2021 till 11/12/2021 are provided in Appendix 2 and Appendix 3. During storm events, chemical responses will result in variations in the general trends of major ions (which will be discussed in later section); therefore, the major ion analyses were only performed for the samples that were acquired without prior raining event (referred to “no-rain” conditions here and throughout).

Stream discharge at each site is plotted from upstream to downstream (Figure 3.17). The discharge of HB5 is plotted separately from BC6 to show the increase in discharge down the main stem of the Hart Brook. Increases in discharges are observed in the downstream sites of HB3 and BC6, which is reasonable because of a larger infiltrating area as moving downstream and the joining tributary passing through HB9 and HB7. Mid-summer is observed to be the “driest period” in this watershed.

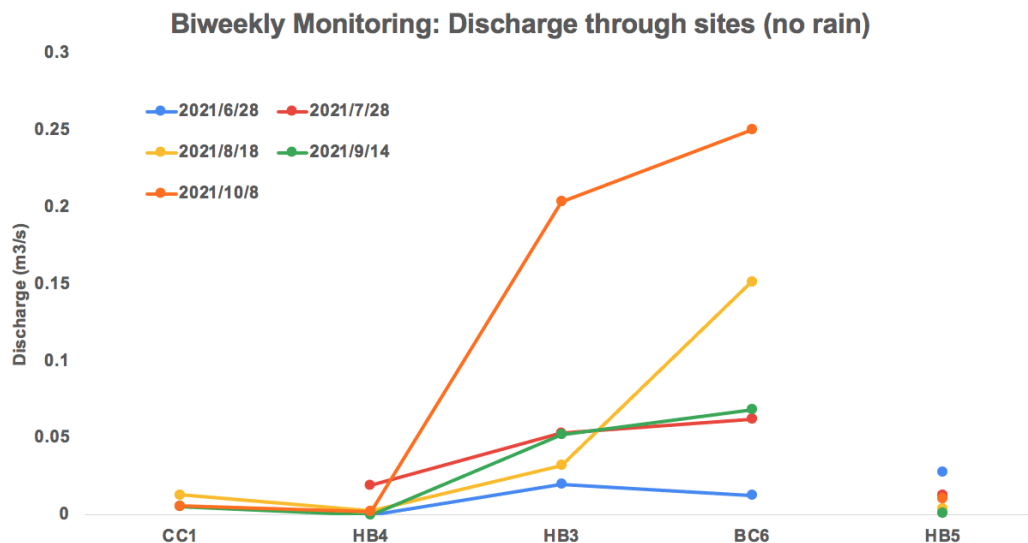
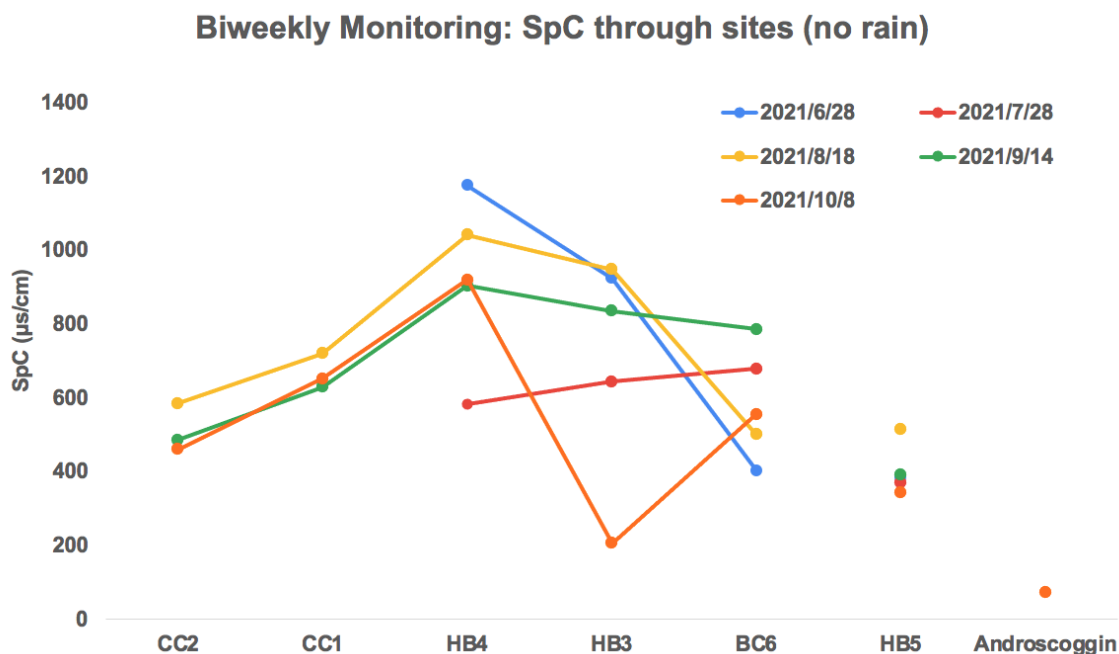


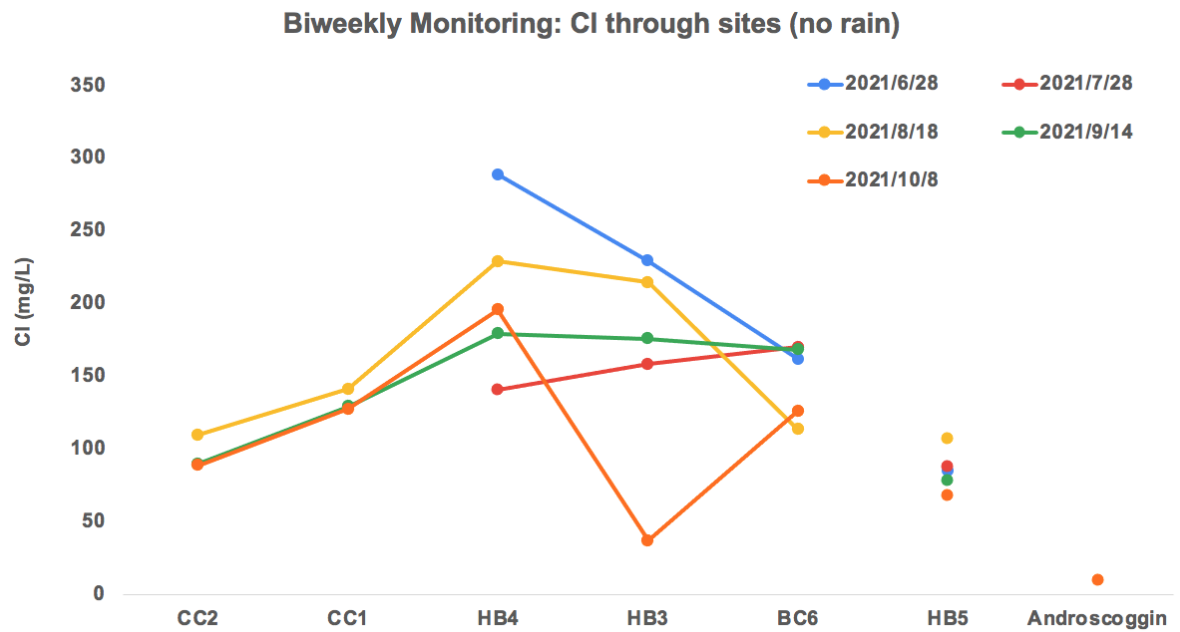
Figure 3.17. Discharge through sites

The Hydrolab data and the ion concentrations were plotted to reveal the spatial variations of the water quality (Figure 3.18). Among these plots, SpC ($\mu\text{S}/\text{cm}$) and Cl^- concentration (mg/L) show almost identical trends with different locations, which is consistent with the strong correlation between these two parameters. Moreover, these values tend to be higher during summer than during fall. HB4 is observed to have the highest SpC, Cl^- concentration, and HCO_3^- concentration among the measured sites (Figure 3.18(a), 3.18(b), 3.18 (c)). Interestingly, SO_4^{2-} concentration is usually found to be the highest at HB3 (Figure 3.18 (d)).

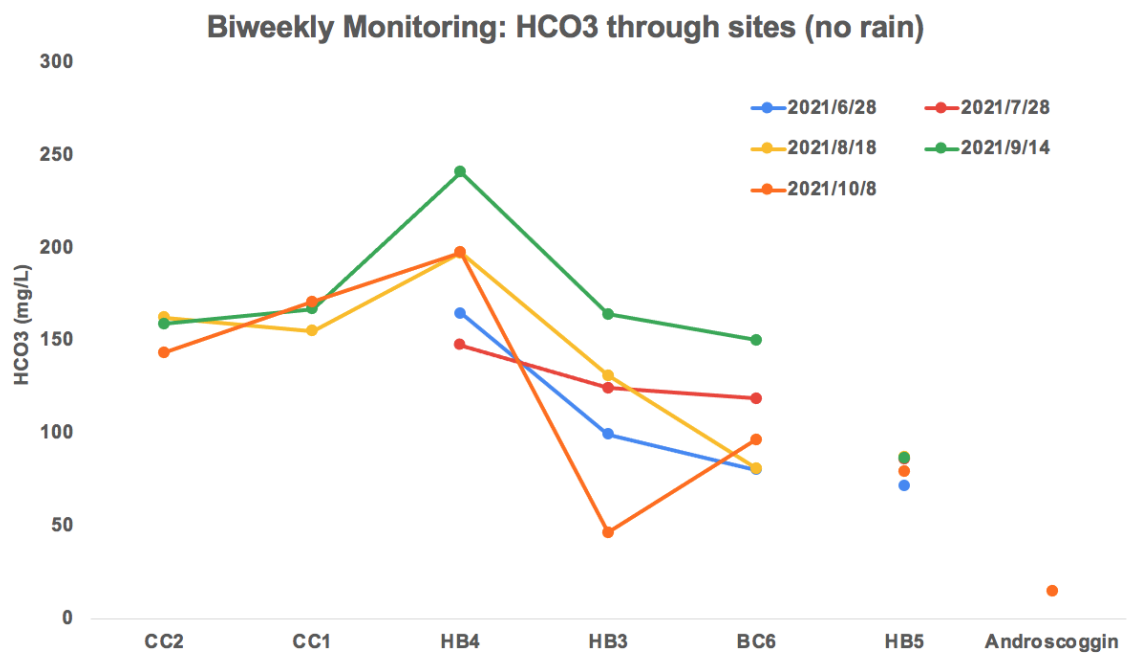
(a).



(b).



(c).



(d).

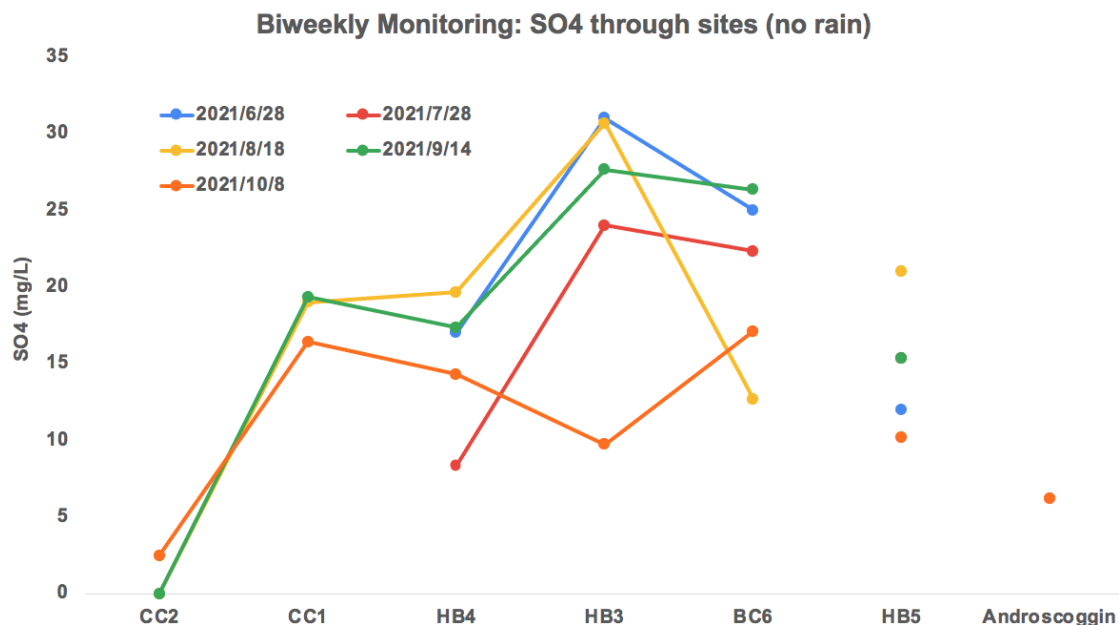
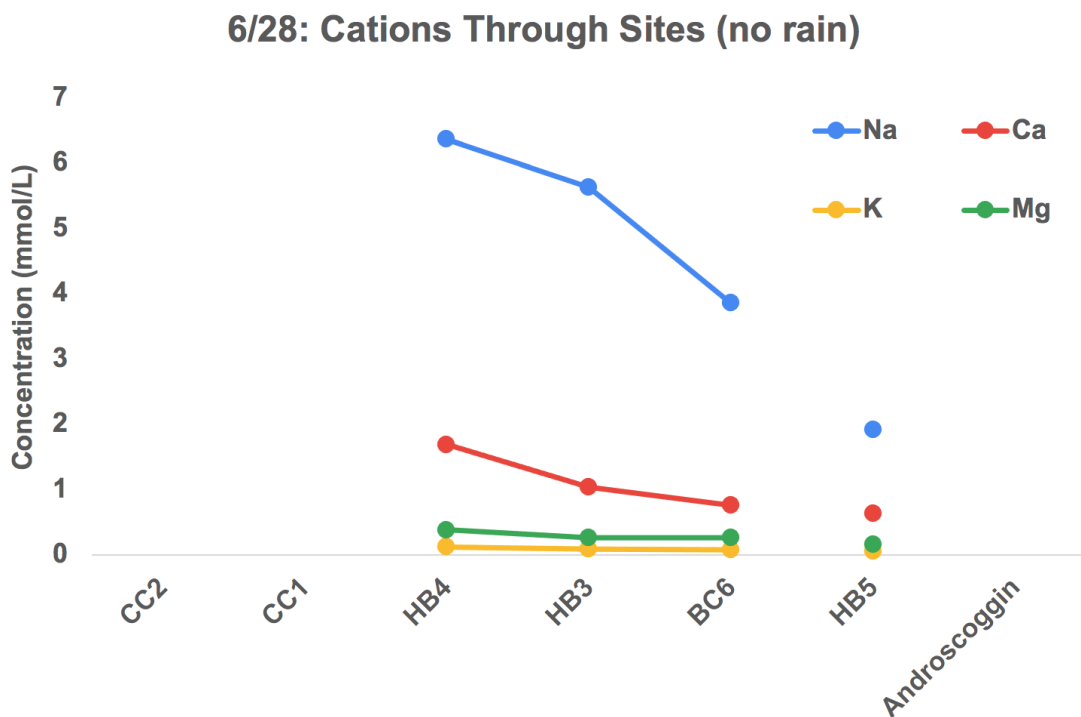
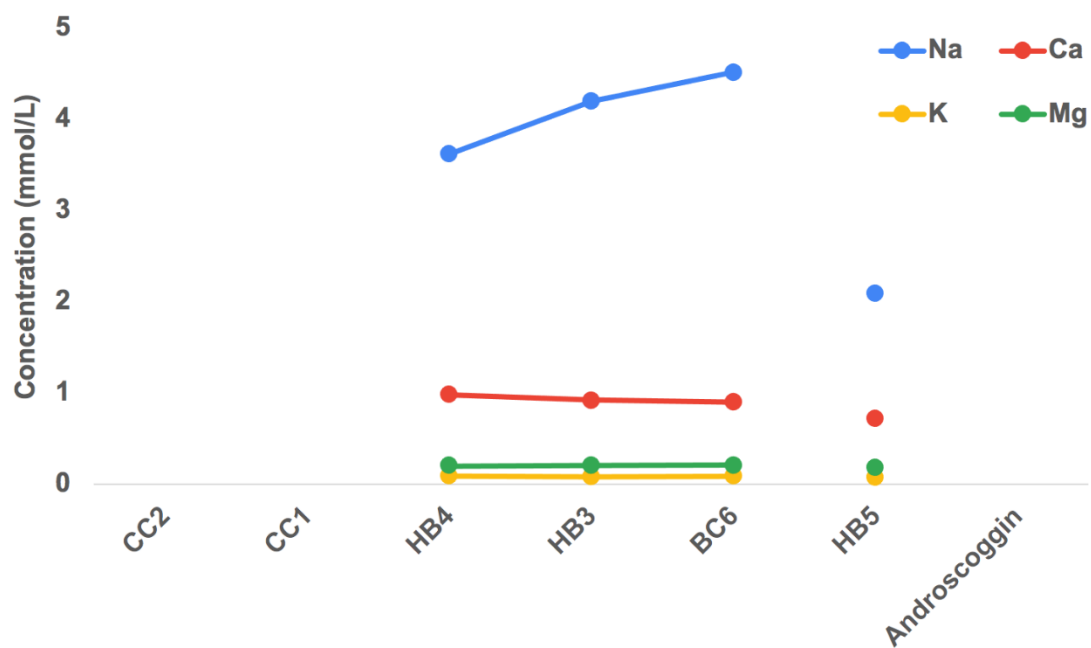


Figure 3.18. Major anions in the watershed (a) SpC through sites, (b) Cl⁻ concentration through sites, (c) HCO₃ concentration through sites, and (d) SO₄²⁻ concentration through sites.

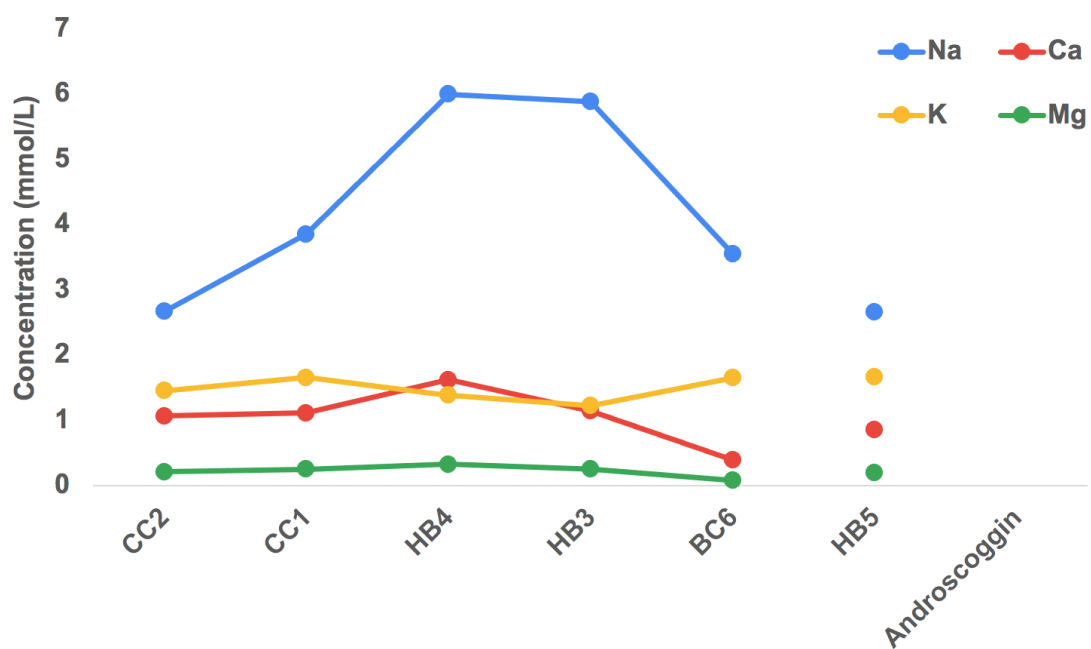
The spatial variation of major cations generally follows the same trend with the analyzed anions (Figure 3.19). Interestingly, no significant increase in any measured cations were observed in HB3 to correspond with its higher SO₄²⁻ concentration.



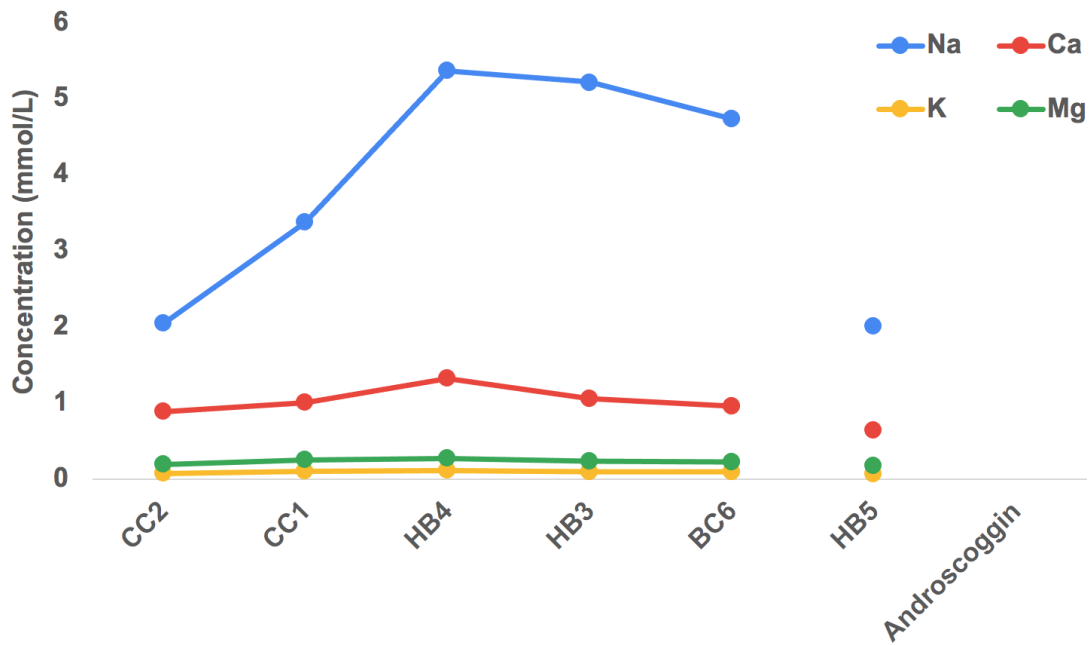
7/28: Cations Through Sites (no rain)



8/18: Cations Through Sites (no rain)



9/14: Cations Through Sites (no rain)



10/8: Cations Through Sites (no rain)

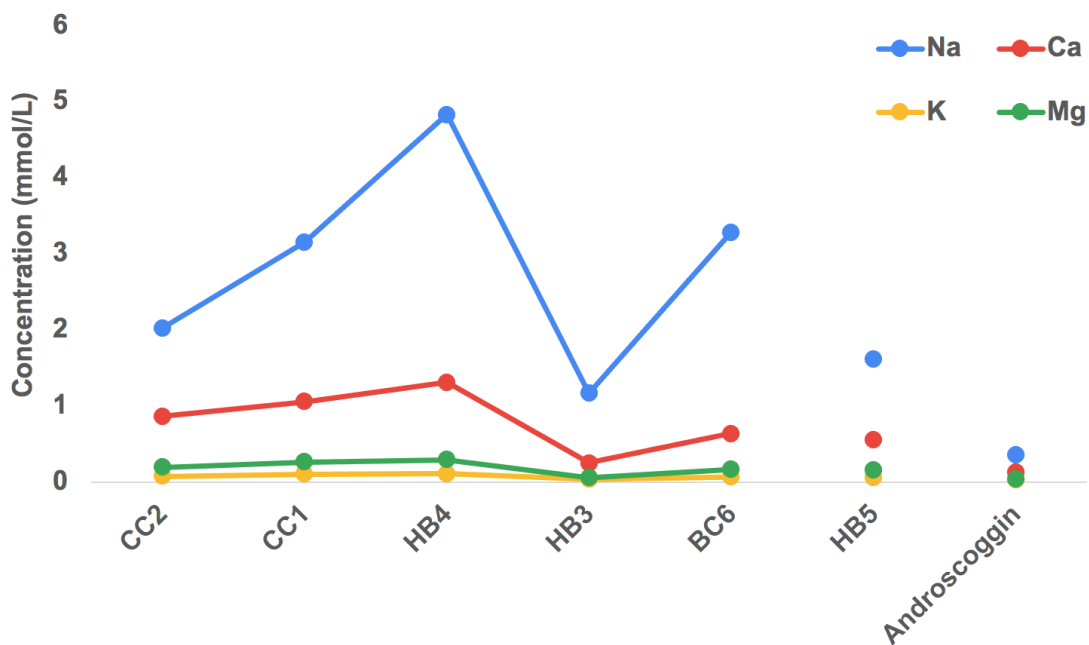


Figure 3.19. Major cations in the watershed.

The Charge-Balance Error for all samples ranged between 0.37% and 9.12% (Appendix 3). Among 36 sample sets, 10 of them are more than 0.5% higher than the expected 5% error. Almost every calculated error value is negative, meaning that total amounts of major anions (Cl^- ,

HCO_3^- , SO_4^{2-}) usually exceeds that of the major cations (Na^+ , Mg^{2+} , K^+ , Ca^{2+}). While it is possible that errors may have existed during the lab procedures, the negative values and the larger error % comparing with the expected value may also indicate that some dissolved species (anions) were not measured, such as $\text{Fe}^{2+/3+}$.

There is a strong linear correlation between the Cl^- and Na^+ concentrations ($R^2 = 0.9928$) (Figure 3.20). This indicates that the primary source of Cl^- contamination is likely NaCl, or road salt. Because the slope is nearly 1, the overall Cl^- input from groundwater recharge may not be very large in this watershed. Alternatively, if significant Cl^- retention does exist, then the soil/water chemistry may not be conducive to soil retention of cations.

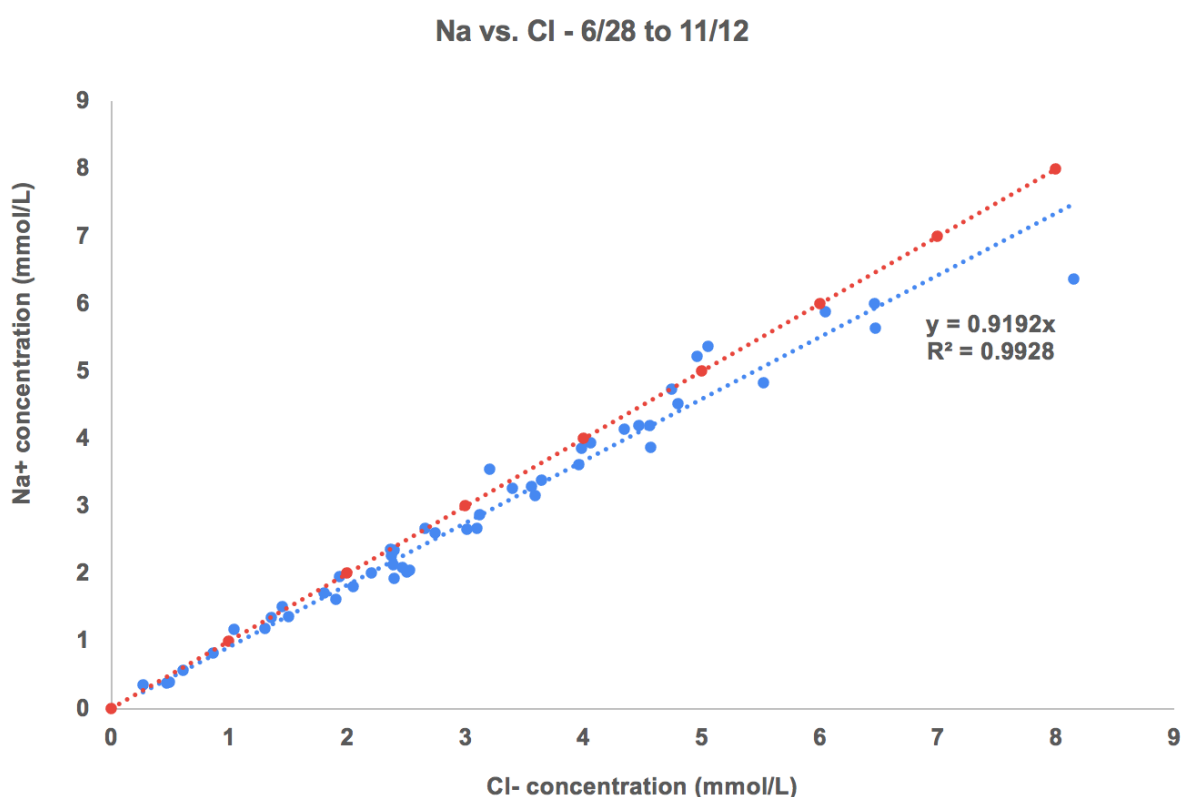


Figure 3.20. Na^+ concentration vs. Cl^- concentration with respect to all data; red line represents the standard 1:1 ratio.

In order to visualize the relative abundance of major ions within water samples, piper diagram is graphed out with GW-Chart provided by USGS (Figure 3.21). For all the samples, Cl^- , Na^+ , and Ca^{2+} are usually the dominant ions, taking up to 74% of anions and 78% and 41% cations, respectively. The Cl^- proportion in the waters is observed to decrease since 6/28/2021, likely due to the dilution processes under the increasing discharge. The diagrams were also plotted for each sample date in Appendix 4 to better reveal the seasonal variation of the water quality.

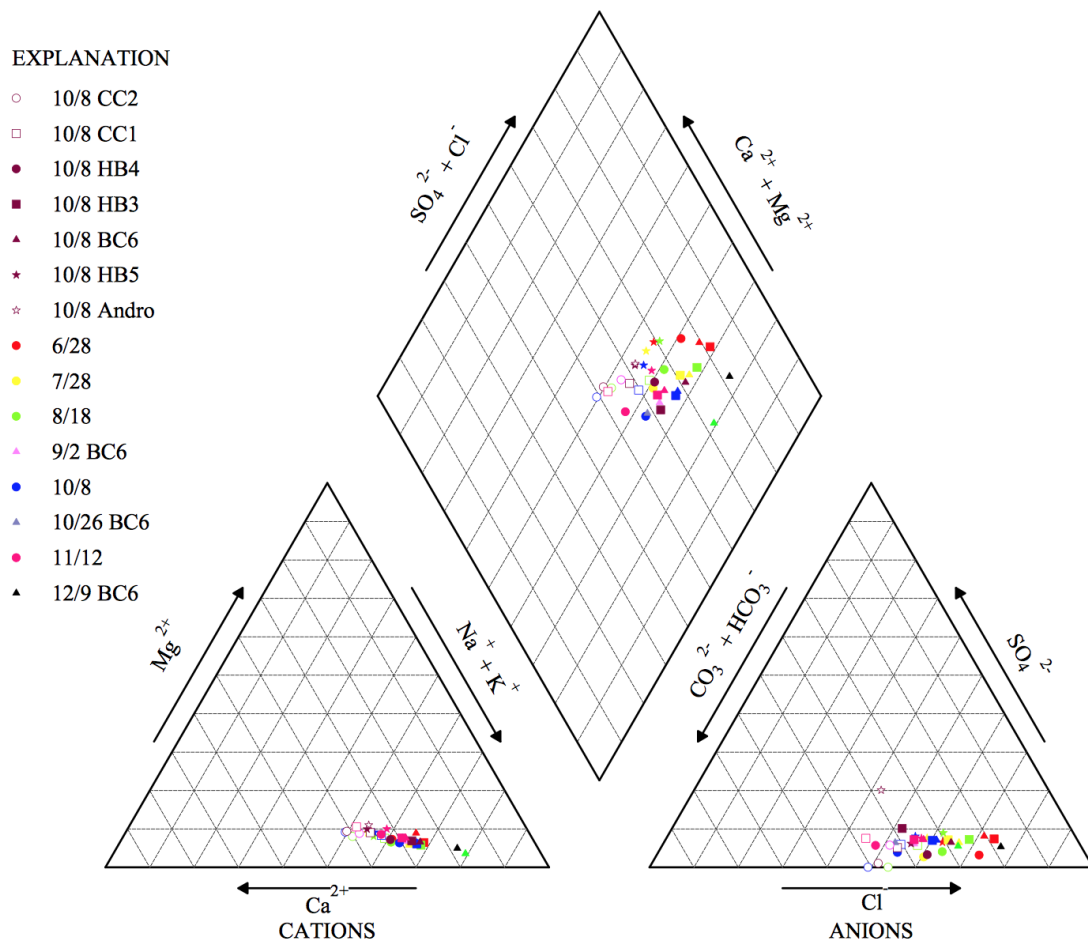


Figure 3.21. Piper diagram of samples from 6/28/2021 to 12/9/2021.

4. Discussion

4.1 Major Ion Concentrations and Seasonal Shifts in Water Type

The measured average major ions from 6/28 to 12/9 within the watershed (include all sites) were provided in Table 4.1. Comparing with the global mean, all the analyzed ions in this watershed have higher concentrations. At the same time, since the concentrations of these ions in the Androscoggin River, which represent the natural rock weathering pattern, are really close or even lower than the value of the global average, the significantly higher concentrations of ions in the Hart Brook suggest that the watershed is contaminated. Among the ions, the concentrations of Na^+ and Cl^- are significantly higher than the global average, indicating the presence of sources of contamination of these ions in the Hart Brook.

	Measured Major Ion Concentration (mg/L)	Concentration (mg/L) in the Androscoggin River	Concentration (mg/L) of Global River Water (Hem, 1985)
Na^+	68.18	8.12	5.15
K^+	3.00	0.99	1.30
Ca^{2+}	28.78	4.95	13.40
Mg^{2+}	4.13	0.94	3.35
Cl^-	113.47	9.59	5.75
HCO_3^-	108.27	14.77	52.00
SO_4^{2-}	14.20	6.19	8.25

Table 4.1. Concentrations of ions in the watershed, the Androscoggin River, and global river water.

The ions in this watershed are dominated by Na^+ and Cl^- , with the average percentage of 58.63% Na^+ among major cations and the average percentage of 58.76% Cl^- among major anions. According to the interpretation of piper diagram, all the sampled sites from the watershed present signals of sodium chloride type during sampling period (Figure 4.1 and Figure 3.21).

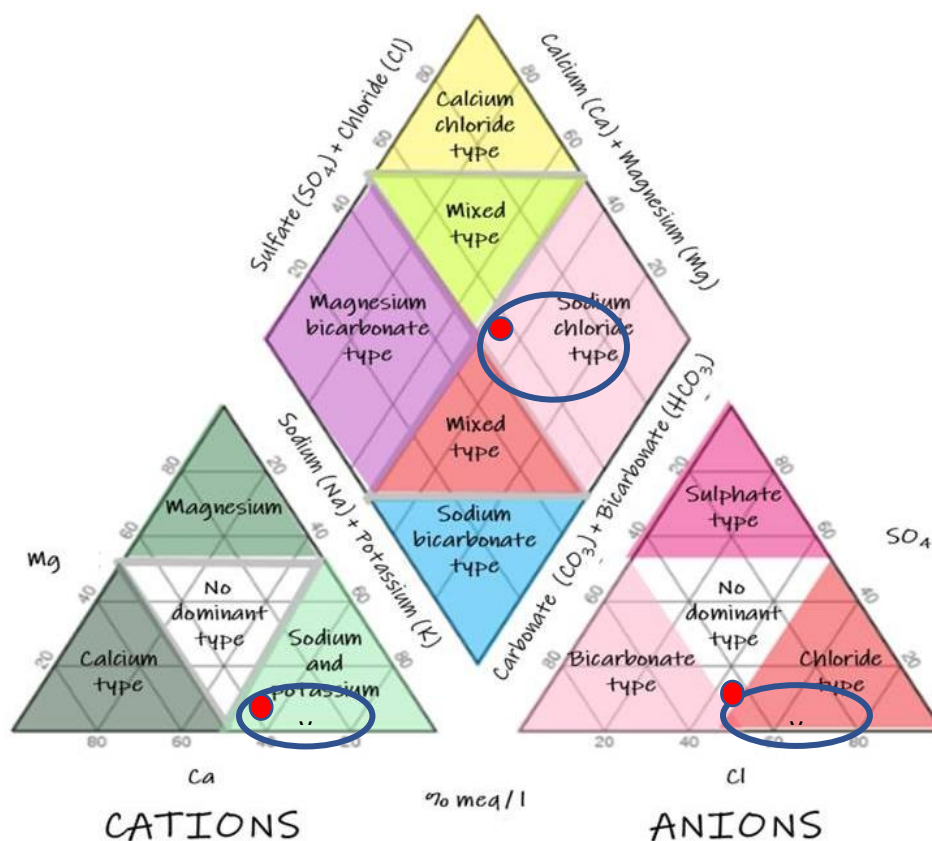


Figure 4.1. Interpretation of piper diagram with blue circles indicating the location of Hart Brook samples and red circles representing the location of the Androscoggin River (Hatari Lab).

These signals are less likely to be caused by natural weathering of bedrocks/surficial geologies because one sample being acquired from the Androscoggin River in 10/8 indicate the river overall is a “mixed type” or “no dominant type”. Instead, road salt is identified to be the major contributor of the NaCl.

Viewing the piper diagram in the sequence from 6/28 to 11/12, the overall trend to move from “sodium chloride type” to “mixed type” is observed (Appendix 4). While CC2 appeared to be “mixed type” by the first sample on 8/18/2021, water from other sites gradually shift to, and almost reaches the “mixed type” by 11/12/2021. Among them, BC6 appeared to be the farthest away from the “mixed type” in all the sampling dates, showing a relatively stable “sodium chloride type” feature. This indicates that BC6 is suffering with the NaCl contamination throughout summer and fall periods. At the same time, a sample from BC6 in 12/9, after the first snow event and thus the first road salt application of 2021 on 12/7, jumped dramatically back to the middle of sodium chloride type. This observation provides a direct evidence that the road salt application is affecting the water type of the stream.

The last snow event of 2020-2021 winter in Lewiston happened on April. Therefore, it is highly likely that the Cl^- kept adding to the stream as baseflow until July, and thus made the

stream appear “sodium chloride type” during midsummer periods. At the same time, as the residence road salt in soils may be mostly exported by August, according to the retention time of 10.5-17.5 weeks proposed by Robinson et al. (2017), the ratio between infiltrated road salt and the groundwater recharge (namely, the Cl^- concentration of groundwater) may be smaller due to more moist condition, and thus leads to the change in stream water type during fall months.

4.2 Spatial Variation in Water Quality

4.2.1. Clean Water in Goff Brook Area

HB5 is the cleanest site monitored, with the Cl^- concentration below 100 mg/L from midsummer to late fall (16.9mg/L-94.4 mg/L). Regarding the guidelines provided by EPA, the site may not have serious road salt pollution problems yet. This may be attributed to its location in a residential area and the relatively higher infiltration rate and lower runoff potential (Hart Brook Watershed Management Plan 2019). Despite that, the concentrations of HCO_3^- , Cl^- , and Na^+ in the site are still significantly larger than the baseline value in the Androscoggin River under no-rain conditions, indicating the existence of non-pointing source of pollution within the area. In addition, its average percentage of Na^+ in major cations and Cl^- in major anions were found to be 52.9% and 58.7%, respectively, suggesting that the water type of the site is still highly affected by the road salt.

4.2.2. Potential Source of Contamination in Industry Area

The upstream site HB4, locating at the Industry section of the watershed, where impervious surfaces were constructed upon the area with minimal infiltration rate, is usually most contaminated with HCO_3^- and Cl^- , which is consistent with previous records (Hart Brook Watershed Management Plan 2019).

HB4 is surrounded by industries and businesses with large parking lots, thus it is possible that salt applied to these impervious covers impair the water body in the site. Besides, HB4 is located at the downstream of an industrial area that is consisted of a poly-lab room, and factories of wine, food and beverage, plumbing fixtures, and industrial motions and controls, which may produce drains containing high acid and metal contents, and thus contaminate the stream (de Almeida et al., 2015).

In order to better understand the source of pollution, CC2 and CC1 that are located at the upstream and within the industrial area, respectively, have been sampled since 8/18/2021 (Figure 2.1). The stream flows: CC2 (upstream industrial zone) → CC1 (within industrial zone) → HB4 (downstream industrial zone). Evidence that all of the concentrations of HCO_3^- , SO_4^{2-} , and Cl^- increase as the stream passes through the industrial area (from CC2 to HB4) suggests that the area is related to the high contamination in HB4 (Figure 3.18 (b), (c), and (d)).

The level of contamination in CC1 is not as serious as that in HB4, despite a drain pipe is

observed right above the sampling point (Figure 4.2). Since the level of contamination in CC1 is significantly higher than that in CC2, but is not as high as that in HB4, the non-point sources of pollution, in addition to the contamination conducted from the industrial zone, may also play a role in HB4.



Figure 4.2. Site condition of CC1 on 8/18/2021.

The concentrations of HCO_3^- (161 mg/L) and Cl^- (100 mg/L) is abnormally high in CC2, regarding its location. Being the most upstream sampling site, CC2's levels of HCO_3^- and Cl^- contamination are still significantly higher than that of the Androscoggin River, and even have surpassed the levels of HB5. Further upstream watershed area of the site is a large forest, where anthropogenic effects appear to be less likely to be introduced. Nevertheless, the evapotranspiration processes in this region may lead to a more humid environment, cause the soil minerals absorb H^+ , and thus introduce HCO_3^- to the stream during ground-water recharge (Hem, 1985). It is possible that CC2 has undergone this natural process, so that observed HCO_3^- concentrations are high but still below the normal value of 200mg/L for most of the surface streams.

Hem (1985) mentioned three ways that Cl^- contents may be introduced to the stream water: (a) chemical weathering of igneous rocks (biotite), (b) fine-grained marine shale and porous rocks that were previously submerged by the sea, and (c) inflows of high-chloride groundwater or industrial wastes. Impurities are possible because the deeper Waterville Formation and the Vassalboro Formation below the watershed are consist of biotite schist, but Hem (1985) also noted that these contributions are very limited. The area upstream of CC2, CC1, HB4 is

surrounded by Stream Alluvium and Marine Regressive Deposits. It is possible that these rocks used to impregnated with NaCl crystal or solution, but it is unlikely that they are still sending out Cl^- today. However, these rocks may form suitable environments for Na^+ and Cl^- retention. Therefore, it is the most possible that the source of Cl^- in CC2 is actually introduced from 1) the surface water runoff from the impervious area near the site and/or 2) the groundwater that takes residence Cl^- in soils from further upstream, outside the watershed.

4.2.3. Downstream Site Conditions

In general, dilution signal of major ion concentrations is observed as one moves downstream of HB4. Since increasing discharge was observed in HB3 and BC6 is where two stems of stream converged, the dilution is caused by the addition of more and more fresh/cleaner water relative to contaminants

Interestingly, the SO_4^{2-} concentration is observed to be the highest at the site of HB3, which is significantly higher than the normal concentration of 10mg/L in relatively unpolluted water source (Hem, 1985). However, no significant increase in cations is observed in the site to correspond with this observation. It is possible that the SO_4^{2-} is bonded with Na^+ and Ca^{2+} , because the difference between these cations in HB4 and HB3 is not as significant as that between the Cl^- in these sites, when HB3 has underwent freshwater dilution. Nevertheless, the source of the SO_4^{2-} remains an unknown.

4.3 Seasonal Variation

4.3.1. Connecting Discharge Measurements with Previous Records

During dry periods, groundwater discharge (i.e., baseflow) is the primary source of stream flow (Caswell, 1987). Historically, in Maine, infiltration rates (groundwater recharge) are low during summer and early fall, increase in late fall, drop in winter, and then increase during the late winter and spring months, as evidenced by records of groundwater levels from the 1970s (Figure 4.4; Caswell, 1987). These seasonal changes in groundwater level are likely due to a combination of the following: an increase in the rate of evapotranspiration and/or a decrease in precipitation in summer and early fall, an increase in precipitation in late fall, freezing up land surface in winter, and then snow/ice melt in late winter and spring (Figure 4.3; Caswell, 1987).

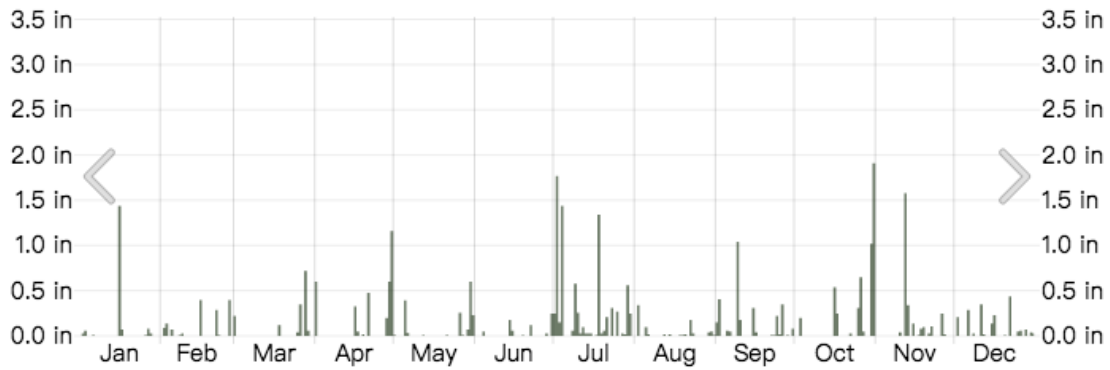


Figure 4.3. Historical daily precipitation in Lewiston in 2021 (weatherspark.com)

The general patterns in monthly stream discharge in the Hart Brook are similar to those established for monthly groundwater levels across Maine in the 1970s (Figure 4.4). Peak stream discharge occurs in the winter and spring months and low discharge occurs in the summer months.

While a warmer winter period is a general trend of the past 75 years, the shorter ice-cover duration is resulted from both later ice cover in fall and earlier ice-cover thaw in spring (Fernandez and Marvinney, 2020). Vegetation die-off and more frequent precipitation events lead to the increase in discharge during mid-fall period; at the same time, the first ice event being monitored this year at Lewiston happened on 12/7, which may provide an explanation that the fall discharge kept increasing because of the lack of frozen effects.

Additionally, it is important to note that the variable nature of the groundwater water levels from the 70s is not captured in the stream data. This may reflect changes in temperature and the hydrologic cycle in Maine over the last 45 years, or may reflect the sampling strategies employed in this study. Regardless, the general patterns of stream discharge in the Hart Brook suggest that baseflow is a major component to streamflow in the Hart Brook throughout the year.

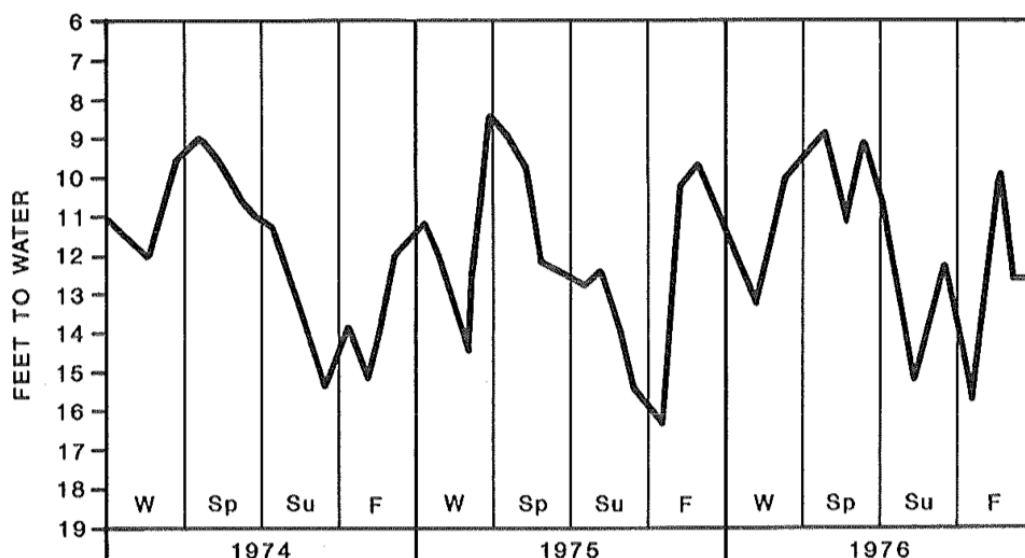


Figure 4.4. Groundwater water-level in Maine (Caswell, 1987)

4.3.2. Road Salt Application and Conductivity

According to Lewiston Public Works (Reggie Poussard, Lewiston Public Work), during the winter season in 2021-2022, 25 road salt treatments were performed in the Hart Brook area from December to February 25. Among these events, 22 of them happened during 12/7-2/17. The dates of these road salt applications coincide with peaks in SpC from BC 6 (Figure 3.13); therefore, every peak of the SpC (equivalently, Cl^- concentration), the increasing Cl^- flux and concentration (Figure 3.12, Figure 3.13, Figure 3.15, Figure 3.16) during Dec., Jan., and Feb. is likely caused by the application of road salt.

Moreover, because the high Cl^- flux and high Cl^- concentration in winter months are caused by the road salt application, it can be predicted that these values will drop significantly to meet similar values as those being recorded in March 2021. I hypothesize that when the temperature rises enough to not produce any snowfall in mid-March, the road salt application will be ceased, and thus the Cl^- flux will decrease without the major contributor of Cl^- input; the Cl^- concentration in the site will also drop significantly in correspond with the increasing discharge led from melting ice cover.

Cl^- concentrations are moderately high in June and July; the concentrations then decrease in early fall and rise during late fall and winter months. Notwithstanding, the Cl^- flux is low during the summer months due to the dry season conditions, and the flux only increases into the fall and winter months. Because road salt is not applied in these fall months, and because baseflow dominates stream flow in summer and fall, it appears as if road salt is retained in the groundwater for more than 6 months, at the very least. This is in apparent agreement with Robinson et al. (2017) who indicated the storage duration of 10.5 weeks to 17.5 weeks. It is

important to note they also suggested the possibility for longer retention times due to drier or more variable moisture condition and slow porewater movement. In addition, different soil types may also result in different holding capacities for the salt contents.

4.4 Surficial Geology and Infiltration Rate Analysis

The total area of the watershed calculated is 8903573 m², which is equivalent to about 2200 acres and is 100 acres larger than historical measurements (Hart Brook Watershed Management Plan 2019). The area of the watershed is calculated by summing up the areas of each surficial geology type in the watershed after projecting the map of the Hart Brook onto the surficial geology map. Therefore, the inconsistency may be caused by the use of different map of Hart Brook and the error introduced during projection processes. The total watershed infiltration rate is estimated to be 20.5%, which is consistent with a statewide estimate of 10-20% infiltration rate in Maine (Caswell, 1987).

The fate of precipitation is to undergo either evapotranspiration, infiltration, and runoff. To calculate the amount of water delivered to the stream annually, precipitation was assumed to either infiltrate the watershed (20.5%; this study), becoming a part of the plant and soil water cycle, under evapotranspiration (35%; Caswell, 1987), or behave as surface runoff (44.5%; Caswell, 1987) (Figure 4.5). Therefore, the total volume of precipitation shunting into the stream and mobilizing Cl⁻ is 65% of the total precipitation delivered to the watershed (Figure 4.5). In the past year, Lewiston received 45.77 inches (1.16 meters) of precipitation (US Climate Data). Hence, theoretically, the total volume of water that makes it into the stream in 2021, at a minimum, was thus $1.16\text{ m} \times 8903573\text{ m}^2 \times 65\% = 6728098\text{ m}^3$. It is important to note that this calculation assumes no input from baseflow, which we know is not true.

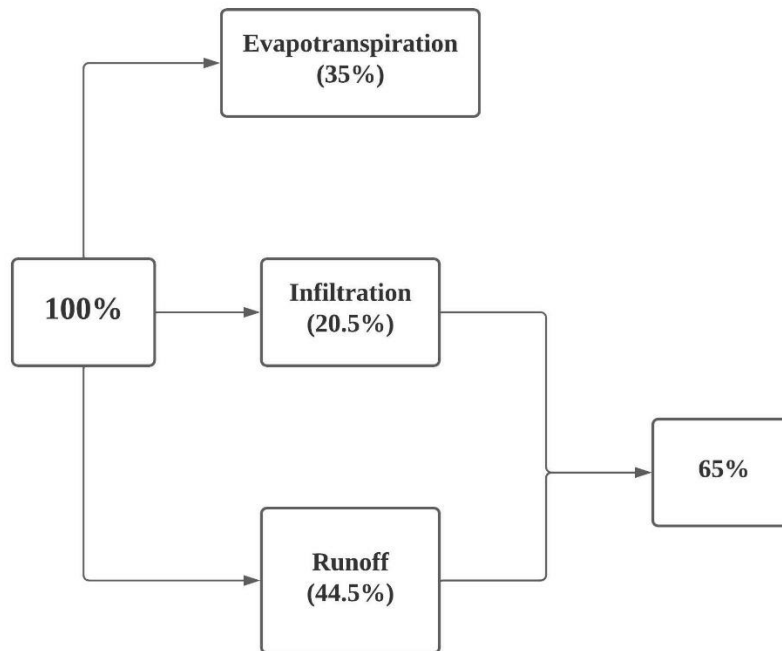


Figure 4.5. Schematic illustrating the fate of the precipitation in the watershed to estimate annual stream flow volume.

4.5 Rough Calculations of Exported Cl^-

With the total volume of water in the stream being estimated, it is possible to determine the average annual Cl^- concentrations expected. In this case, we divide the total mass of road salt applied to the watershed (as mg of Cl^-) by the total volume of water flowing through the streams over the course of the year. The assumptions here are that there are no seasonal changes in water or Cl^- input, and there is no contribution of water baseflow. These assumptions are inherently flawed, but they provide very coarse estimates to guide our thinking in the transport of road salt in the watershed.

With all of that in mind, the amount of road salt applied to the Hart Brook watershed in 2020 is determined based on the lane lengths ratio between Lewiston and Hart Brook as: $M_{(\text{Road Salt in HB})} = M_{(\text{Road Salt in Lew})} \times \frac{\text{Lane Lengths}_{(\text{HB})}}{\text{Lane Lengths}_{(\text{Lew})}}$. Table 4.2. is the compiled data of the extrapolation of the road salt application amounts in Hart Brook from the 2020 application amounts data in the Lewiston.

	Lewiston	Hart Brook
Lane Length (km)	359.66	35.42
Road Salt (tons)	4435	704

Table 4.2. Road salt application amounts in the Hart Brook

The total road salt being applied in the watershed is determined to be 704 tons (Table

4.2). The theoretical average concentration of Cl^- throughout the year is thus 63.5 mg/L.

When compared to the measured values, the total annual discharge volume 13614711 m^3 was determined by multiplying the average discharge of the year by the amount of the time a year, which is about the 2 times of the estimated discharge volume (Table 4.3). While the average measured Cl^- concentration 129.6 mg/L, twice of the theoretical value, the amount of Cl^- in the stream appears to be at least four times higher than the amount of Cl^- that was applied by the government to the roads in 2020.

	Literature/Theoretical Value	Measurements
Area (acres)	2100	2200
Infiltration Rate	10-20%	20.5%
Average Cl^- conc. (mg/L)	63.5	129.6
Road Salt (tons)	704	3178
Discharge (m^3)	6728098	13614711

Table 4.3. Calculations of annual Cl^- exportation

Further information is derived by summing the total Cl^- flux measured throughout for the year (1.93×10^{12} mg). This requires some assumptions and corrections during the interpretations of the SpC values. The largest correction of SpC values in this study occurs during period of September to November; SpC recordings below 65 $\mu\text{S}/\text{cm}$ are neglected because this is the baseline value observed from the Androscoggin River that should be below the values within the watershed. However, the lowest SpC being manually measured during a storm in the site is about 246 $\mu\text{S}/\text{cm}$; even during the middle of a very heavy and continuous storm event the values rarely appear below 100 $\mu\text{S}/\text{cm}$. Therefore, the correction approach may still be underestimating the average SpC values in these months as some values above 65 $\mu\text{S}/\text{cm}$ may still be invalid values provided by the sensor that is buried by sediments. At the same time, the actual average discharge may also be higher than that being estimated, because the potentially largest spring discharge mentioned in both articles by Caswell (1985), Fernandez, and Marvinney (2020) was not measured and not taken into the calculation. Therefore, it is highly unlikely that this study is underestimating the annual Cl^- flux.

The discrepancy between the actual Cl^- export and the Cl^- input from the government is potentially even larger because the road salt application amounts in the winter season of 2021-2022 is reported to be less than those in 2020-2021. While the estimated annual application amounts of road salt are 704 tons in this study, with the data from 2020-2021, the Lewiston Public Work states that the application amounts of road salt in this season is about 375 tons, because the government is trying to reduce the application amounts by applying 23.3% road salt brine (1 tons of road salt = 1000 gallons of liquid salt brine).

This discrepancy suggests that there are extra sources of Cl^- and road salt in this watershed

other than that which was applied by the Department of Transportation, City of Lewiston every year. Possible explanations for the presence of excess road salt include (1) groundwater Cl^- inputs from years of accumulation, including Cl^- retained in soils and those retained in the subsurface dam for stormwater protection, or from sources outside of the watershed as the surface water watershed boundaries do not necessarily coincide with the groundwater divides, (2) surface water Cl^- inputs from anthropogenic sewages and wastes other than road salt, and/or (3) additional application of road salt by individual companies and residences. The Hart Brook watershed has 22% ISC, thus it is possible that individuals are applying road salt to deice the parking lots and etc. These applications are not regulated and will continue to contribute to the salinization of the Hart Brook with time.

In summary, these back-of-the-envelope calculations and estimates suggest that there is more salt in the system than is laid down by the City of Lewiston on the public roads. Lewiston applies ~704 tons of road salt contains 4.27×10^{11} mg of Cl^- , but the total mass of Cl^- from the average Cl^- flux is about 1.93×10^{12} mg (equivalently, ~3178 tons of NaCl). In other words, there appears to be about 3.5 times more road salt coming through the Hart Brook stream than is applied annually by the city of Lewison. (Table 4.3).

4.6 Precipitation Event Analysis

One storm event occurred during 7/8/2021-7/12/2021, and was monitored at BC6 throughout the period. There had been no rain for at least two weeks prior to this precipitation event.

4.6.1 Storm Hydrograph

During the storm event, the largest precipitation of 0.86 inch was observed at 7/9 11:56 a.m. The largest discharge at BC6 happened 6 hours later, at about 6:00 p.m. (Figure 4.6 and Figure 4.7). The lag time in the watershed at BC6 is thus **6 hours**.

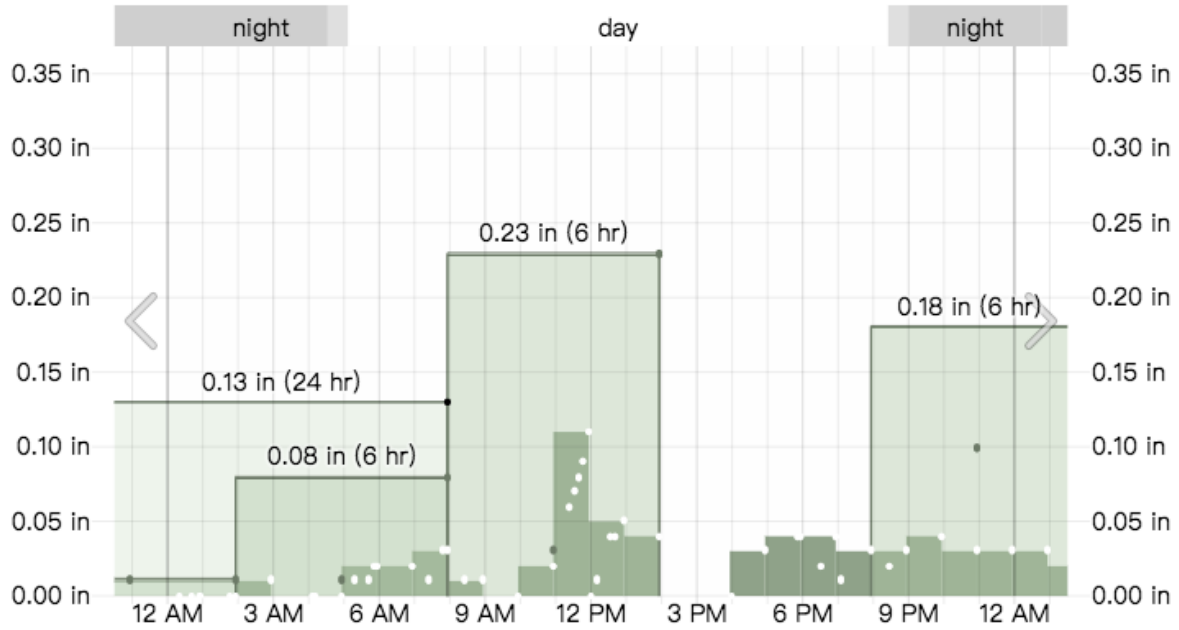


Figure 4.6. Precipitation on 7/9/2021 (Weatherspark.com)

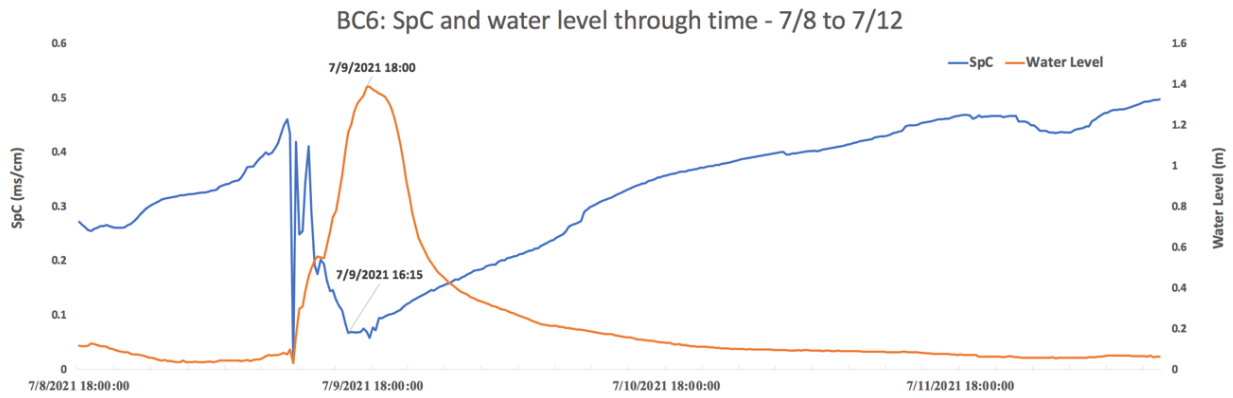


Figure 4.7. Logger data for BC6 from 7/8 to 7/12.

Baseflow is reestablished once the stream discharge (water level) returns to pre-storm levels. This appears to occur after 7/11/2021 6:00 p.m., and indicates a return to baseflow after 24 hours. This is supported by the empirically determined relationship between peak discharge, and areas of a watershed presented in Fetter (2018) as follows:

$D = 0.827A^{0.2}$, where D is the number of days between the storm peak and the end of overland flow and A is the drainage basin area. For this storm in the Hart Brook, $D = 0.827 \times (8.903573 \text{ km}^2)^{0.2} \approx 1.28 \text{ days}$. This is in pretty good agreement with the hydrograph interpretation.

4.6.2 Base Flow Separation

The SpC of base flow and runoff is assigned to be 786 $\mu\text{S}/\text{cm}$ and 59 $\mu\text{S}/\text{cm}$, which is the highest and the lowest SpC being observed from the conductivity sensor during the smallest and the largest discharge period (5/26 and 7/9), respectively. The calculated baseflow contribution thus ranges from 0 to 60.39% (Stewart et al., 2007).

4.6.3 First Flush Analysis

The MFFs ratio is graphed by plotting the normalized cumulative Cl^- mass observed in the stream against the normalized cumulative runoff volumes throughout the storm event (Figure 4.8). A comparison between the data from Hart Brook and the interpretative schematic provided by Shamseldin et al. (2011) in Figure 1.3 of this thesis indicates that the Hart Brook experiences a moderate first flush event accompanied with fast dilution.

For this storm event, an intersection is observed between the MFFs ratio line with the standard MFF line at 4:15 p.m. on 7/9/2021 (Figure 4.8). In other words, prior to this point in time, stream flow was dominated by runoff with high SpC (and Cl^-) load. After 4:15pm, runoff appears to diminish significantly, and baseflow becomes important, with a lower Cl^- load. From this curve, it presents a 4-hour lag between peak precipitation and the end of runoff.

By plotting out the variation of Cl^- mass during the storm, 4:15 p.m. is also observed as the lowest point between two peaks of Cl^- mass (Figure 4.9). Because, at 4:15pm, the runoff appears to have diminished significantly (Figure 4.8), it is possible that the second peak in Cl^- mass represents the time when the Cl^- introduced through infiltration of surface contaminants reaches the maximum, so that the infiltration recharges the stream 7 hours after the maximum runoff reaches. This time difference **is also consistent with the lag time of the watershed, suggesting the speed of the infiltration during storm event.**

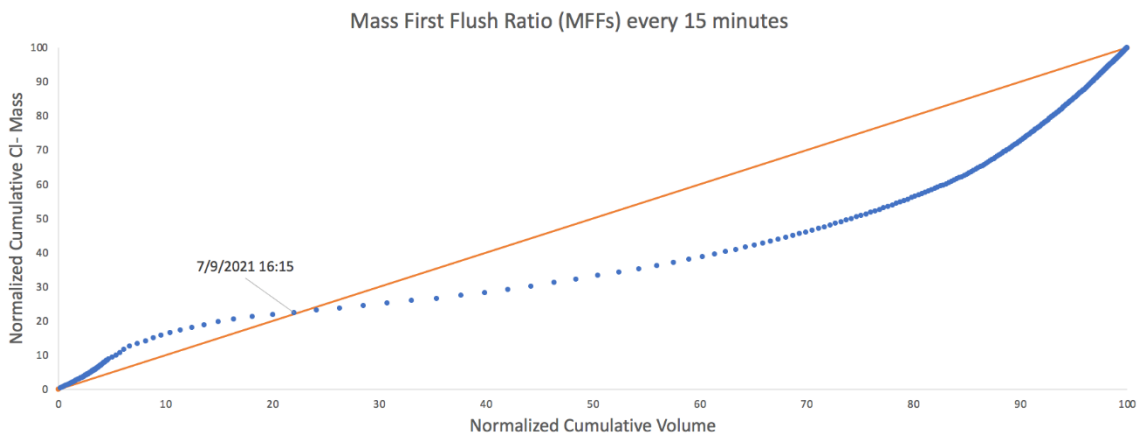


Figure 4.8. MFF of the storm event at BC6 between 7/8/2021 - 7/12/2021.

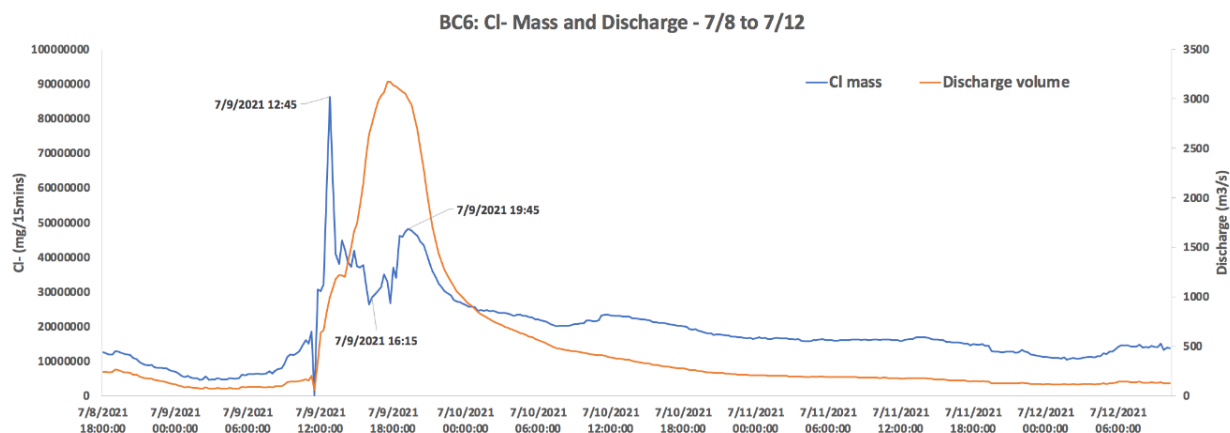


Figure 4.9. Cl^- mass and discharge variations during storm at BC6 from 7/8/2021 to 7/12/2021.

4.6.4. Chemical Responses

During the storm events, the correlation between Cl^- concentration and SpC is even stronger during storm events. The slope of the equation defining the relationship between Cl^- concentration and SpC (Cl^- against SpC) is 0.8878; whereas the ratio increases to 0.9525 during the storm period.

Variation was observed for the molar ratio between Na^+ and Cl^- during the storm (Figure 4.10). The molar ratio is closer to 1:1 during the storm, suggesting that the road salt is more likely to be input to the stream via runoff during rain events than via groundwater discharge during regular low flows.

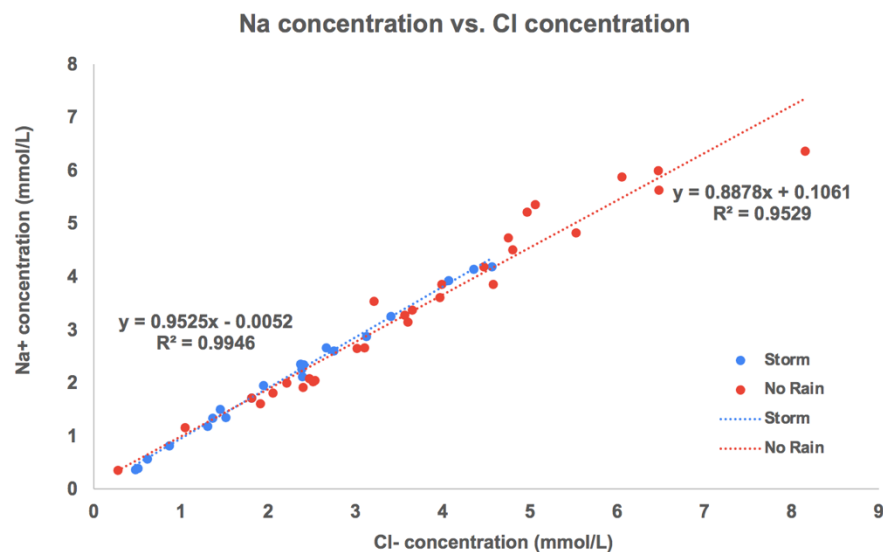


Figure 4.10. Molar ratio between Na^+ and Cl^- under storm and no-rain condition

Conclusion and Recommendations

The Hart Brook watershed is contaminated with various pollutants. Road salt appears to be the major contributor for Cl^- contamination in the Hart Brook watershed. Despite the efforts joined by the government in reducing road salt application amounts for each snow event, part of the stream is still surpassing EPA's chronically toxic Cl^- concentration level during summer and winter. The hotspots of Cl^- contamination are consistent with previous data, and are located mostly around the Industrial section of the watershed. In addition, this study also shows possibility for the further upstream area in the Industrial section to introduce contamination to the stream.

Continuous input of Cl^- during summer and fall periods are observed in this study, alongside with the increasing discharge in fall months. Together with the molar ratio of Na:Cl below 1:1, road salt retention is identified in this watershed, and the storage time is suggested to be longer than half a year. In addition, a weak/moderate first flush event is observed during a storm in midsummer, indicating the remaining road salt on the surface even during summer period.

The total annual export amounts of NaCl from the watershed is about 4 times the theoretical input amounts of NaCl reported from the Lewiston Department of Transportation. This discrepancy is likely to be introduced from 1) unregulated private application of de-icing salts, 2) wastewater with high Cl^- contents, 3) road salt retention from previous years, including those retained in the soils and those retained in subsurface reservoirs for stormwater protections, and 4) groundwater sources with high Cl^- contents from the outside of the watershed.

In order to further understand the reason behind the significantly larger Cl^- export from this watershed, it is important to investigate the % ISC belonging to private owners and to estimate the amounts of salt being applied annually in these ISCs. More detailed topography on the subsurface of the watershed may also be helpful, regarding the Cl^- contributions from subsurface stormwater dams and the possibility of outside groundwater sources.

Moreover, the retention mechanisms in this watershed remain unclear. As being mentioned by Robinson and Hasenmueller (2017), salt retention time is closely related to the holding-capacity the recovery time of soils, and the storage capacity may be affected by soil types and be exhausted with intense Cl^- input. Therefore, controlled experiments with local core samples from the watershed to identify the detailed soil types within the area and to investigate their corresponding salt retention times may be worth conducting.

References

- Arnold Jr, C. L., and Gibbons, C. J., 1996, Impervious surface coverage: the emergence of a key environmental indicator: *Journal of the American planning Association*, v. 62, no. 2, p. 243-258.
- Brabec, E., Schulte, S., and Richards, P. L., 2002, Impervious Surfaces and Water Quality: A Review of Current Literature and Its Implications for Watershed Planning: *Journal of Planning Literature*, v. 16, no. 4, p. 499-514.
- Benbow, M. E., and Merritt, R. W., 2004, Road-salt toxicity of select Michigan wetland macroinvertebrates under different testing conditions: *Wetlands*, v. 24, no. 1, p. 68-76.
- Castellote, M., Andrade, C., and Alonso, C., 2001, Measurement of the steady and non-steady-state chloride diffusion coefficients in a migration test by means of monitoring the conductivity in the anolyte chamber. Comparison with natural diffusion tests: *Cement and Concrete Research*, v. 31, no. 10, p. 1411-1420.
- Cunningham, M. A., O'Reilly, C. M., Menking, K. M., Gillikin, D. P., Smith, K. C., Foley, C. M., Belli, S. L., Pregnall, A. M., Schlessman, M. A., and Batur, P., 2009, The suburban stream syndrome: evaluating land use and stream impairments in the suburbs: *Physical Geography*, v. 30, no. 3, p. 269-284.
- Fetter, C.W., 2018, *Applied hydrogeology*, Waveland Press.
- de Almeida, M., Vargas-Zerwes, F., Ferreira-Bastos, L., Ben da Costa, A., de Souza-Schneider, R. d. C., Machado, Ê. L., and Kohler, A., 2015, Cation and anion monitoring in a wastewater treatment pilot project: *Revista Facultad de Ingeniería Universidad de Antioquia*, no. 76, p. 82-89.
- Godwin, K. S., Hafner, S. D., and Buff, M. F., 2003, Long-term trends in sodium and chloride in the Mohawk River, New York: the effect of fifty years of road-salt application: *Environmental Pollution*, v. 124, no. 2, p. 273-281.
- Gu, C., Cockerill, K., Anderson, W. P., Shepherd, F., Groothuis, P. A., Mohr, T. M., Whitehead, J. C., Russo, A. A., and Zhang, C., 2019, Modeling effects of low impact development on road salt transport at watershed scale: *Journal of Hydrology*, v. 574, p. 1164-1175.
- Hem, J. D., 1985, *Study and interpretation of the chemical characteristics of natural water*, Department of the Interior, US Geological Survey.
- Hildreth, Carol T., 2002, *Surficial geology of the Lewiston 7.5-minute quadrangle, Androscoggin County, Maine: Maine Geological Survey, Open-File Report 02-164*, 6 p.. Maine Geological Survey Publications. 283.
http://digitalmaine.com/mgs_publications/283
- Holland, A. F., Sanger, D. M., Gawle, C. P., Lerberg, S. B., Santiago, M. S., Riekerk, G. H. M., Zimmerman, L. E., and Scott, G. I., 2004, Linkages between tidal creek ecosystems and

- the landscape and demographic attributes of their watersheds: *Journal of Experimental Marine Biology and Ecology*, v. 298, no. 2, p. 151-178.
- Howard, K. W., and Haynes, J., 1993, Groundwater contamination due to road de-icing chemicals—salt balance implications: Geoscience Canada.
- Kaushal, S. S., Duan, S., Doody, T. R., Haq, S., Smith, R. M., Johnson, T. A. N., Newcomb, K. D., Gorman, J., Bowman, N., and Mayer, P. M., 2017, Human-accelerated weathering increases salinization, major ions, and alkalization in fresh water across land use: *Applied geochemistry*, v. 83, p. 121-135.
- Kaushal, S. S., Groffman, P. M., Likens, G. E., Belt, K. T., Stack, W. P., Kelly, V. R., Band, L. E., and Fisher, G. T., 2005, Increased salinization of fresh water in the northeastern United States: *Proceedings of the National Academy of Sciences*, v. 102, no. 38, p. 13517-13520.
- Kaushal, S. S., Likens, G. E., Pace, M. L., Utz, R. M., Haq, S., Gorman, J., and Grese, M., 2018, Freshwater salinization syndrome on a continental scale: *Proceedings of the National Academy of Sciences*, v. 115, no. 4, p. E574-E583.
- Kelly, V. R., Lovett, G. M., Weathers, K. C., Findlay, S. E. G., Strayer, D. L., Burns, D. J., and Likens, G. E., 2008, Long-Term Sodium Chloride Retention in a Rural Watershed: Legacy Effects of Road Salt on Streamwater Concentration: *Environmental Science & Technology*, v. 42, no. 2, p. 410-415.
- Kim, H., Jeong, H., Jeon, J., and Bae, S., 2016, The Impact of Impervious Surface on Water Quality and Its Threshold in Korea: *Water*, v. 8, no. 4, p. 111.
- Klein, R. D., 1979, Urbanization and stream quality impairment 1: *JAWRA Journal of the American Water Resources Association*, v. 15, no. 4, p. 948-963.
- Liu, Z., Wang, Y., Li, Z., and Peng, J., 2013, Impervious surface impact on water quality in the process of rapid urbanization in Shenzhen, China: *Environmental Earth Sciences*, v. 68, no. 8, p. 2365-2373.
- Maine Legislature, Standards for Classification of Estuarine and Marine Waters, Title 38, Chapter 3, Subchapter 1, Article 4-A, <https://www.mainelegislature.org/legis/statutes/38/title38sec465-B.html>
- Osberg, Philip H., Hussey, Arthur M., II, and Boone, Gary M. (editors), 1985, Bedrock geologic map of Maine: Maine Geological Survey, 1 plate, correlation chart, tectonic inset map, metamorphic inset map, color geologic map, cross sections, scale 1:500,000. Maine Geological Survey Maps. 23. http://digitalmaine.com/mgs_maps/23
- Peinado-Guevara, H., Green-Ruíz, C., Herrera-Barrientos, J., Escolero-Fuentes, O., Delgado-Rodríguez, O., Belmonte-Jiménez, S., and Ladrón de Guevara, M., 2012, Relationship between chloride concentration and electrical conductivity in groundwater and its

- estimation from vertical electrical soundings (VESs) in Guasave, Sinaloa, Mexico: *Ciencia e investigación agraria*, v. 39, no. 1, p. 229-239.
- Perera, N., Gharabaghi, B., and Noehammer, P., 2009, Stream chloride monitoring program of City of Toronto: implications of road salt application: *Water Quality Research Journal*, v. 44, no. 2, p. 132-140.
- Robinson, H. K., and Hasenmueller, E. A., 2017, Transport of road salt contamination in karst aquifers and soils over multiple timescales: *Science of The Total Environment*, v. 603-604, p. 94-108.
- Robinson, H. K., Hasenmueller, E. A., and Chambers, L. G., 2017, Soil as a reservoir for road salt retention leading to its gradual release to groundwater: *Applied Geochemistry*, v. 83, p. 72-85.
- Rubin, J., Garder, P. E., Morris, C. E., Nichols, K. L., Peckenham, J., McKee, P., Stern, A., and Johnson, T. O., 2010, *Maine's Winter Roads: Salt, Safety, Environment and Cost*.
- Schueler, T., 2003, *Impacts of impervious cover on aquatic systems*: Center for Watershed Protection. Ellicott City, MD.
- Shambaugh, A., and Vermont, W., 2008, *Environmental Implications of Increasing Chloride Levels in Lake Champlain and Other Basin Waters*: Vermont Agency of Natural Resources, Department of Environmental Conservation.
- Shamseldin, A., 2011, *First Flush Analysis in the Auckland Region*, Prepared by Auckland UniServices Ltd. for Auckland Regional Council
- Slattery, H. R., 2018, *Urbanization: Impact on Dissolved Oxygen and Sedimentation in the Hart Brook Watershed (Lewiston, Maine)* [Thesis]: Bates College.
- Snodgrass, J. W., Moore, J., Lev, S. M., Casey, R. E., Ownby, D. R., Flora, R. F., and Izzo, G., 2017, Influence of Modern Stormwater Management Practices on Transport of Road Salt to Surface Waters: *Environmental Science & Technology*, v. 51, no. 8, p. 4165-4172.
- Snowfall Totals and Certification, 2022, *Snowfall Totals History for Lewiston, 04240*: https://certifiedsnowfalltotals.com/storm_history/history/ME/67/36521/Lewiston%2C%2004240 (accessed February 2022).
- Stenstrom, M. K., and Kayhanian, M., 2005, *First flush phenomenon characterization*: California Department of Transportation Division of Environmental Analysis, No. CTSW-RT-05-073.02. 6.
- Stewart, M., Cimino, J., and Ross, M., 2007, Calibration of base flow separation methods with streamflow conductivity: *Groundwater*, v. 45, no. 1, p. 17-27.
- STS, M., 2020, *Scientific Assessment of Climate Change and Its Effects in Maine: A Report by the Scientific and Technical Subcommittee (STS) of the Maine Climate Council (MCC)*. Augusta, Maine.

- Su, Y., 2007, Storm water runoff first flush modeling and treatment with a hydrodynamic device: Ohio University.
- Sun, H., Huffine, M., Husch, J., and Sinpatanasakul, L., 2012, Na/Cl molar ratio changes during a salting cycle and its application to the estimation of sodium retention in salted watersheds: *Journal of Contaminant Hydrology*, v. 136-137, p. 96-105.
- U.S. Climate Data, 2022, Climate Lewiston - Maine:
<https://www.usclimatedata.com/climate/lewiston/maine/united-states/usme0213>
(accessed January 2022).
- USGS Water Science School, 2018, How Streamflow is Measured: https://www.usgs.gov/special-topics/water-science-school/science/how-streamflow-measured?qt-science_center_objects=0#overview (accessed June 2021).
- Wilson, R. W., and Grosell, M., 2003, Intestinal bicarbonate secretion in marine teleost fish—source of bicarbonate, pH sensitivity, and consequences for whole animal acid–base and calcium homeostasis: *Biochimica et Biophysica Acta (BBA) - Biomembranes*, v. 1618, no. 2, p. 163-174.
- City of Lewiston Public Works. 2019. Hart Brook Watershed Management Plan 2019:
<http://www.ci.lewiston.me.us/stormwater/hartbrook/index.htm> (accessed June 2021).
- Zuidema, S., Wollheim, W. M., Mineau, M. M., Green, M. B., and Stewart, R. J., 2018, Controls of chloride loading and impairment at the river network scale in New England: *Journal of environmental quality*, v. 47, no. 4, p. 839-847.

GIS Layers

Carol T. Hildreth, Surficial Geology of the Lewiston Quadrangle, Maine [Map]. 1:24000. Maine: Maine Geological Survey, 2002.

Nate Kane, MaineDOT Public Roads [Map]. Augusta, Maine, U.S.: Maine Department of Transportation, 2019.

Appendix 1: Field Work Schedule

Time	CC2	CC1	HB4	HB3	BC6	HB5	Andro
6/28/2021			T, D, P, O, C, H, S, L, I	T, D, P, O, C, H, S, L, I	T, D, P, O, C, H, S, L, I	T, D, P, O, C, H, S, L, I	
7/08/2021			T, D, L, I	T, D, L, I	T, D, L, I	T, D, L, I	
7/09/2021					T, D, L, I		
7/10/2021			T, D, L, I	T, D, L, I	T, D, L, I	T, D, L, I	
7/12/2021			T, D, L, I	T, D, L, I	T, D, L, I	T, D, L, I	
7/27/2021			T, D, P, O, C, H, S, L, I	T, D, P, O, C, H, S, L, I	T, D, P, O, C, H, S, L, I	T, D, P, O, C, H, S, L, I	
8/18/2021	T, D, P, O, C, H, S, L, I	T, D, P, O, C, H, S, L, I	T, D, P, O, C, H, S, L, I	T, D, P, O, C, H, S, L, I		T, D, P, O, C, H, S, L, I	
8/20/2021					T, D, P, O, C, H, S, L, I		

T: Temperature

D: Discharge

C: SpC

O: DO

P: pH

H: HCO₃⁻

S: SO₄²⁻

L: Cl⁻

I: major cation

Appendix 1 (Continued)

Time	CC2	CC1	HB4	HB3	BC6	HB5	Andro
8/20/2021					T, D, P, O, C, H, S, L, I		
9/02/2021					T, D, P, O, C, H, S, L, I		
9/14/2021	T, D, P, O, C, H, S, L, I	T, D, P, O, C, H, S, L, I	T, D, P, O, C, H, S, L, I	T, D, P, O, C, H, S, L, I	T, D, P, O, C, H, S, L, I	T, D, P, O, C, H, S, L, I	T, D, P, O, C, H, S, L, I
10/08/2021	T, D, P, O, C, H, S, L, I	T, D, P, O, C, H, S, L, I	T, D, P, O, C, H, S, L, I	T, D, P, O, C, H, S, L, I	T, D, P, O, C, H, S, L, I	T, D, P, O, C, H, S, L, I	
10/26/2021					T, D, P, O, C, H, S, L, I		
11/12/2021	T, D, P, O, C, H, S, L, I	T, D, P, O, C, H, S, L, I	T, D, P, O, C, H, S, L, I	T, D, P, O, C, H, S, L, I	T, D, P, O, C, H, S, L, I	T, D, P, O, C, H, S, L, I	
12/9/2021					T, D, P, O, C, H, S, L, I		

T: Temperature

D: Discharge

C: SpC

O: DO

P: pH

H: HCO₃⁻

S: SO₄²⁻

L: Cl⁻

I: major cation

Appendix 2: Hydrolab Data

Site	Date	Temperature (°C)	SpC (ms/cm)	DO (mg/L)	pH
HB4	06/28/2021	22.87	1.176	2.99	7.53
HB3	06/28/2021	20.82	0.923	6.60	7.22
BC6	06/28/2021	23.33	0.402	5.35	7.35
HB5	06/28/2021	21.17	0.383	6.40	7.51
HB4	07/08/2021		0.717		
HB3	07/08/2021		0.233		
BC6	07/08/2021		0.301		
HB5	07/08/2021		0.403		
BC6	07/09/2021		0.434		
HB4	07/10/2021		0.399		
HB3	07/10/2021		0.408		
BC6	07/10/2021		0.407		
HB5	07/10/2021		0.499		
HB4	07/12/2021		0.581		
HB3	07/12/2021		0.674		
BC6	07/12/2021		0.712		
HB5	07/12/2021		0.563		
HB4	07/28/2021		0.582	8.55	6.57
HB3	07/28/2021		0.644	8.59	7.02
BC6	07/28/2021		0.679	8.60	7.19
HB5	07/28/2021		0.370	8.30	7.39
CC2	08/18/2021	20.91	0.584	9.69	7.51
CC1 (mix)	08/18/2021	24.88	0.720	20.44	7.73
CC1 (orange)	08/18/2021	20.33	0.867	13.00	7.49
CC1 (black)	08/18/2021	25.74	0.671	8.66	7.70
HB4	08/18/2021	23.38	1.041	11.83	7.80
HB3	08/18/2021	19.83	0.947	12.23	7.74
BC6	08/20/2021	21.21	0.500	11.92	6.25
HB5	08/18/2021	20.89	0.513	12.95	8.16
CC2	09/14/2021	17.12	0.486	2.61	6.79
CC1	09/14/2021	22.61	0.629	9.89	8.68
HB4	09/14/2021	19.09	0.903	7.55	8.24
HB3	09/14/2021	15.98	0.835	8.76	7.51
BC6	09/14/2021	17.57	0.786	9.09	7.75
HB5	09/14/2021	16.68	0.390	13.18	7.48
CC2	10/08/2021	17.01	0.460	7.98	6.71
CC1	10/08/2021	19.11	0.652	9.04	8.21
HB4	10/08/2021	16.38	0.920	10.32	8.23
HB3	10/08/2021	17.29	0.205	8.78	7.48
BC6	10/08/2021	15.26	0.555	9.16	7.46
HB5	10/08/2021	15.30	0.344	8.46	7.47
Androscoggin	10/08/2021	18.85	0.072	8.53	7.22
CC2	11/05/2021		0.358		
CC1	11/12/2021		0.129		
HB4	11/12/2021		0.173		
HB3	11/12/2021		0.245		
BC6	11/12/2021		0.277		
HB5-1	11/12/2021		0.105		
HB5-2	11/12/2021		0.110		

Appendix 3: Major Ion Analysis Results

Sample Site	Date	As1890	Pb2203	K7664	Mg2795	Ca4226	Na5895	Cl-	HCO3	SO4	Charge-Balance Error
HB4	6/28	-0.01	-0.03	5.03	9.38	67.82	146.39	289.06	164.90	17.00	-2.55%
HB3	6/28	0.02	0.01	3.68	6.54	41.86	129.47	229.47	99.43	31.00	-2.31%
BC6	6/28	-0.02	-0.03	3.17	6.49	30.77	88.77	162.14	80.33	25.00	-3.21%
HB5	6/28	-0.02	-0.03	2.30	4.08	25.45	44.19	85.02	71.60	12.00	-3.17%
HB4	7/8	-0.02	-0.03	2.93	3.82	30.15	96.26	161.67			
HB3	7/8	-0.02	-0.03	1.41	1.75	12.20	34.57	51.34			
BC6	7/8	-0.02	-0.03	1.70	2.13	14.41	44.77	68.73			
HB5	7/8	-0.02	-0.04	2.38	4.15	25.85	48.75	84.65			
BC6	7/9	-0.02	-0.03	2.46	3.19	21.47	59.82	97.33			
HB4	7/10	-0.02	-0.03	2.55	2.73	21.54	52.06	84.33			
HB3	7/10	-0.02	-0.03	2.64	2.82	19.28	54.23	84.00			
BC6	7/10	-0.02	-0.03	2.45	2.81	18.37	53.93	85.14			
HB5	7/10	-0.02	-0.03	3.20	4.48	28.79	61.31	94.40			
HB4	7/12	-0.02	-0.03	2.69	3.74	30.59	74.88	120.56			
HB3	7/12	-0.02	-0.03	3.14	4.17	30.09	90.42	144.12			
BC6	7/12	-0.02	-0.03	3.14	4.32	29.88	95.23	154.19			
HB5	7/12	-0.02	-0.03	3.06	4.77	32.23	66.10	110.65			
HB4	7/28	0.01	-0.02	3.38	4.85	39.18	83.04	140.50	147.65	8.33	-4.00%
HB3	7/28	0.01	-0.02	3.30	5.00	36.82	96.41	158.47	124.51	24.00	-3.58%
BC6	7/28	0.01	-0.02	3.49	5.03	36.07	103.70	170.23	118.96	22.33	-2.87%
HB5	7/28	0.00	-0.02	2.56	4.29	28.62	47.86	87.45	86.09	15.33	-3.30%
CC2	8/18	0.01	-0.02	3.01	5.16	42.79	61.27	109.98	162.43	0.00	-4.18%
CC1	8/18	0.01	-0.02	4.33	6.12	44.63	88.56	141.38	155.27	19.00	-1.73%
HB4	8/18	0.01	-0.02	5.43	7.95	64.90	137.80	229.37	197.33	19.67	-0.44%
HB3	8/18	0.01	-0.02	4.20	6.13	45.62	135.20	214.60	131.10	30.67	-0.40%
BC6	8/20	0.01	-0.02	2.95	1.98	15.59	81.46	113.68	81.21	12.67	-2.59%
HB5	8/18	0.01	-0.02	3.15	4.73	34.46	61.01	106.79	87.25	21.00	-0.37%

(Concentrations in the unit of ppm)

Appendix 3 (Continued)

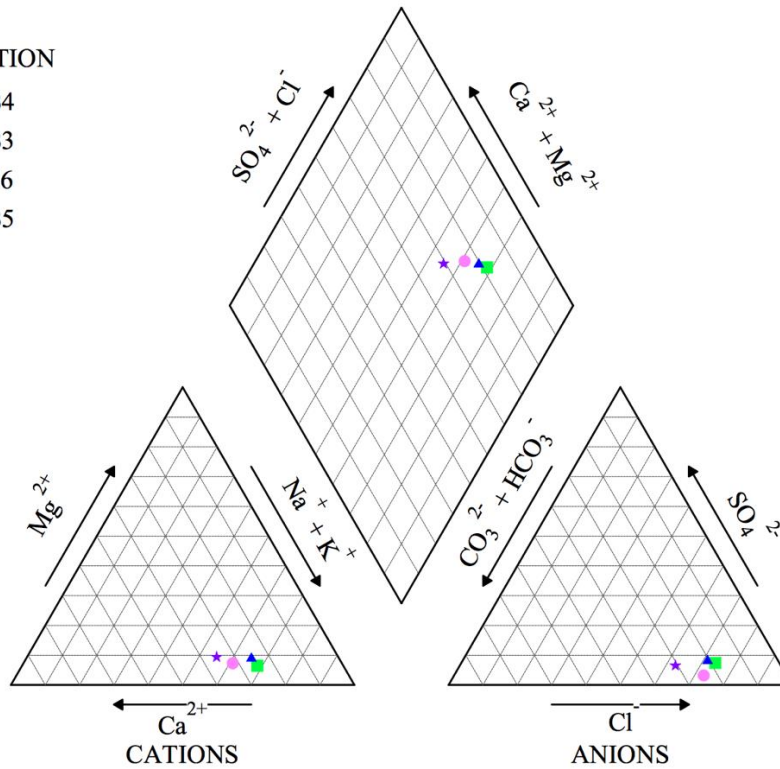
Sample Site	Date	As1890	Pb2203	K7664	Mg2795	Ca4226	Na5895	Cl-	HCO3	SO4	Charge-Balance Error
BC6	9/2	0.00	0.00	2.54	2.25	15.94	39.33	63.99	72.49	9.33	-7.26%
CC2	9/14	0.00	0.00	2.85	4.75	35.44	47.08	89.78	159.07	0.00	-9.12%
CC1	9/14	0.01	0.00	4.08	6.04	40.29	77.59	129.31	167.13	19.33	-6.28%
HB4	9/14	0.01	-0.02	4.46	6.70	53.10	123.30	179.39	241.18	17.33	-3.85%
HB3	9/14	0.00	-0.02	3.80	5.84	42.41	119.90	175.88	164.44	27.67	-2.00%
BC6	9/14	0.00	-0.02	3.71	5.57	38.41	108.80	168.34	150.35	26.33	-3.73%
HB5	9/14	0.00	-0.02	2.30	4.08	25.77	46.07	78.22	86.81	15.33	-3.46%
CC2	10/8	0.00	0.00	3.00	4.79	34.66	46.54	88.90	143.63	2.47	-7.53%
CC1	10/8	0.01	0.00	4.17	6.47	42.28	72.44	127.51	170.93	16.42	-6.65%
HB4	10/8	0.01	0.00	4.37	7.10	52.53	111.00	195.79	197.78	14.30	-5.33%
HB3	10/8	0.00	0.00	1.39	1.53	10.08	26.80	36.92	46.54	9.73	-4.61%
BC6	10/8	0.00	0.00	2.59	3.97	25.56	75.47	126.17	96.65	17.12	-5.25%
HB5	10/8	0.00	-0.01	2.13	3.74	22.32	37.10	67.67	79.20	10.18	-5.06%
Andro	10/8	0.00	0.00	0.99	0.94	4.95	8.12	9.59	14.77	6.19	4.58%
BC6	10/26	0.00	0.00	2.49	2.08	13.05	30.84	48.13	65.78	8.07	-7.80%
CC2	11/5	0.00	0.00	2.67	3.81	27.32	41.61	72.76	104.93	10.98	-5.90%
CC1	11/12	0.00	0.00	2.65	1.57	9.38	12.95	21.58	39.15	4.87	-4.80%
HB4	11/12	0.00	0.00	2.46	1.58	10.27	18.88	30.60	50.56	4.91	-8.04%
HB3	11/12	0.00	0.00	2.65	1.84	11.74	27.32	46.20	52.13	8.01	-7.65%
BC6	11/12	0.11	0.00	2.79	2.07	12.73	31.16	53.50	54.81	8.99	-7.51%
HB5_1	11/12	0.00	0.00	2.64	0.91	4.75	8.53	16.90	17.67	3.02	-4.96%
HB5_2	11/12	0.00	-0.01	2.64	0.94	4.75	8.88	17.71	20.36	3.12	-7.78%
BC6	12/9	0.00	0.00	2.70	5.24	31.72	151.80	249.18	101.57	23.67	-2.80%

(Concentrations are expressed in the unit of ppm)

Appendix 4: Piper Diagram of Each Sample Set

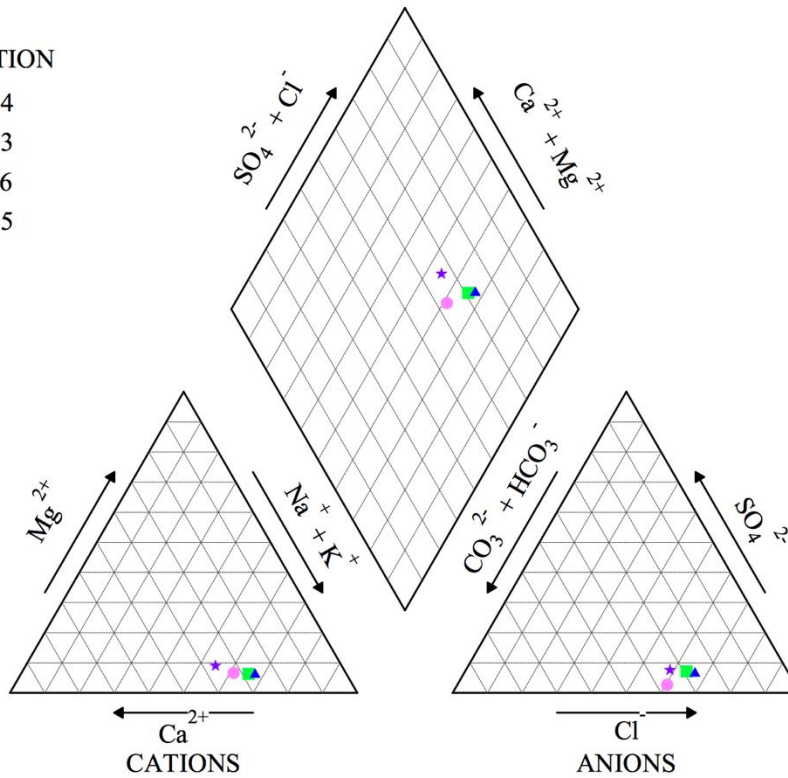
EXPLANATION

- 6/28 HB4
- 6/28 HB3
- ▲ 6/28 BC6
- ★ 6/28 HB5



EXPLANATION

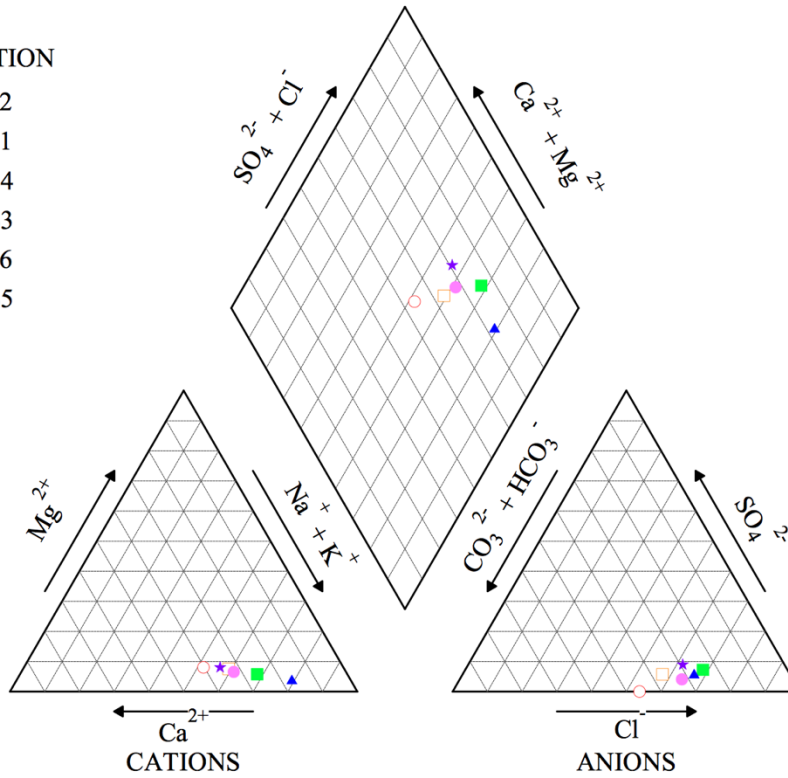
- 7/28 HB4
- 7/28 HB3
- ▲ 7/28 BC6
- ★ 7/28 HB5



Appendix 4 (Continued)

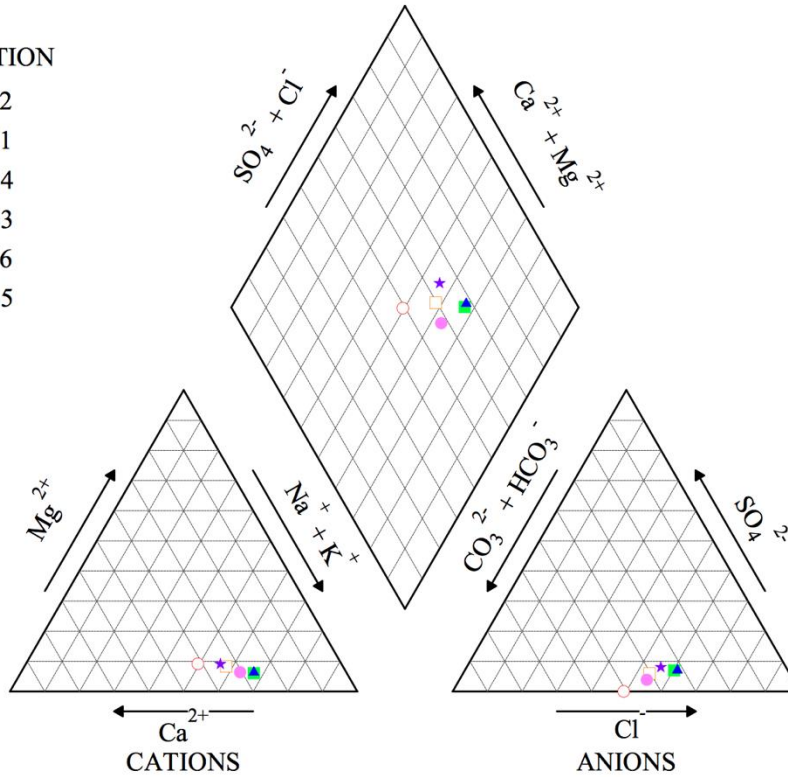
EXPLANATION

- 8/18 CC2
- 8/18 CC1
- 8/18 HB4
- 8/18 HB3
- ▲ 8/20 BC6
- ★ 8/18 HB5



EXPLANATION

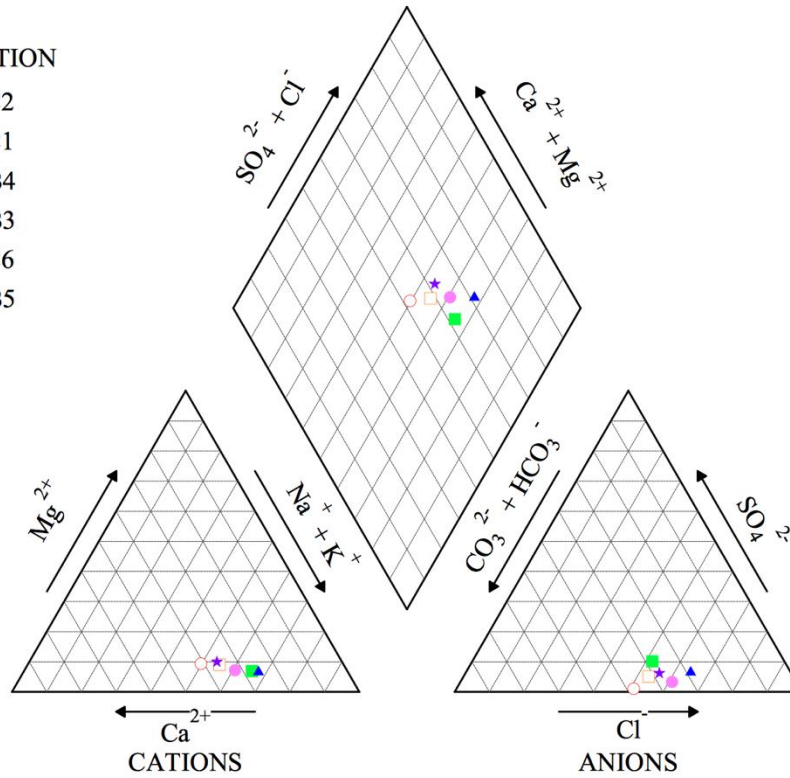
- 9/14 CC2
- 9/14 CC1
- 9/14 HB4
- 9/14 HB3
- ▲ 9/14 BC6
- ★ 9/14 HB5



Appendix 4 (Continued)

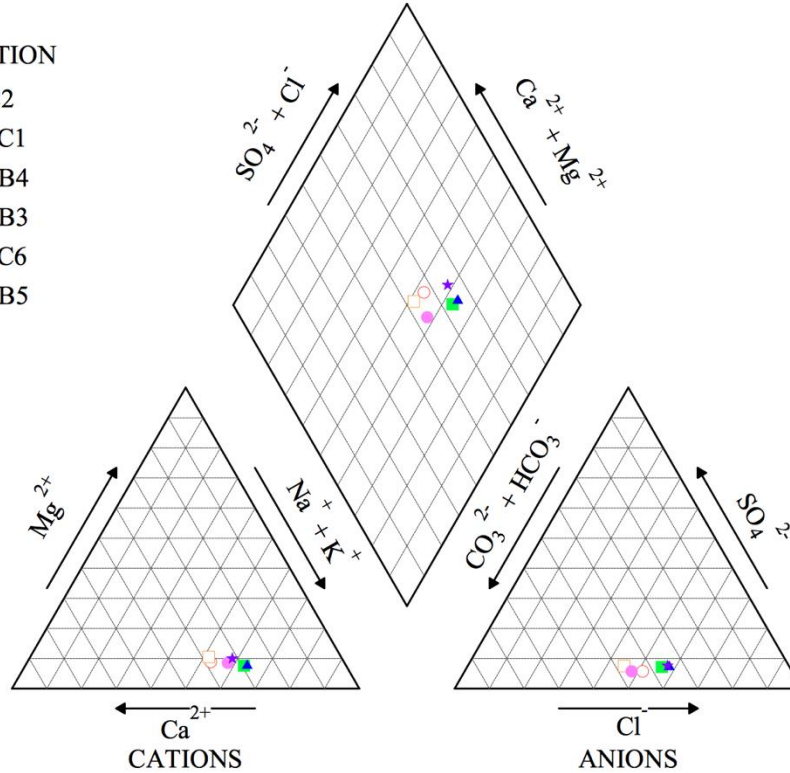
EXPLANATION

- 10/8 CC2
- 10/8 CC1
- 10/8 HB4
- 10/8 HB3
- ▲ 10/8 BC6
- ★ 10/8 HB5



EXPLANATION

- 11/5 CC2
- 11/12 CC1
- 11/12 HB4
- 11/12 HB3
- ▲ 11/12 BC6
- ★ 11/12 HB5



Appendix 4 (Continued)

EXPLANATION

▲ 12/9 BC6

